ol. 133 No. 2, May 1, 1981 ISSN 0378-4304
omputer Techniques and Optimization, Vol. 5 No. 2)

ANALYTICA CHIMICA ACTA

International journal devoted to all branches of analytical chemistry

COMPUTER TECHNIQUES AND OPTIMIZATION

ELSEVIER SCIENTIFIC PUBLISHING COMPANY

ANALYTICA CHIMICA ACTA

International journal devoted to all branches of analytical chemistry
Revue internationale consacrée à tous les domaines de la chimie analytique
Internationale Zeitschrift für alle Gebiete der analytischen Chemie

PUBLICATION SCHEDULE FOR 1981 (incorporating the section on Computer Techniques an Optimization).

	J	F	M	A	M	J	J	A	S	O	N	D
Analytica Chimica Acta	123	124/1	124/2	125	126	127	128	129	130/1	130/2	131	132
Section on Computer Techniques and Optimization		133/1			133/2			133/3			133/4	

Scope. *Analytica Chimica Acta* publishes original papers, short communications, and reviews dealing with ever aspect of modern chemical analysis, both fundamental and applied. The section on *Computer Techniques an Optimization* is devoted to new developments in chemical analysis by the application of computer techniques and b interdisciplinary approaches, including statistics, systems theory and operation research. The section deals with th following topics: Computerized acquisition, processing and evaluation of data. Computerized methods for th interpretation of analytical data including chemometrics, cluster analysis, and pattern recognition. Storage and retrieva systems. Optimization procedures and their application. Automated analysis for industrial processes and quali control. Organizational problems.

Submission of Papers. Manuscripts (three copies) should be submitted as designated below for rapid and efficien handling:

Papers from the Americas to: Professor Harry L. Pardue, Department of Chemistry, Purdue University, West Lafayette IN 47907, U.S.A.

Papers from all other countries to: Dr. A. M. G. Macdonald, Department of Chemistry, The University, P.O. Box 363 Birmingham B15 2TT, England.

For the section on *Computer Techniques and Optimization:* Dr. J. T. Clerc, Universität Bern, Pharmazeutisches Institut Sahlistrasse 10, CH-3012 Bern, Switzerland.

American authors are recommended to send manuscripts and proofs by INTERNATIONAL AIRMAIL.

Submission of an article is understood to imply that the article is original and unpublished and is not being considered for publication elsewhere. Upon acceptance of an article by the journal, the author(s) resident in the U.S.A. will be asked to transfer the copyright of the article to the publisher. This transfer will ensure the widest dissemination of information under the U.S. Copyright Law.

Information for Authors. Papers in English, French and German are published. There are no page charges. Manuscripts should conform in layout and style to the papers published in this Volume. Authors should consult Vol. 121, p. 353 for detailed information. Reprints of this information are available from the Editors or from: Elsevier Editorial Services Ltd., Mayfield House, 256 Banbury Road, Oxford OX2 7DE (Great Britain).

Reprints. Fifty reprints will be supplied free of charge. Additional reprints (minimum 100) can be ordered. An order form containing price quotations will be sent to the authors together with the proofs of their article.

Advertisements. Advertisement rates are available from the publisher.

Subscriptions. Subscriptions should be sent to: Elsevier Scientific Publishing Company, P.O. Box 211, 1000 AE Amsterdam, The Netherlands. The section on *Computer Techniques and Optimization* can be subscribed to separately.

Publication. *Analytica Chimica Acta* (including the section on *Computer Techniques and Optimization*) appears in 11 volumes in 1981. The subscription for 1981 (Vols. 123–133) is Dfl. 1639.00 plus Dfl. 198.000 (postage) (total approx. U.S. $942.00). The subscription for the *Computer Techniques and Optimization* section only (Vol. 133) is Dfl. 149.00 plus Dfl. 18.00 (postage) (total approx. U.S. $86.00). Journals are sent automatically by airmail to the U.S.A. and Canada at no extra cost and to Japan, Australia and New Zealand for a small additional postal charge. All earlier volumes (Vols. 1–121) except Vols. 23 and 28 are available at Dfl. 164.00 (U.S. $84.00), plus Dfl. 13.00 (U.S. $6.50 postage and handling, per volume.

Claims for issues not received should be made within three months of publication of the issue, otherwise they cannot be honoured free of charge.

Customers in the U.S.A. and Canada who wish to obtain additional bibliographic information on this and other Elsevier journals should contact Elsevier/North Holland Inc., Journal Information Center, 52 Vanderbilt Avenue, New York, NY 10017. Tel: (212) 867-9040.

Analytica Chimica Acta, 133 (1981) 109—123
Computer Techniques and Optimization
Elsevier Scientific Publishing Company, Amsterdam — Printed in The Netherlands

EXTENSION OF THE SMITH PREDICTOR

CHARLES J. HERGET and JACK W. FRAZER*

Lawrence Livermore Laboratory, University of California, Livermore, California 94550 (U.S.A.)

(Received 7th July 1980)

SUMMARY

An effective means of controlling non-linear systems with time delays by use of a digital computer is presented. A model of the system is required, and an extension of Smith's method is used. The method is demonstrated on an experimental enzyme reactor containing a saturating element and a large delay relative to the time constants of the system. The time optimum control of the experimental system as well as PID control is used to demonstrate the effectiveness of the method.

Efficient methods for controlling large-scale chemical processing plants are needed to reduce environmental pollution, improve product yield and quality, and conserve energy. The development of integrated circuit technology has resulted in inexpensive micro- and mini-computers powerful enough for sophisticated automation and control applications. In addition, many chemical instruments capable of on-line measurements and analysis are available or under development. A profile of a process obtained with these instruments can be used directly by computers to control the process. In spite of this increased availability of hardware, computer automation and control of chemical processes has proceeded slowly, possibly because of the complexity of chemical systems and the lack of communication between associated disciplines. Typical complexities are the large number of process variables, strong interaction among process variables, process delays, the need for good control models for non-linear distributed processes and incorporation of control bounds in the controller design, and system disturbances and noise that are difficult to characterize.

In order to provide a systematic procedure to approach these difficult problems, a laboratory bench scale apparatus with a problem environment similar to that found in a commercial pilot plant has been built, and an interdisciplinary team of chemists, engineers and mathematicians organized at this laboratory. The goals are to characterize quickly complex chemical reactions, determine optimum operating conditions, and develop control algorithms to achieve these optimum conditions under adverse conditions.

This paper deals with the problem of non-linear systems with time delays and the time optimum control of systems with time delays. Preceding papers

0378—4304/81/0000—0000/$02.50

from this research project have treated the problem of characterizing chemical processes [1, 2] and the sensitivity of the Smith predictor to parameter variations [3]. Time delays are well known to have detrimental effects in feedback control systems. Smith [4] introduced a method for designing controllers to overcome the difficulties introduced by time delays. This method, known as the Smith predictor, requires a model of the process and time delay be built into the controller. If in fact the actual process were to behave exactly as predicted by the model, the detrimental effects of the time delay could be eliminated totally; however, in practice there is always a mismatch between the model and the actual process.

The Smith predictor was originally formulated for linear, time-invariant systems consisting of a single input (control) and a single output. Several papers have shown that Smith's technique can also be applied to digital control systems [5, 6] and multivariable systems [6—8]. In this paper, it will be shown how Smith's approach can be applied to a much larger class of general, non-linear systems with delays. As with Smith's original work, the detrimental effects of the time delays are completely eliminated if the model is an exact representation of the actual system. In practice, there will always be some mismatch, and so this approach must be viewed as a design philosophy rather than a proven theory.

The method will be demonstrated on the previously mentioned laboratory bench scale apparatus. Non-linearities in the system appear in the form of limits on the pumping rates of the motors. The time optimum control of this system will be implemented in order to provide a nontrivial demonstration of the method.

The time optimum control of chemical processes has been considered by various workers [9—14]. In each case, the authors were interested in analog control, and the time delays were assumed to be small compared to the system time constant. Also, the methods presented were easy to implement as analog controllers which resulted in time optimum or nearly time optimum control. In this paper, the exact solution of the time optimum control of a second-order system by a digital controller will be implemented. The algorithm is based on that of Desoer and Wing [15]. Since there is always a mismatch between the model and the actual system, some form of corrective feedback is desirable after the completion of a time optimum control sequence. In this application, a PID controller will be used to maintain the desired set point after time optimum control has been used to achieve a change in set point. The extended form of the Smith predictor will be used to compensate for time delays.

THE EXTENDED PREDICTOR

There are several ways of explaining how the Smith predictor works. Here, the Smith predictor appropriate for a linear, time invariant, single input, single output control system is briefly explained; then the generalization to

multivariable, possibly non-linear systems with multiple delays will be given, with implementation by a digital controller.

In this paper, functions of time, e.g., $u(t)$ and $x(t)$, are denoted by lower case letters with t denoting time. The corresponding Laplace transforms of the time functions are denoted by upper case letters, e.g., $U(s)$ and $X(s)$, with s denoting the complex variable argument of the Laplace transform. A vector or matrix is denoted by boldface letters, e.g., $\mathbf{x} = (x_1 \ldots, x_n)^T$ where the superscript T denotes transpose. The derivative of a function of time, $f(t)$, is denoted by $f'(t)$.

Figure 1 outlines the implementation of the Smith predictor in a linear, time invariant, single input, single output, control system. The actual system to be controlled is shown within the upper set of dashed lines. It consists of an input, $U(s)$, the system transfer function, $G(s)$, the system output before delay, $X(s)$, a dead time, d, and the measured output, $Y(s)$. The input to the overall system is the set point, $Y_d(s)$. To implement the Smith predictor, a model of the system is simulated. The model is shown within the lower set of dashed lines. The input to the model is the same function, $U(s)$, which is the input to the true system. The transfer function $G_m(s)$ is the model approximation to the transfer function $G(s)$. The model output before delay, $X_m(s)$, is the predicted value of $X(s)$ of the model. Since $X_m(s)$ appears in the simulation, it is available to the controller whereas $X(s)$ is not. The model contains a time delay, d_m, with output $Y_m(s)$, the value of $Y(s)$ predicted by the model. The transfer function $G_c(s)$ is the compensation network, usually a proportional plus integral (PI) or proportional plus integral plus derivative (PID) control.

It is apparent that if the model transfer function, $G_m(s)$, is exactly equal to $G(s)$, if the model delay, d_m, is exactly the same as the true system delay, d, and if the initial conditions on the system model are the same as the initial conditions on the actual system, then $Y(s)$ and $Y_m(s)$ will be identical. If this

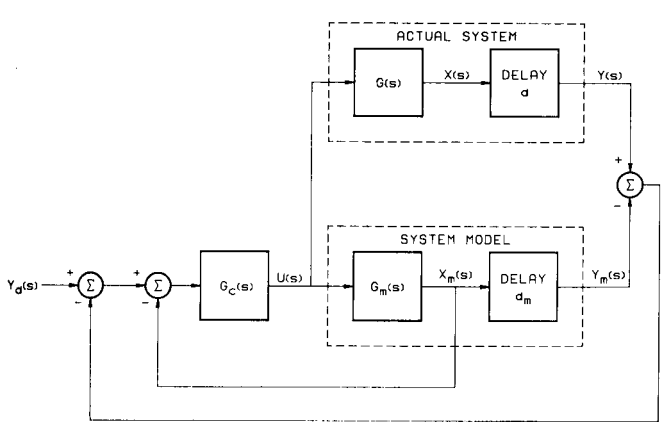

Fig. 1. Implementation of the Smith predictor. $Y_d(s)$ set point; $U(s)$ control; $X(s)$ system output before delay; d system dead time; $Y(s)$ system output after delay; $G_c(s)$ controller compensation network; $G(s)$ system transfer function; $G_m(s)$ model transfer function; $X_m(s)$ model output before delay; d_m model delay; $Y_m(s)$ model output after delay.

is so, then the simplified form shown in Fig. 2 will be equivalent to the complete implementation shown in Fig. 1. The advantage of the simplified model is that design of $G_c(s)$ can be done by classical control system methods. There is no time delay in the feedback loop. Classical design procedures can be applied, or standard methods for tuning PI or PID networks can be used.

In practice, the system model will never be an exact representation of the actual system, and eventually there will be some non-zero difference between $y(t)$ and $y_m(t)$. The implementation (Fig. 1) shows that this difference is fed back on the outer feedback path. The errors from system modeling will eventually be eliminated for a fixed set point if the compensation, $G_c(s)$, contains an integrator and the overall system is stable.

It can be observed that the only use of the fact that $G(s)$ is a transfer of a linear system is to facilitate the design of the compensation $G_c(s)$. Furthermore, $G_c(s)$ was assumed to be a transfer function in order to design it by classical methods. Whether the actual system is linear or not, an approach similar to Smith's can be used to arrive at a method to design the controller based on a system without delay.

It will be convenient to use state variable notation to facilitate the description of the system. Let $\mathbf{x}(t)$ denote the state of the actual system before delay, which is assumed to be of dimension n. Let $\mathbf{u}(t)$ denote the control vector of dimension r. Let p be the number of measured output variables where $p \leqslant n$. It will be assumed that the state variables can be selected in such a way that the measured output vector, $\mathbf{y}(t)$, is given by

$$\mathbf{y}(t) = \begin{bmatrix} x_1(t - d_1) \\ \vdots \\ x_p(t - d_p) \end{bmatrix} \tag{1}$$

where $d_i \geqslant 0$ corresponds to the delay of the x_i state variable for $i = 1, \ldots, p$. Although this is not the most general case, it includes most situations encountered in applications, the most frequent being $p = 1$. The vector $\mathbf{d} = (d_1, \ldots, d_p)^T$ will be called the delay vector. It will be assumed that the state of the true system satisfies the (possibly non-linear) system of first order

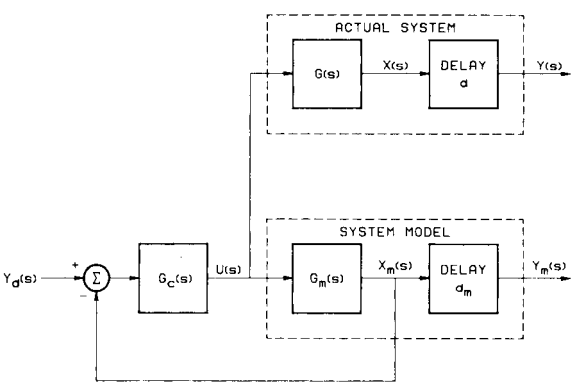

Fig. 2. Simplified form of the Smith predictor.

ordinary differential equations

$$\mathbf{x}'(t) = \mathbf{f}[\mathbf{x}(t), \mathbf{u}(t)] \tag{2}$$

where $\mathbf{f}$ is a suitably defined function on $R^n \times R^r$ into R^n.

Implementation of the controller which follows the same approach as Smith's for linear systems is shown in Fig. 3. The actual system is shown within the upper set of dashed lines. The block labeled DELAYS $\mathbf{d}$ and MEASURE implies that $\mathbf{y}(t)$ is related to $\mathbf{x}(t)$ by eqn. (1). Since $\mathbf{x}(t)$ depends on $\mathbf{x}(0)$ for $t \geqslant 0$, the initial condition $\mathbf{x}(0)$ is shown. Shown within the lower set of dashed lines is the model of the system which is simulated on a computer on-line. The vector $\mathbf{x}_m(t)$ is the model's approximation to $\mathbf{x}(t)$, $\mathbf{x}_m(0)$ is the model's estimate of $\mathbf{x}(0)$, $\mathbf{d}_m = (d_{1m}, \ldots, d_{pm})^T$ is the model's approximation to the delay vector $\mathbf{d}$, and $\mathbf{y}_m(t)$ is related to $\mathbf{x}_m(t)$ by

$$\mathbf{y}_m(t) = \begin{bmatrix} x_{1m}(t - d_{1m}) \\ \vdots \\ x_{pm}(t - d_{pm}) \end{bmatrix}.$$

The block labeled STATE ESTIMATOR indicates that a current estimate of the true state $\mathbf{x}(t)$ is to be made based on $\mathbf{x}_m(t)$, $\mathbf{y}_m(t)$, and $\mathbf{y}(t)$. The ad hoc estimator proposed below is an immediate extension of Smith's original suggestion. The study of optimum estimators for this application would be an important area for further research. The proposed state estimate is given by

$$\hat{\mathbf{x}}(t) = \mathbf{x}_m(t) + \begin{bmatrix} \mathbf{y}(t) \\ \mathbf{0} \end{bmatrix} - \begin{bmatrix} \mathbf{y}_m(t) \\ \mathbf{0} \end{bmatrix} \tag{3}$$

where the $\mathbf{0}$ vectors are of dimension $n - p$. The controller then determines $\mathbf{u}(t)$ based on $\mathbf{x}_d$ and $\hat{\mathbf{x}}(t)$. No specific design procedure is proposed; however, it should be noted that an estimate of the full state vector, $\hat{\mathbf{x}}(t)$, is available to the controller, and thus many of the state variable design techniques can be applied.

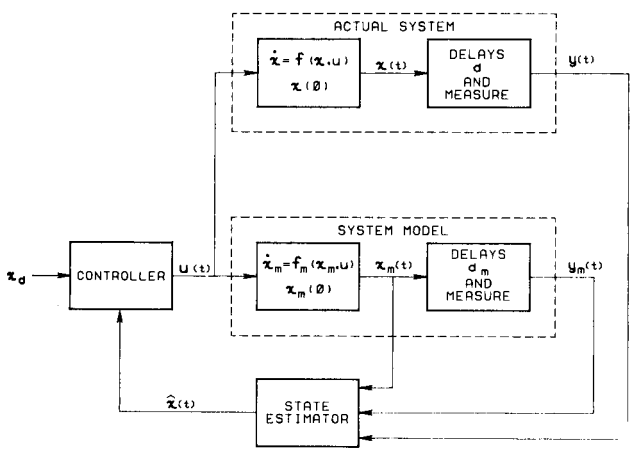

Fig. 3. Implementation of the extended predictor.

As with the classical Smith predictor, if the model's system equations, $\mathbf{f}_m$, are exactly equal to the true system equations, $\mathbf{f}$, if the model's delay vector, $\mathbf{d}_m$, is exactly the same as the true delay vector, $\mathbf{d}$, and if the initial conditions on the system model, $\mathbf{x}_m(0)$, are the same as the initial conditions on the true system, $\mathbf{x}(0)$, then $\mathbf{y}(t)$ and $\mathbf{y}_m(t)$ will be identical for all $t \geqslant 0$. If this is so, then the simplified form shown in Fig. 4 will be equivalent to the complete implementation shown in Fig. 3. The advantage of the simplified model is that the controller can be designed by state variable methods for systems without delay.

The digital implementation of the extended predictor is shown in Fig. 5. Since the modifications required to Fig. 3 are fairly obvious, a detailed discussion will not be presented. The times indicated by t_j denote the sampling times, i.e., $t_j = jT$ for $j = 0, 1 \ldots$ where T is the sampling period.

The design of controllers for non-linear systems is very much dependent on the specific system under consideration. Probably the most widely documented non-linear control system design problem is the one in which saturation of the control variable occurs. One well suited control strategy for this situation is the time optimum control.

TIME OPTIMUM CONTROL

The time optimum control of a second-order system is discussed here. Since time delays have been taken into account by the extended predictor described in the preceding section, the simplified model shown in Fig. 6 will be considered. The time optimum control strategy is well known. Continuous time systems have been discussed by Kirk [16]. For sampled data systems, the method of Desoer and Wing [15] is used here. Time optimum control strategy is described below for continuous time systems and sampled data systems.

The differential equation describing the dynamic system shown in Fig. 6 is

$$x''(t) + 2\zeta\omega_n x'(t) + \omega_n^2 x(t) = K\omega_n^2 u(t) \tag{4}$$

where K, ζ, and ω_n are known, non-negative parameters of the system. Let

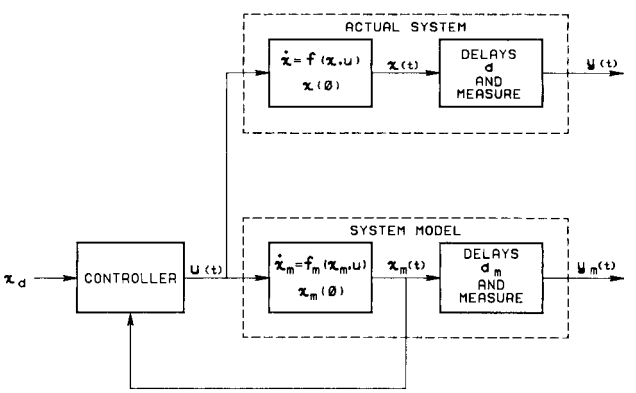

Fig. 4. Simplified form of the extended predictor.

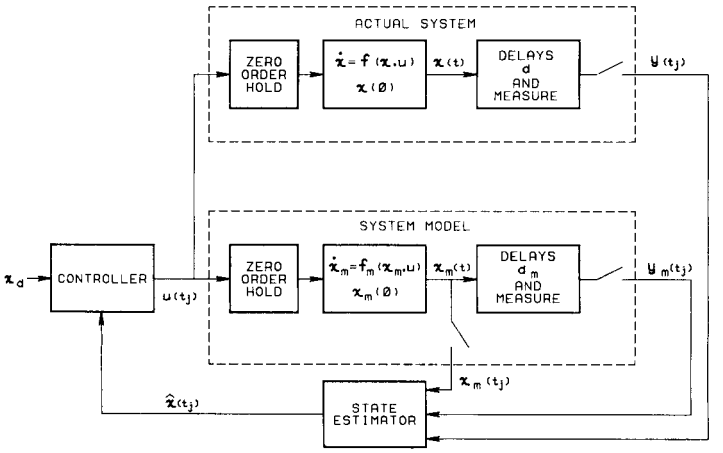

Fig. 5. Digital implementation of the extended predictor.

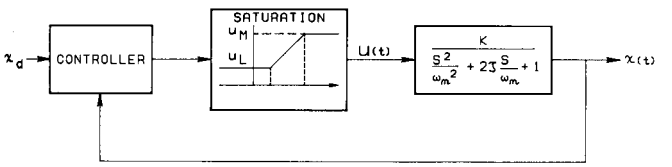

Fig. 6. Block diagram of saturating system.

the state vector $\mathbf{x}(t)$ be given by $\mathbf{x}(t) = [x(t), x'(t)]^T$. It is assumed that the control $u(t)$ is constrained to lie between the limits u_L and u_M where $u_L < u_M$. In Fig. 6. positive values of these two quantities are shown to be in accordance with the constraints on the pumping motors rates in the experimental system (see below).

In all cases, it will be assumed that the system is initially at steady state at some value, say $\mathbf{x}_0 = (x_0, 0)^T$. It is then desired to transfer the system to a new operating point, say $\mathbf{x}_d = (x_d, 0)^T$, in minimum time. Obviously, x_d must be such that $Ku_L \leqslant x_d \leqslant Ku_M$. The optimum control requires that if $x_d > x_0$, the maximum $u(t)$ should be applied initially up until some time, t_s, and then switched to the minimum $u(t)$ until a final time, t_f. After t_f, the control $u(t) = u_d = x_d/K$ is applied to remain at the new set point in steady state. The form of the control is shown in Fig. 7. The unknowns are t_s and t_f. These quantities are found from a phase plane plot, i.e., a plot of x' vs. x. To obtain a phase plane plot, eqn. (4) is written in the state variable form

$$\begin{bmatrix} x'(t) \\ x''(t) \end{bmatrix} = \begin{bmatrix} 0 & 1 \\ -\omega_n^2 & -2\zeta\omega_n \end{bmatrix} \begin{bmatrix} x(t) \\ x'(t) \end{bmatrix} + \begin{bmatrix} 0 \\ K\omega_n^2 \end{bmatrix} u(t). \tag{5}$$

The solution to eqn. (5) is obtained for values of $u = u_L$ and $u = u_M$, and x' is plotted versus x to obtain the phase plane shown in Fig. 8. The arrows indicate the direction of motion as t increases. The control $u = u_M$ is used until the correct position and velocity, x and x', are achieved at which the

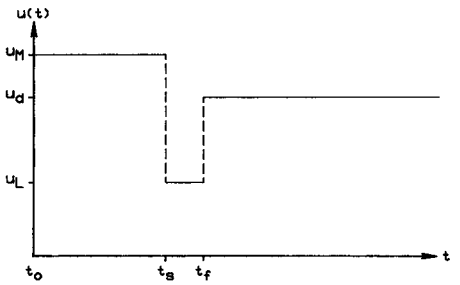

Fig. 7. Form of the optimal control, $x_d > x_0$.

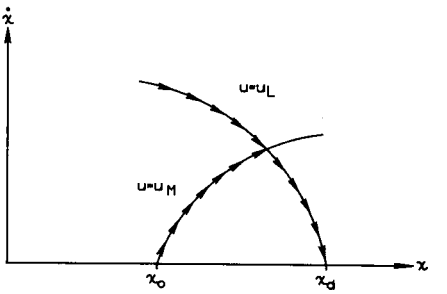

Fig. 8. Phase plane trajectory.

control $u = u_L$ will bring the system to rest at the precise time $x(t_f) = x_d$. Estimates of both $x(t)$ and $x'(t)$ are known in the extended predictor. If $x'(t)$ is not measured, its estimated value will still be available from the system model. The model will generate $x_m(t)$ and $x'_m(t)$ where the initial conditions $x_m(0) = x_0$ and $x'_m(0) = 0$ are used. If $x_d < x_0$, a strategy reversed from that just described is used, as illustrated in Figs. 9 and 10. The optimum control, $u(t)$, is always a function of $x(t)$, $x'(t)$, and x_d, which can be found from the relative location of these quantities in the phase plane. The appropriate regions are shown in Fig. 11. The curve with arrows directed toward the desired steady state operating point, $(x_d, 0)$, is called the switching curve. If $x'(t) > 0$, and the state $x(t)$, $x'(t)$ lies on the switching curve, the control $u(t) = u_L$ will bring the system to the desired steady state in minimum time. If $x'(t) < 0$, and the state $x(t)$, $x'(t)$ lies on the switching curve, the control $u(t) = u_M$ will be optimum.

If the state $[x(t), x'(t)]$ lies to the left of the switching curve, the control $u(t) = u_M$ is applied until $x(t)$ and $x'(t)$ are such that the upper switching curve is reached, and then $u(t) = u_L$ is applied. Similarly, if the state $[x(t), x'(t)]$ lies to the right of the switching curve, the control $u(t) = u_L$ is applied until the lower switching curve is reached, and then $u(t) = u_M$ is applied.

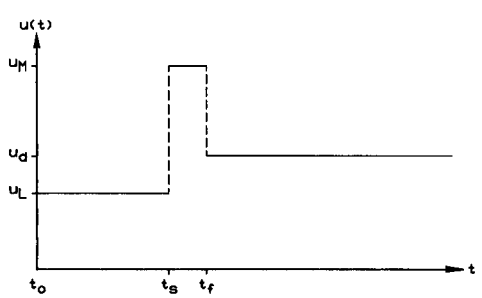

Fig. 9. Form of the optimal control, $x_d < x_0$.

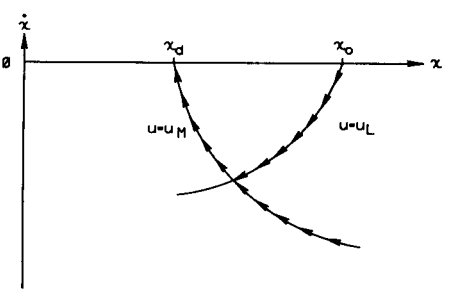

Fig. 10. Phase plane trajectory, $x_d < x_0$.

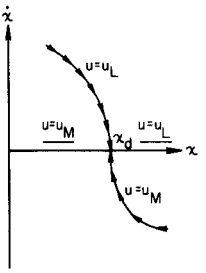

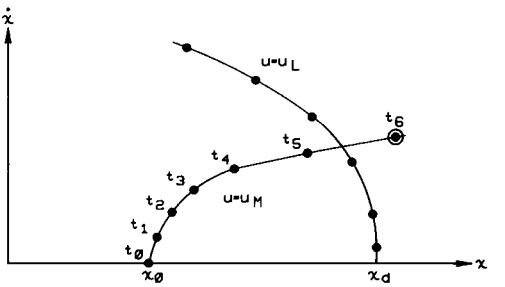

Fig. 11. Switching curve in the phase plane.

Fig. 12. Sampled data phase plane trajectory.

Once the desired state, $(x_d, 0)$, has been achieved, the control $u_d = x_d/K$ is applied to stay at steady state.

The preceding discussion applies to continuous time control systems which can be switched at precisely the correct time from one extreme value to the other. If a digital computer is used to determine the control, measurements of the system are available only at the sampling times, and the control is usually held constant between sampling times. In this case, the implementation of the minimum time control law becomes slightly more complicated. To illustrate, a possible phase plane plot for the dynamic system described by the differential equation in eqn. (4) is shown in Fig. 12. In this case $x(t)$ and $x'(t)$ are known only at the sampling times, $t_j = jT$, $j = 0, 1 \ldots$. The positions in the phase plane of the trajectory $x(t_j)$, $x'(t_j)$ are shown by the filled circles in Fig. 12. If the system starts from steady state at $(x_0, 0)$, and if $u(t) = u_M$ is applied, the system will have the values of $x(t_j)$, $x'(t_j)$ shown at times $t_1, \ldots, t_5$ shown in this example. Also shown by the points along the line marked $u = u_L$ are positions in the phase plane from which it is possible to reach $(x_d, 0)$ using $u(t) = u_L$. The point at time t_6 is circled to show that the switching curve would be crossed if $u(t) = u_M$ were applied over the interval $t_5 < t < t_6$. Since it is extremely unlikely that a position on the curve $u = u_M$ will coincide with a point on the curve $u = u_L$ at a sampling time, the optimum control for a sampled data system will be different from that of a continuous time control system. In this case, the optimum control is not unique [15]. It turns out that, in general, there must be two sampling intervals over which the control is not at one of its saturated values. The non-uniqueness results from the fact that there are various possibilities for choosing the time intervals for the non-saturated controls. A modification of the method developed by Desoer and Wing [15] was implemented for this study. The modification is described in Appendix 2.

The general form of the minimum time control for a sampled data system is shown in Fig. 13. For this illustration, the control over the interval $t_5 < t < t_6$ is less than u_M so that the state $[x(t_6), x'(t_6)]$ lies on the critical curve [15]. The control $u(t) = u_L$ is applied until the system is within one sampling time of reaching $(x_d, 0)$. In the example shown in Fig. 13, this occurs at

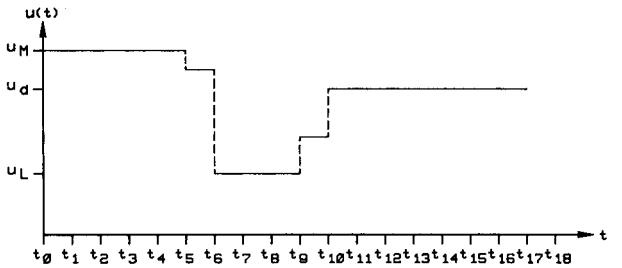

Fig. 13. Form of the optimal control for a sampled data system.

time t_9. The control over the interval $t_9 < t < t_{10}$ is such that $[x(t_{10}), x'(t_{10})] = (x_d, 0)$. After time t_{10}, the control $u_d = x_d/K$ is applied to maintain the new steady-state condition.

EXPERIMENTAL RESULTS

The extended predictor was implemented in the control of the experimental enzyme reactor outlined in Fig. 14. Input reagents are pumped into the system via stepping motors whose pumping rates are controlled by the digital computer. In this experiment, enzyme (alkaline phosphatase), substrate (*p*-nitrophenylphosphate), buffer (2-amino-2-methyl-1-propanol), and diluent (water) were pumped into the mixer. The substrate was pumped at a constant rate, the enzyme served as the controlled or manipulated variable, the buffer was pumped at a rate to maintain constant pH, and the diluent was pumped at a rate to maintain a constant flow rate through the system. A series of four delay loops and valves permits sixteen possible pathlengths which determine the time allowed for the reaction to occur. The product

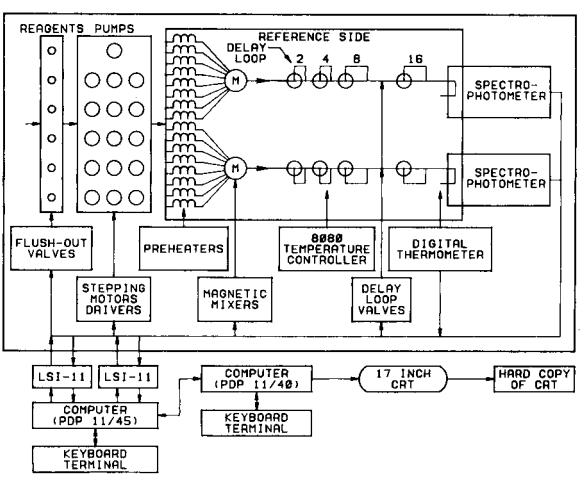

Fig. 14. Functional block diagram of the computerized apparatus showing the flow system and major components.

formed in this enzyme catalyzed reaction is *p*-nitrophenolate. The light absorption of the solution is measured by a spectrophotometer located at the end of the delay lines. The output of the spectrophotometer is sampled every period, converted to digital form, and input to the digital computer. The concentration of the product is determined from the measured absorption, and fed back to the controller which determines the rate at which to pump enzyme, thus completing the feedback loop. A block diagram which illustrates each of the functions just described is shown in Fig. 15.

The sampled data time optimum control algorithm described in Appendix 2 was implemented. A second-order model with dead time was found for the experimental system by an open loop non-linear parameter identification method which is described in Appendix 1. Although a very good fit to the data could be achieved with the second-order model, the actual experimental system is much more complex. In order to ensure that the desired set point would be maintained in spite of variations in the model, a PID controller was used after the time optimum control sequence was executed. This procedure was also recommended by Latour et al. [10]. The parameters of the PID controller were tuned as described in Herget et al. [3]. The parameters listed in Table 1 were used for this experiment.

The parameters of the system identified by the non-linear parameter identifier described in Appendix 1 are shown in Table 2. The parameters K, ω_n, and ζ are defined in Fig. 6 for the second-order system without delay, and delay is denoted by d.

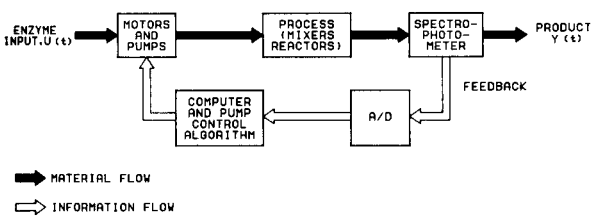

Fig. 15. Block diagram of the enzyme control system.

TABLE 1

Parameters of experimental system

pH	10.0	Delay path volume	10 ml
Substrate concentration	3 mmol l^{-1}	Temperature	30°C
Total flow rate	7 ml min^{-1}	Sampling period	1 s

TABLE 2

Identified system model parameters

K	1.399 μmol U^{-1}	ζ	0.8668
ω_n	0.05853 s^{-1}	d	58.61 s

The system was allowed to reach steady state at a product concentration of 10 μmol l^{-1} under PID control. A step change in product to 20 μmol l^{-1} was commanded. After a step change is requested, the controller is switched to the time optimum control strategy. It can be seen from Fig. 13 that the optimum control takes on four distinct values before assuming the final value $u_d = x_d/K$. The control logic used here was that after the time optimum control algorithm had executed four distinct values, the control would be switched back to PID. The initial conditions set on the PID controller were set as if the system had been in steady state at the new set point. The resulting step response is shown in Fig. 16. For comparison, the step response of the system under PID control only is shown also. The PID controller was tuned assuming there was no saturation. It can be seen that the time optimum controller, which makes optimum use of the saturation limits, provides a considerable improvement in achieving the new set point.

The digital implementation of the extended predictor shown in Fig. 5 was thoroughly tested on the experimental system with a number of control algorithms. Besides time optimum and PID, deadbeat and near time optimum control algorithms, e.g., Kuo [17], were tested. In all cases, the extended predictor was demonstrated to be a powerful technique for controlling non-linear systems with large time delays. The dead time in the experimental system was purposely chosen to be much larger than the time constants of the dynamic system. It should be noted that the system is non-linear even with PID control, and it was found to be essential to include the saturation in the system model with PID control in order to achieve satisfactory performance.

The time optimum control algorithm was used to illustrate a nontrivial application; however, satisfactory results could never be achieved with the time optimum algorithm alone, i.e., the PID controller following the time optimum sequence was essential to eliminate unavoidable modeling errors.

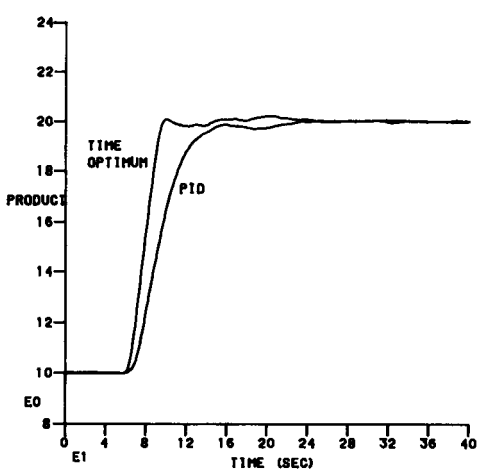

Fig. 16. Time optimum and PID control.

The time optimum control was found to be extremely sensitive to modeling errors. However, in situations where the time improvement justifies the added complexity, the time optimum control followed by PID was shown to be effective.

This work was performed under the auspices of the U.S. Department of Energy under contract number W-7405-ENG-48, and partially funded by OBES.

APPENDIX 1

The parameter identification algorithm used in this study is described here. The dynamic model relating enzyme to product was assumed to have the form shown in Fig. A1.

The system is operated open loop to gather the parameter identification data. The enzyme concentration is the input, $u(t_j)$, where t_j denotes the sampling time. The output concentration, $y(t_j)$, is also sampled. The parameters c_1, c_2, c_3, and c_4 are related to K, ζ, ω_n, and d as follows:

$$c_1 = \omega_n^2;\ c_2 = 2\zeta\omega_n;\ c_3 = K\omega_n^2;\ c_4 = d.$$

The enzyme concentration is held constant until steady state is reached. Call y_0 the corresponding product at steady state. Beginning at time $t = 0$, an arbitrary sequence $u(0), u(t_1), \ldots, u(t_N)$ is applied where $t_j = jT, j = 0, 1, \ldots, N$ and T is the sampling time. Let $\mathbf{x}(t) = [x(t), x'(t)]^T$. Then $\mathbf{x}(0) = (y_0, 0)^T$ since the system is at steady state. The resulting output sequence $y(0), \ldots, y(t_N)$ is measured. The system shown in Fig. A1 is simulated for a given set of $c_1, \ldots, c_4$. Let $\mathbf{c} = (c_1, \ldots, c_4)^T$. For the given input sequence $u(0), \ldots, u(t_N)$, the resulting output sequence will be dependent on c, say $y_c(0), \ldots, y_c(t_N)$. A cost function $J(\mathbf{c})$ is defined by

$$J(\mathbf{c}) = \sum_{j=0}^{N} [y(t_j) - y_c(t_j)]^2$$

i.e., the sum of the squares of the residuals between the measured $y(t_j)$ and the model output $y_c(t_j)$. A non-linear parameter identification algorithm, the Levenberg–Marquardt algorithm from the International Mathematics and Statistics Library (IMSL), was used to minimize $J(\mathbf{c})$. The fit of the model to the actual measured data is shown in Fig. A2. The identification model parameters are listed in Table 2.

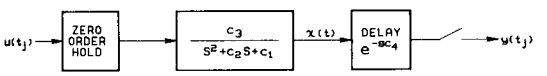

Fig. A1. Dynamic model of enzyme reactor.

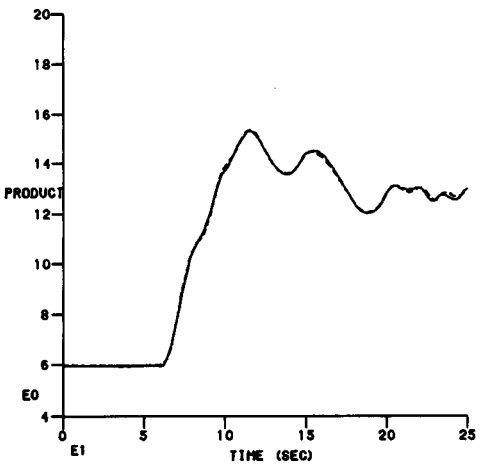

Fig. A2. Control parameter fit. (—) Model fit; (---) actual data.

APPENDIX 2

The modification required of Desoer and Wing's algorithm [15] to account for a desired final state not at the origin of the state space is presented here.

It is assumed that the dynamic behavior of the system is described by the second order, ordinary differential equation in eqn. (4). Let $\mathbf{x}_0 = (x_0, 0)^T$ and $\mathbf{x}_d = (x_d, 0)^T$. The time optimum problem considered here is to go from $\mathbf{x}_0$ to $\mathbf{x}_d$ in minimum time. By a change of variables, it is possible to select a new set of state variables so that the final state is at the origin, as considered by Desoer and Wing [15].

To achieve the new set of variables, let $\xi(t) = x(t) - x_d$. Then $\xi'(t) = x'(t)$, and so the point $(x_d, 0)$ corresponds to the point $(0, 0)$ in (ξ, ξ') state variables. Let $u_d = x_d/K$ and $\psi(t) = u(t) - u_d$. The differential equation for $\xi(t)$ is

$$\xi''(t) + 2\zeta\omega_n \xi'(t) + \omega_n^2 [\xi(t) + x_d] = K\omega_n^2 [\psi(t) + u_d]$$

or

$$\xi''(t) + 2\zeta\omega_n \xi'(t) + \omega_n^2 \xi(t) = K\omega_n^2 \psi(t) \tag{A1}$$

The problem is now to find the control $\psi(t)$ which will take the state $[\xi(t), \xi'(t)]$ from $(x_0 - x_d, 0)$ to $(0, 0)$ in minimum time. The control $u(t)$ is related to $\psi(t)$ by $u(t) = \psi(t) + u_d$.

REFERENCES

1 J. W. Frazer, L. P. Rigdon, H. R. Brand, C. L. Pomernacki and T. A. Brubaker, Anal. Chem., 51 (1979) 1747.
2 C. L. Pomernacki, H. L. Brand, T. A. Brubaker and J. W. Frazer, Anal. Chim. Acta, 112 (1979) 287.

3 C. J. Herget, C. L. Pomernacki and J. W. Frazer, Anal. Chim. Acta, 122 (1980) 403.
4 O. J. M. Smith, Instrum. Soc. J., 6 (1959) 28.
5 J. E. Marshall, Int. J. Control, 19 (1974) 933.
6 J. O. Gray and P. W. B. Hunt, Electron Lett., 7 (1971) 131.
7 G. Alevisakis and D. E. Seborg, Chem. Eng. Sci., 29 (1974) 373.
8 B. Garland and J. E. Marshall, in M. J. Gregson (Ed.), Recent Theoretical Developments in Control, Academic Press, New York, 1978.
9 L. B. Koppel and P. R. Latour, Ind. Eng. Chem. Fundam., 4 (1965) 463.
10 P. R. Latour, L. B. Koppel and D. R. Coughanowr, Ind. Eng. Chem. Process Des. Dev., 7 (1968) 345.
11 P. R. Latour, L. B. Koppel and D. R. Coughanowr, Ind. Eng. Chem. Process Des. Dev., 6 (1967) 452.
12 D. A. Mellichamp, Ind. Eng. Chem. Process Des. Dev., 9 (1970) 494.
13 T. J. McAvoy, Ind. Eng. Chem. Process Des. Dev., 11 (1972) 71.
14 A. H. Bohl and T. J. McAvoy, Ind. Eng. Chem. Process Des. Dev., 15 (1976) 24.
15 C. A. Desoer and J. Wing, IRE Trans. Autom. Control, AC-6 (1961) 5.
16 D. E. Kirk, Optimal Control Theory, Prentice-Hall, Englewood Cliffs, N.J., 1970.
17 B. C. Kuo, Digital Control Systems, SRL Publishing Co., Champaign, IL, 1977.

Analytica Chimica Acta, 133 (1981) 125—136
Computer Techniques and Optimization
Elsevier Scientific Publishing Company, Amsterdam — Printed in The Netherlands

TARGET FACTOR ANALYSIS OF INFRARED SPECTRA OF MULTICOMPONENT MIXTURES†

MATTHEW McCUE and EDMUND R. MALINOWSKI*

Department of Chemistry and Chemical Engineering, Stevens Institute of Technology, Hoboken, New Jersey 07030 (U.S.A.)

(Received 1st September 1980)

SUMMARY

The target factor analysis (t.f.a.) error criteria discussed earlier are applied to Fourier-transform infrared spectra in order to determine, without any prior knowledge of the experimental error, the number and identities of components in a series of related multicomponent mixtures. The t.f.a. method is also used for quantitative analysis and is compared to regression analysis, which force-fits the data and does not compensate for an impurity of small but measurable quantity. In addition, it is shown how an impurity in a single mixture can be detected, identified, and quantified. An actual experimental example is presented, using solutions of *o*-xylene, *m*-xylene, *p*-xylene, and ethylbenzene in cyclohexane, with chloroform as an impurity.

Malinowski and McCue [1] have applied target factor analysis (t.f.a.) to the mass spectral data of a series of related mixtures containing the same components in varying proportions. They showed how, in addition to determining the number of species, t.f.a. can be used to test individually for the presence of suspected components and to determine the composition of each mixture quantitatively. In the present paper, t.f.a. will be applied to F.t.i.r. absorbance data of multicomponent mixtures in order to determine the number, identities, and concentrations of the absorbing components without any prior knowledge of the experimental error. This is achieved by means of newly developed t.f.a. error criteria [2, 3]. The method should also find use with high-quality dispersive infrared spectrophotometers that provide digital output.

Spectral stripping and the ratio method, the current procedures used to effect qualitative analyses in F.t.i.r. spectroscopy, are limited in application. Spectral stripping, also known as difference or subtractive spectroscopy, can sometimes be used to identify an unknown constituent in a mixture, provided that the identities of the other constituents are known. In this method, one successively subtracts the stored absorbance spectra (suitably scaled) of the other components until only the unknown component spectrum remains. This final spectrum is then used for identification purposes. In con-

†Paper presented at Metrochem 80, ACS New York Section, South Fallsburg, October 1980.

0378—4304/81/0000—0000/$02.50

trast, t.f.a. allows one to test individually for suspected components; the identities of the other absorbing species need not be known. The ratio method [4] has been used to determine the absorbance spectra of the individual components in related mixtures without prior knowledge of the constituents. The method requires n mixtures, where n is the number of components involved. Partly because each component must have a spectral region where it alone absorbs, the method has been restricted to two- and three-component mixtures. By contrast, t.f.a. does not require such regions of non-overlapping behavior. A large number of components can therefore be determined.

The simple method of solving simultaneous equations [5] and least-squares multiple regression analysis [6] can be used to analyze mixtures quantitatively from their absorbance spectra. However, these techniques cannot be used to identify components in a series of related mixtures. If there are unidentified components, in addition to those known to be present, determinations based solely on the absorptivities of the known constituents will lead to erroneous results. With t.f.a., however, it is often possible to identify all the components. The complete set of absorptivities can then be used to quantify the components accurately.

DESCRIPTION OF THE METHOD

In order to be factor-analyzable, each point in a data matrix must be a linear sum of product terms. The absorbances at different wavenumbers of related multicomponent solutions, whose individual components obey Beer's law, satisfy this condition. Each absorbance value is a linear sum of contributions from the individual components:

$$A(i, \alpha) = \sum_{j=1}^{n} a(i, j)\, F(j, \alpha) \qquad (1)$$

where $F(j, \alpha) = b(\alpha)\, c(j, \alpha)$; $A(i, \alpha)$ is the absorbance of solution α at wavenumber i; $a(i, j)$ is the absorptivity of component j at wavenumber i; $b(\alpha)$ is the pathlength of the cell used for solution α; $c(j, \alpha)$ is the concentration of component j in solution α, and n is the number of absorbing species.

A detailed, mathematical formulation of t.f.a. is readily available [7]. An overview of t.f.a. as it applies to F.t.i.r. absorbance data follows. Consider a data matrix of absorbance values, constructed so that the rows correspond to the different wavenumbers and the columns to the different solutions of a series. Generally, the wavenumbers are equally spaced, although this is not necessary. In order to determine the number of absorbing species and to test for the presence of suspected components by means of the error criteria [2, 3, 7], the data matrix should contain at least $2n$ rows and $2n$ columns. In practice, more than $2n$ wavenumbers are generally used because digitizing the wavenumber scale more frequently requires little extra effort. Obtaining

$2n$ mixtures containing the same components but in different concentrations, poses a much more difficult and time-consuming problem.

Abstract factor analysis (a.f.a.), the first step in t.f.a., decomposes the data matrix into abstract factors. The number of factors needed to account for the data to within experimental error is equal to the number of absorbing components. Once the number of factors has been determined, t.f.a. can be used to test for the presence of individual suspected components. The absorbance values of each suspected component, measured at the same wavenumbers and experimental conditions that were used to construct the data matrix, are input as a test vector. If desired, the absorbance test vector may be converted to an absorptivity test vector by dividing each absorbance value by the concentration—pathlength product. In fact, the absorbance values can be divided by any constant without affecting the error criteria involved in evaluating the worthiness of the test vector as a true factor.

If all n components are identified from the target-testing procedure, a quantitative analysis of each solution can be made by means of combination target factor analysis [7] or regression analysis [6]. Both computational procedures make use of more than n wavenumbers. The familiar method of using n wavenumbers to solve n simultaneous equations for each solution can also be used [5]. The n wavenumbers are chosen to be the best possible so that each component has a fairly strong and distinctive absorbance at, at least, one wavenumber.

In the t.f.a. procedure, the test vectors of all the components present are entered in combination. Here it is important that each test vector be composed of absorptivities. A column cofactor matrix [F] is calculated from $[F] = [T]^{-1}[C^{\ddagger}]$, where $[C^{\ddagger}]$ is the abstract column factor matrix obtained from a.f.a. using n factors and [T] is the transformation matrix determined by the target transformation least-squares procedure, using the combination set of test vectors. From the column cofactors $F(j, \alpha)$, which comprise [F], and the known pathlengths $b(\alpha)$, the composition of each solution is readily calculated (see above). The ratios of the cofactors $F(j, \alpha)$ for a given solution α are the same as the corresponding concentration ratios. That is,

$$F(1, \alpha) : F(2, \alpha) : \ldots : F(j, \alpha) : \ldots : F(n, \alpha) =$$

$$c(1, \alpha) : c(2, \alpha) : \ldots : c(j, \alpha) : \ldots : c(n, \alpha) \qquad (2)$$

Consequently, if one is interested only in the mole fractions (or weight fractions) of the absorbing components, the pathlength need not be known. This is the case for a series of unknown mixtures that have been diluted in a solvent in order to minimize deviations from Beer's law and to allow the use of cells of longer pathlength.

At a later time, a single solution containing the same components as the series can be analyzed quantitatively in the following way. A column vector is formed from the absorbance values of this solution and added to the computer-stored data matrix. Combination t.f.a. is then carried out as before.

The time needed to obtain the original computer-stored data matrix is well worth the effort if unknowns containing the same components are routinely encountered. A valuable feature of this approach is that the presence of an impurity in the single solution will appear as an extra factor. The use of one wavenumber for each known constituent to solve a set of simultaneous equations [5] would result in erroneous concentrations, with no indication that an additional component was present. The presence of an impurity may not be apparent from a visual examination of the spectrum. The use of chromatography to monitor samples for impurities may be time-consuming. If desired, test vectors can be fed into the t.f.a. program in order to identify the impurity. Once identified, combination t.f.a. can be used to quantify the impurity as well as the other components. If more than one impurity is present in the single solution, only one extra factor will appear. In this case, the impurities cannot be identified or quantified.

The factor analysis approach is statistically superior to solving n simultaneous equations because a larger number of wavenumbers is used. Furthermore, time need not be spent in selecting the n best wavenumbers. However, in the t.f.a. technique, absorbance values must be digitized at sufficiently frequent intervals to permit adequate representation for each component. This is especially important when sharp peaks are involved. Factor analysis of spectra with sharp peaks at arbitrary, equally spaced wavenumbers also requires increased spectrophotometric resolution, when compared with obtaining data at the n best wavenumbers. Usually, the n best wavenumbers are situated at peak maxima, where instrumental deviations from Beer's law are small. With arbitrary digitization, most of the wavenumbers characterized by fairly large absorbance values are on the sides of peaks, where instrumental deviations from Beer's law are large. High resolution is therefore essential. Also, lack of precision in wavenumber measurement will lead to larger absorbance errors on the sides of peaks than at peak maxima.

APPLICATIONS

To illustrate the method, a series of nineteen solutions was prepared with cyclohexane as the solvent; cyclohexane is almost completely transparent over the wavenumber range used. Solutions 1—10 contained various mixtures of *o*-xylene, *m*-xylene, *p*-xylene, and ethylbenzene as solutes. Because of overlap of the component spectra, the concentrations of these compounds cannot be determined independently by selecting wavenumbers unique to each component. In addition to the four components, solutions 11 and 12 contained small amounts of chloroform to simulate an impurity. The remaining seven solutions (13—19) were the single-solute solutions needed to construct the test vectors. The molarities of the nineteen solutions estimated from the solution preparation data, are given in Tables 1—3. All these values had an estimated r.m.s. error of ±2.4%, except the chloroform value of solution 12 (see Table 2), which had an estimated r.m.s. error of ±3.6%.

TABLE 1

Comparison of the estimated molarities of *o*-xylene, *m*-xylene, *p*-xylene, and ethylbenzene in ten cyclohexane solutions with the molarities obtained by t.f.a. of data matrix A, by solving simultaneous equations, and by regression analysis

Solution (α)	*o*-Xylene molarities				*m*-Xylene molarities			
	Estimated[a]	T.f.a.[b]	Simultaneous equations[c]	Regression analysis[d]	Estimated[a]	T.f.a.[b]	Simultaneous equations[c]	Regression analysis[d]
1	0.0352	0.0364	0.0356	0.0364	0.0346	0.0356	0.0348	0.0356
2	0.0482	0.0499	0.0483	0.0498	0.0828	0.0842	0.0834	0.0842
3	0.0120	0.0125	0.0120	0.0125	0.0236	0.0240	0.0234	0.0240
4	0.0584	0.0595	0.0584	0.0594	0.0117	0.0124	0.0119	0.0124
5	0.0238	0.0249	0.0237	0.0249	0.0456	0.0465	0.0458	0.0465
6	0.0713	0.0719	0.0700	0.0718	0.0586	0.0595	0.0586	0.0595
7	0.0843	0.0838	0.0803	0.0837	0.0304	0.0313	0.0301	0.0313
8	0.0120	0.0130	0.0124	0.0130	0	0.0000	0.0003	0.0000
9	0.0058	0.0066	0.0061	0.0066	0.0057	0.0055	0.0059	0.0055
10	0	0.0002	0.0000	0.0003	0.0691	0.0694	0.0691	0.0694
Av. diff.[e]		0.00086	0.00067	0.00085		0.00068	0.00024	0.00067
R.m.s. diff.[f]		0.00095	0.00134	0.00094		0.00081	0.00030	0.00080
	p-Xylene molarities				Ethylbenzene molarities			
1	0.0344	0.0352	0.0351	0.0352	0.0347	0.0349	0.0348	0.0349
2	0.0118	0.0123	0.0123	0.0123	0	0.0016	0.0005	0.0017
3	0.0236	0.0236	0.0236	0.0236	0.0830	0.0824	0.0817	0.0823
4	0.0454	0.0466	0.0465	0.0466	0.0235	0.0255	0.0236	0.0256
5	0.0571	0.0578	0.0578	0.0578	0.0117	0.0127	0.0121	0.0128
6	0.0057	0.0062	0.0061	0.0062	0.0057	0.0083	0.0065	0.0084
7	0.0118	0.0125	0.0124	0.0125	0.0186	0.0211	0.0188	0.0212
8	0.0824	0.0832	0.0832	0.0832	0.0474	0.0470	0.0473	0.0470
9	0.0698	0.0710	0.0710	0.0710	0.0574	0.0571	0.0575	0.0570
10	0	−0.0001	−0.0001	−0.0001	0.0693	0.0663	0.0679	0.0662
Av. diff.[e]		0.00066	0.00060	0.00065		0.00143	0.00052	0.00150
R.m.s. diff.[f]		0.00075	0.00071	0.00075		0.00174	0.00070	0.00180

[a] Based on the solution preparation data. [b] Based on t.f.a. of 35 absorbance values, at 4 cm^{-1} intervals between 682 and 818 cm^{-1}, for each solution. [c] Obtained by using the four best wavenumbers to solve four simultaneous equations for each solution. [d] Based on the regression analysis of 35 absorbance values, at 4 cm^{-1} intervals between 682 and 818 cm^{-1}, for each solution. [e] Average of the absolute values of the differences from the estimated molarities. [f] R.m.s. difference from the estimated molarities.

For each of the nineteen solutions, thirty-five absorbance values were obtained at 4 cm^{-1} intervals from 682—818 cm^{-1}. The error, estimated from replicate determinations, for these absorbances was between 0.001 and 0.002 absorbance units. The data were used in the factor analyses and regression analyses described below. In addition, the absorbances at 741.02, 767.40, 794.28, and 696.77 cm^{-1} (the four best wavenumbers) were obtained for the ten solutions in Ta e 1 and the first four solutions in Table 3. These wavenumbers correspond to the maximum absorbance values for *o*-xylene, *m*-xylene, *p*-xylene, and ethylbenzene, respectively, over the 682—818 cm^{-1} region. A comparison between the molarities (determined by using the absorbances at these four wavenumbers to solve simultaneous equations) and those determined by t.f.a. and regression analysis could therefore be made.

Chemicals, equipment and data handling

Cyclohexane (Burdick and Jackson), the three isomeric xylenes (Matheson, Coleman, and Bell; 99+ mol%, chromatoquality) ethylbenzene (Aldrich; 99%), chloroform (Matheson, Coleman and Bell; spectroquality), toluene (Fisher certified ACS), and 1,2,4-trimethylbenzene (Baker grade) were used without further purification.

The solutions were prepared using volumetric flasks and graduated pipets. The estimated molarities were calculated from the nominal volumes delivered. A two-step dilution procedure was used for each solution.

Spectra were obtained with a Nicolet (Nicolet Instrument Corp., Madison, Wisc.) Model 7199 F.t.i.r. spectrophotometer, a computer-controlled interferometer equipped with a Globar source, a Ge/KBr beam splitter, and a deuterated triglycine sulfate detector. A Model SL-3, fixed-length amalgam-

TABLE 2

Comparison of the estimated solute molarities of two cyclohexane solutions containing small amounts of chloroform, with the molarities obtained by t.f.a. and by regression analysis

Solute	Solution 11 molarities			Solution 12 molarities		
	Estimated[a]	T.f.a.[b]	Regression analysis[c]	Estimated[a]	T.f.a.[d]	Regression analysis[c]
o-Xylene	0.0093	0.0102	0.0113	0.0093	0.0098	0.0101
m-Xylene	0.0864	0.0881	0.1057	0.0864	0.0867	0.0926
p-Xylene	0.0136	0.0143	0.0143	0.0136	0.0136	0.0136
Ethylbenzene	0.0274	0.0285	0.0294	0.0274	0.0260	0.0263
Chloroform	0.00834	0.00852	—	0.00278	0.00283	—

[a]Based on the solution preparation data. [b]Obtained by t.f.a. of data matrix B, constructed from the absorbances of solutions 1—10 (see Table 1) and solution 11. [c]Obtained by regression analysis, using only the absorptivities of *o*-xylene, *m*-xylene, *p*-xylene, and ethylbenzene. [d]Obtained by t.f.a. of data matrix C, constructed from the absorbances of solutions 1—10 and solution 12.

TABLE 3

Molarities of single-solute cyclohexane solutions estimated from the solution preparation data and used to obtain the test vector absorptivities

Solute	Molarities	Solute	Molarities
o-Xylene	0.0478	Chloroform	0.0161
m-Xylene	0.0814	Toluene	0.0542
p-Xylene	0.0812	1,2,4-Trimethylbenzene	0.1083
Ethylbenzene	0.0817		

sealed cell (International Crystal Laboratories, Elizabeth, N.J.) with sodium chloride windows was used throughout. Its pathlength, as determined by the method of interference fringes [8], was 0.02106 cm.

For each solution, an interferogram with the cell containing solution and a separate background interferogram with the cell containing pure cyclohexane were obtained. Each interferogram was the result of 50 signal-averaged scans using 16,384 data points (nominal resolution 1 cm^{-1}). The average measurement time for each interferogram was about 175 s. The interferograms were transformed into single-beam spectra with Happ—Genzel apodization, using 65,536 transform points (2 times zero-filling). The Happ—Genzel function multiplies each data point i by $0.54 + 0.46 \cos [\pi |n_i - Z| / 2(NDP - Z)]$, where n_i is the displacement of point i from the start of scan, Z is the location of the zero path difference, and NDP is the total number of data points. The actual resolution (FWHM criterion [9]), degraded somewhat by the apodization, was 1.42 cm^{-1}. In each case, the solution single-beam spectrum was ratioed against that of the background and then converted to an absorbance spectrum. The absorbance contributions of the cell and cyclohexane were eliminated by the ratioing.

The data-handling capabilities of the Model 7199 minicomputer allowed an automatic printout of the absorbances to be obtained. The factor analyses were carried out by a FORTRAN IV program [10]. An APLSF program was developed to carry out the regression analyses. All computations were made with a Digital Equipment Corporation DEC system-1090 computer.

Results

A 35 row × 10 column data matrix A was first formed from the absorbances of solutions 1—10 (see Table 1). Abstract factor analysis was done by using the principal component analysis mathematical procedure [7]. The theory of errors [2, 7] was used to determine the number of absorbing components (factors). This involved evaluating the real error (RE), the imbedded error (IE), and the indicator function (IND), using $n = 1$ to $n = 9$ factors to reproduce the data (see Table 4). To calculate these quantities, only the number of rows and columns in the data matrix, the eigenvalues, and n were needed. For data matrix A, the real error at $n = 4$, 0.0011, fell within the estimated error range (0.0010—0.0020), giving evidence for four

TABLE 4

Results of abstract factor analysis of three data matrices constructed from solution absorbances

	Data matrix A: solutions 1—10[a]				Data matrix B: solutions 1—10 and 11[a]			
n	Eigenvalue	*RE*[b]	*IE*[c]	*IND* × 10⁴[d]	Eigenvalue	*RE*[b]	*IE*[c]	*IND* × 10⁴[d]
1	3.511398	0.06352	0.02009	7.84	3.903064	0.06694	0.02018	6.69
2	0.783311	0.04173	0.01866	6.52	0.849379	0.04777	0.02037	5.90
3	0.366018	0.02227	0.01220	4.55	0.557809	0.02399	0.01253	3.75
4	0.121286	0.00110	0.00070	0.31	0.139592	0.00937	0.00565	1.91
5	0.000093	0.00096	0.00068	0.39	0.021247	0.00109	0.00073	0.30
6	0.000061	0.00085	0.00066	0.53	0.000089	0.00096	0.00071	0.38
7	0.000038	0.00078	0.00065	0.86	0.000061	0.00084	0.00067	0.53
8	0.000030	0.00069	0.00062	1.74	0.000038	0.00077	0.00065	0.85
9	0.000018	0.00067	0.00063	6.66	0.000029	0.00068	0.00061	1.69
10	0.000016	—	—	—	0.000017	0.00066	0.00063	6.60
11					0.000015	—	—	—

	Data Matrix C: solutions 1—10 and 12[a]			
1	3.809839	0.06493	0.01958	6.49
2	0.822667	0.04553	0.01942	5.62
3	0.514778	0.02223	0.01161	3.47
4	0.135377	0.00348	0.00210	0.71
5	0.002711	0.00109	0.00073	0.30
6	0.000088	0.00096	0.00071	0.38
7	0.000061	0.00084	0.00067	0.53
8	0.000037	0.00077	0.00065	0.85
9	0.000030	0.00068	0.00061	1.69
10	0.000017	0.00066	0.00063	6.58
11	0.000015	—	—	—

[a]See Table 1 for the compositions of solutions 1—10 and Table 2 for the compositions of solutions 11 and 12. [b]Root-mean-square difference between experimental data and hypothetical errorless data. [c]Root-mean-square difference between data reproduced by a.f.a. and hypothetical errorless data. [d]Used to determine the number of factors without prior knowledge of the experimental error.

absorbing components. This conclusion was substantiated by the indicator function reaching a minimum at $n = 4$ and by the fact that the imbedded error did not decrease appreciably beyond $n = 4$.

Test vectors were constructed from the absorptivities of seven solutes (Table 3) to determine their presence in the ten solutions. The test vectors were entered into the t.f.a. program using four factors. The theory of errors for t.f.a. [3, 7] was used to determine whether each test vector was a successful target. The target error criteria involved calculating values for AET (the apparent error in the target test vector, i.e., the r.m.s. difference between the predicted vector and the target test vector), REP (the real error in the

predicted vector), and RET (the real error in the target test vector). These errors, which are readily calculated from information generated during the target analysis, are related by the expression: $(AET)^2 = (REP)^2 + (RET)^2$. *RELI* and *SPOIL* function values were calculated from the *AET*, *REP*, and *RET* values as follows:

$$RELI = \{1 - [((RET)^2 - (RET)^2_{est})/(AET)^2]\}^{1/2} \quad (3)$$

$$SPOIL = RET/REP \quad (4)$$

Both the *RELI* and *SPOIL* values were used to judge the validity of each target test vector as a true factor. The *RELI* function is preferred when an estimate of the real error in the target test vector, $(RET)_{est}$, is available from a knowledge of the experimental error in the data used to construct the test vector.

The *AET*, *REP*, *RET*, $(RET)_{est}$, *RELI*, and *SPOIL* values calculated for the seven components tested are listed in Table 5. Since the test vector data were obtained under the same experimental conditions as the absorbance values comprising the data matrix, the $(RET)_{est}$ value associated with each test vector was obtained by dividing the real error by the product of the pathlength and concentration given in Table 3. A *RELI* value greater than 0.5 indicates that the component tested for is present. The results in Table 5 indicate that *o*-xylene, *m*-xylene, *p*-xylene, and ethylbenzene were present and that chloroform, toluene, and 1,2,4-trimethylbenzene were not. This was in agreement with the known compositions (see Table 1). The *SPOIL* function criterion was also applied. The extremely large *SPOIL* values for chloroform, toluene, and 1,2,4-trimethylbenzene indicated that these components were not present. The values for *o*-xylene, *m*-xylene, *p*-xylene, and ethylbenzene were all below 3.5, confirming the presence of these components.

The absorptivities $a(i, j)$, in units of 1 mol^{-1} cm^{-1}, of the four components present were fed into the t.f.a. program as a combination set, yielding a set

TABLE 5

Target testing of absorptivities with data matrix A to determine components present in solutions 1—10

Target	*AET*	*REP*	*RET*	$(RET)_{est}$[a]	*RELI*	*SPOIL*
o-Xylene	1.96	0.57	1.88	1.10	0.63	3.30
m-Xylene	0.72	0.58	0.42	0.64	1.21	0.72
p-Xylene	0.83	0.57	0.60	0.65	1.04	1.07
Ethylbenzene	1.30	0.59	1.16	0.64	0.67	1.97
Chloroform	201	1.13	201	3.26	0.017	180
Toluene	66.6	0.53	66.6	0.97	0.017	130
1,2,4-Trimethylbenzene	36.6	0.023	36.6	0.48	0.013	1600

[a]Estimated from the *RE* value obtained from a.f.a. using four factors.

of cofactors $F(j, \alpha)$. The concentrations $c(j, \alpha)$, in mol l^{-1}, were then obtained from $F(j, \alpha) = b(\alpha)\ c(j, \alpha)$. The molarities determined by t.f.a. are presented in Table 1, along with those obtained by solving simultaneous equations. Excellent agreement with the estimated values was found throughout. For *m*-xylene and ethylbenzene, the method of simultaneous equations gave better agreement.

The absorbance spectra of solutions 11 and 12, along with the spectrum of pure chloroform in cyclohexane, are shown in Fig. 1. Solutions 11 and 12 each contained small amounts of chloroform, in addition to the four components present in solutions 1—10. The compositions, estimated from the solution preparation data, of solutions 11 and 12 are given in Table 2. The molarity of chloroform in solution 11 was 5.8% of the total solute molarity. In solution 12, only 2.0% of the total solute molarity was due to chloroform. As shown in Fig. 1, the chloroform peak overlaps with one of the *m*-xylene peaks and appears as a shoulder in the solution 11 spectrum. The existence of an absorbance contribution from chloroform is not evident from a visual examination of the solution 12 spectrum.

The absorbance values of solution 11 were added to data matrix A to form a 35 × 11 data matrix B. Likewise, the absorbances of solution 12 were added to data matrix A to form a 35 × 11 data matrix C. These two matrices were subjected to a.f.a. The *RE*, *IE*, and *IND* criteria, listed in Table 4 together with the eigenvalues, were used to determine the number of absorbing components. In both cases, the *RE* was between 0.001 and 0.0020 at $n = 5$. The *IE* and *IND* functions also clearly indicated five factors. Thus, the existence of a fifth absorbing component in the two series of eleven solutions was determined even though the fifth component (chloroform) was present in only one of eleven solutions in both data sets, even though the chloroform concen-

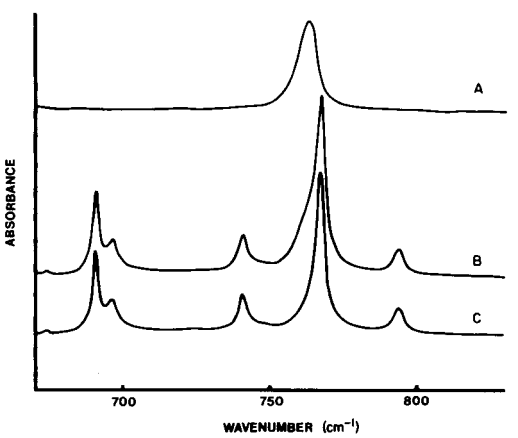

Fig. 1. Absorbance spectra of chloroform and solutions in which chloroform was detected as an impurity and quantified: (A) 0.0161 M chloroform in cyclohexane (see Table 3); (B) solution 11 (see Table 2); (C) solution 12 (see Table 2).

tration was low, and even though the chloroform peak completely overlapped with one of the *m*-xylene peaks. Furthermore, the spectra of solutions 1—10 were taken almost two weeks earlier than the spectra solutions 11 and 12. During this interim time period, the spectrophotometer was used for other experiments, at different instrument settings.

Data matrices B and C were target-tested, using five factors, for the seven solutes in Table 3. The *RELI* and *SPOIL* criteria indicated the presence of *o*-xylene, *m*-xylene, *p*-xylene, and ethylbenzene and the absence of toluene and 1,2,4-trimethylbenzene in both data sets. Target tests also clearly identified chloroform as the fifth factor, as shown in Table 6.

Since the test vector data and the solution data were obtained under the same experimental conditions, the *RET* and *REP* values should be equal for valid factors [3]. A *SPOIL* value of one is therefore expected. The zero *SPOIL* for chloroform in data matrix C was assigned because the calculated *REP*, which is only an approximation, exceeded the *AET*. Theoretically, this is not possible from the equation $(AET)^2 = (REP)^2 + (RET)^2$, but since the *SPOIL* should approach zero as the *REP* approaches the *AET*, the *SPOIL* was assigned a value of zero, indicating a valid factor.

Combination t.f.a. was applied to data matrices B and C. Input of the five valid absorptivity test vectors in combination yielded cofactors $F(j, \alpha)$ from which the concentrations $c(j, \alpha)$ were obtained. For both data sets, the *o*-xylene, *m*-xylene, *p*-xylene, and ethylbenzene molarities of solutions 1—10 were in close agreement with those obtained earlier by factor analysis of data matrix A. The t.f.a.-calculated chloroform molarities for solutions 1—10 were all close to zero (between −0.00001 and 0.00022 mol l^{-1}), as expected. The t.f.a.-determined molarities in solutions 11 and 12 are compared with the estimated values in Table 2. Excellent agreement was found for all five components; the agreement for chloroform was better than 2.2%. Thus, chloroform was identified and accurately quantified in solutions 11 and 12 by t.f.a.

For comparison, regression analyses were also carried out on the twelve multicomponent solutions, each presumed to contain four components, using exactly the same data as in the factor analysis studies. The concentrations were determined by means of the regression equation

$$[C] = (1/b)\ \{([E]^T[E])^{-1}[E]^T[A]\} \qquad (5)$$

TABLE 6

Target test identifications of chloroform as the impurity in solutions 11 and 12

	Data matrix	*AET*	*REP*	*RET*	$(RET)_{est}$[b]	*RELI*	*SPOIL*
B:	Solutions 1—10 and 11[a]	11.1	7.9	7.7	3.2	0.77	0.97
C:	Solutions 1—10 and 12[a]	20.4	23.9	0	3.2	1.01	0

[a]See Tables 1 and 2 for compositions. [b]Estimated from the *RE* values obtained from a.f.a. using five factors.

where [C] is a 4 × 12 concentration matrix, b is the pathlength, [E] is a 35 × 4 absorptivity matrix consisting of the same absorptivities used to construct the test vector combination set for data matrix A, and [A] is a 35 × 12 matrix of the experimental absorbances, i.e., absorbance values of 12 solutions measured at 35 different wavenumbers.

The combination t.f.a. and regression analysis concentrations for solutions 1—10, which did not contain any measurable impurity, were found to be almost identical (see Table 1), as expected. A proper regression analysis computation for solutions 11 and 12 would include the chloroform absorptivities, since chloroform is present in these two solutions. However, the chloroform impurity can be neither tested for, nor identified by regression analysis as it can be by t.f.a. Carrying out regression analyses for solutions 11 and 12 using only the absorptivities of *o*-xylene, *m*-xylene, *p*-xylene, and ethylbenzene resulted in some concentrations which differed significantly from the estimated values (see Table 2). In particular, the discrepancy is large for *m*-xylene, which completely overlaps the chloroform peak. In contrast, the t.f.a. concentrations (see Table 2) were all in close agreement with the estimated values.

The authors are grateful to Dr. Antoinette J. Hockman of this Department and to Dr. Timothy R. Hart of the Department of Physics and Engineering Physics for their help with the F.t.i.r. spectrophotometer, which was purchased under National Science Foundation Grant SER 77-06938. This paper is taken in part from a dissertation submitted in partial fulfillment of Ph.D. requirements (M.McC.).

REFERENCES

1 E. R. Malinowski and M. McCue, Anal. Chem., 49 (1977) 284.
2 E. R. Malinowski, Anal. Chem., 49 (1977) 606, 612.
3 E. R. Malinowski, Anal. Chim. Acta, 103 (1978) 339.
4 T. Hirschfeld, Anal. Chem., 48 (1976) 721.
5 R. P. Bauman, Absorption Spectroscopy, Wiley, New York, 1962, pp. 403—412.
6 A. E. McDowell and H. L. Pardue, J. Pharm. Sci., 67 (1978) 822.
7 E. R. Malinowski and D. G. Howery, Factor Analysis in Chemistry, J. Wiley, New York, 1980.
8 E. D. Olsen, Modern Optical Methods of Analysis, McGraw-Hill, New York, 1975, p. 205.
9 R. J. Bell, Introductory Fourier Transform Spectroscopy, Academic Press, New York, 1972, p. 64 (eqn. 6-1).
10 E. R. Malinowski, D. G. Howery, P. H. Weiner, J. M. Soroka, P. T. Funke, R. B. Selzer and A. Levinstone, FACTANAL Target Transformation Factor Analysis, Program 320, Quantum Chemistry Program Exchange, Indiana University, Bloomington, IN, 1976.

Analytica Chimica Acta, 133 (1981) 137—150
Computer Techniques and Optimization
Elsevier Scientific Publishing Company, Amsterdam — Printed in The Netherlands

EINSATZ VON RECHENANLAGEN IN DER EMISSIONS-SPEKTROCHEMIE
II Teil. Aufstellung, Bewertung und Linearisierung der analytischen Eichgeraden†

MIKULÁŠ MATHERNY*

Lehrstuhl für Chemie der Hüttenmännischen Fakultät der Technischen Hochschule, CS-043 85 Košice (Tschechoslowakei)

JOZEF ONDÁŠ

Ostslowakische Eisenwerke VEB, Abt. Rechenzentrum, CS-044 54 Košice (Tschechoslowakei)

(Eingegangen den 17 Marz 1980)

SUMMARY

The Use of Computers in Emission Spectroscopy. Part 2. Establishment, Evaluation and Linearization of Analytical Calibration Curves

The problems of establishing optimum linear calibration plots for atomic emission spectrometry are described, particularly when photographic recording techniques are employed. The calculation procedure, based on the least-squares method, generates additional statistical values which permit linearity to be checked. As the desired linearity is not always achieved at the first attempt, the process is repeated after exclusion of unreliable input data.

ZUSAMMENFASSUNG

Die vorliegende Arbeit beschäftigt sich mit den Problemen beim Aufstellung von optimalen analytischen Eichgeraden für die atomare Emissionsspektrochemie bei photographischer Registrierung. Bei der Berechnungsprozedur, die auf der Methode de kleinsten Quadrate beruht, werden auch weitere statistische Hilfswerte ermittelt die letzen Endes auch die Prüfung der Linearität erlauben. Da aber in der ersten Berechnungsstufe nicht immer die gewünschte Linearität erreicht wird, ist der Rechengang durch eine weitere Prozedur ergänzt, die unzuverlässige Eingangsdaten ausschliesst.

Bei der Aufstellung von analytischen Eichkurven ist eine Gerade der gewünschte Speziallfal. Deswegen müssen alle vernünftige Bestrebungen unternommen werden um diesen Speziallfall zu erreichen. Der wesentliche Vorteil der analytischen Eichgeraden gegenüber den Eichkurven liegt darin, dass diese bessere Kontrollmöglichkeiten ihres Verlauf bieten [1, 2], und gleichzeitig auch die Ermittlung der Werte der Nachweisgrenzen [3] erlauben. Die experimentelle Vorbereitung der Grundeingangsdaten für die analytischen

†Vorgetragen an der II. Bulgarischen nationalen Analytischen Konferenz, Goldene-Sand-Küste bei Varna, September 1976. Teil I: Anal. Chim. Acta, 112 (1979) 277.

0378—4304/81/0000—0000/$02.50

Eichgeraden fusst entweder in synthetischen Modellmischungen (Eichmischungen, Etalons usw.), die auch Neben- sowie Spurenelemente beinhalten, oder man verwendet natürliche Eichproben (Bezugsproben) die meistens durch nasschemische Methoden eben auf die Nebenuns Spurenelemente analysiert wurden. Dieser letztgenannte Weg ist nur dann zu empfehlen, wenn die Modellierung des krystallochemischen Charakters des Eichmatrixes bedeutende Schwierigkeiten bereitet. Für jeden Fall muss man aber die Bezugsproben sowie einige typische analytische Proben, unabhängig von der Art der Vorbereitung und Bestimmung der Konzentrationswerte der Neben- und Spurenelemente, auf die Elimination der Matrixeffekte zu prüfen [4]. Für eine Eichprozedur sind prinzipiell nur solche Proben zugelassen, die dieselben Matrixeffekte aufweisen wie die typische analysierenden Proben.

ALLGEMEINE THEORETISCHE GEDANKENGÄNGE

Eine analytische Eichgerade (Abb. 1) muss immer und ausschliesslich für eine bestimmte Spannweite der Konzentrationswerte $\langle c_{X,\min}; c_{X,\max} \rangle$ aufgestellt werden [5]. Die entsprechende Formel für die emissionspektrochemischen Methoden stütz sich auf die Arbeiten von Lomakin [6], und Scheibe und Schnettler [7]. Für die Bezugslinienmethode hat aber diese empirische Formel ganz konsequent nur Malpica [8] angewendet. Sie wird meistens in logarithmischer Form verwendet:

$$\Delta Y_{X,R} = A_{X,R} + B_X \log c_X \qquad (1)$$

(Die angewendeten Symbole sind in Tabelle 1 erklärt.) Kaiser [3] hat nachdrücklich betont, dass trotz des empirischen Charakters der diskutierten Formel eine direkter logischer Zusammenhang wischen den Logarithmen der analytischen Konzentrationswerte und den auf Messungen beruhenden ΔY-Werten besteht.

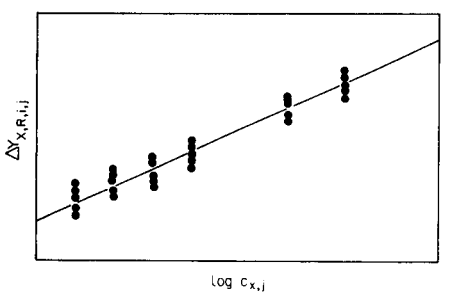

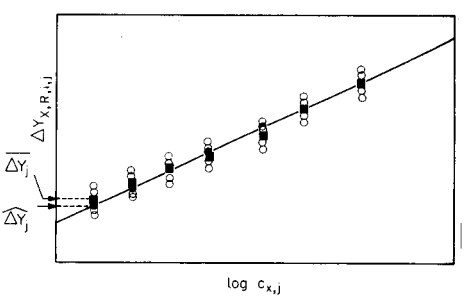

Abb. 1. Schematische Darstellung einer spektrochemischen Eichgerade mit allen experimentell ermittelten $\Delta Y_{X,R,i,j}$-Werten.

Abb. 2. Veranschaulichung der Lage der $\overline{\Delta Y_j}$- und $\widehat{\Delta Y_j}$-Werte auf einer analytischen Eichgeraden.

TABELLE 1

Erläuterung der angewendeten Symbole

c_X	analytischer Konzentrationswert
$A_{X,R}$	Parameter der analytischen Eichgerade; schnitt-punkt der Eichgerade mit der Y-Achse für $c_X = 1$
B_X	Parameter der analytischen Eichgerade; Richtungstangente der Eichgerade; relative Empfindlichkeit der Methode
S	Schwärzungswert
a_i	Transparenzwert ($a_i = T \times 10^3$)
I	relativer Intensitätswert einer Spektrallinie oder des Untergrundes
$Y = \log I$	
$\Delta Y = Y_x - Y_R$	
r	Korrelationskoeffizient
R	Bestimmtheitsmass in %
s	Standardabweichung
t_c	Testwert, abgeleitet von experimentellen Angaben
t_{tab}	tabellierter Testwert der S- oder F-Verteilung
t_0	berechneter Testwert der S- oder F-Verteilung
f	Freiheitsgrad
S [%]	statistische Sicherheit
K, M, P	Endzahlwerte
$G1$ bis $G4$	γ-Werte
$k1$ bis $k4$	k-Transformationskonstanten
Subskripten	
i, j, q	bedeuten immer eine Reihenfolge von Werten
X	bezieht den Wert auf eine analytische Linie oder auf deren Untergrund
R	bezieht den Wert auf eine Bezugslinie oder auf deren Untergrund
$L + U$	bezieht den Wert auf eine nichtkorrigierte Linie (Bruttowert)
U	bezieht den Wert ausschliesslich auf der Untergrund

Die Aufstellungsprozedur [1, 5, 9] verlangt eine Anfangsmatrix der experimentellen Angaben $\{\Delta Y_{X,R,i,j}, \log c_{X,j}\}$, wobei $i = 1,..., K$, $K \epsilon \langle 3, 15 \rangle$ und $j = 1,..., M$, $M \epsilon \langle 4, 20 \rangle$ ist. K stellt dabei die Zahl der wiederholten Spektren für einen gewissen analytischen Konzentrationswert $c_{X,j}$, und M die Gesamtzahl der zur Eichung angewendeten Bezugskonzentrationswerte dar. Die $\Delta Y_{X,R,i,j}$-Werte ergeben sich immer aus der Differenz zweier Y-Werte, die aber von den gemessenen Schwärzungswerten S, oder aber von den Transparenzwerten proportionalen a_i-Werten ($a_i = T\, a_{max}$) abgeleitet werden müssen. Der ΔY-Differenzwert kann aber prinzipiell auf vier Wege gebildet werden, abhängig davon, ob und wie man die Untergrundkorrektur [10] vornimmt. Die vier möglichen Eingabematrizen, von den die Y- und schliesslich auch die ΔY-Werte abgeleitet werden, finden sich in Tabelle 2. Die Schwärzungswerte sind erstens zwangsläufig in die Y-Werte und teilweise auch in die relativen Intensitätswerte I ($I = 10^Y$) umzusetzen. Für diese komplexe Operation eignet sich das Unterprogramm TRANSL [11] falls man die l-Transformation [12] bevorzugt, oder aber das Unterprogramm TRANSP [11], falls sich die allgemeine P-Transformation [13] besser für die angewendete Emulsion eignet.

TABELLE 2

Schema der vier möglichen Anfangsmatrizen

Bezeichnung	Matrixstruktur	Bestimmung
$(T = 0)$	$\{c_{X,j}, S_{X,L+U,i,j}, S_{R,L+U,i,j}\}$	Ohne Untergrundkorrektur
$(T = 1)$	$\{c_{X,j}, S_{X,L+U,i,j}, S_{X,U,i,j}, S_{R,L+U,i,j}\}$	Untergrundkorrektur bei X
$(T = 2)$	$\{c_{X,j}, S_{X,L+U,i,j}, S_{X,U,i,j}, S_{R,L+U,i,j}, S_{R,U,i,j}\}$	Untergrundkorrektur bei X und R
$(T = 3)$	$\{c_{X,j}, S_{X,L+U,i,j}, S_{R,L+U,i,j}, S_{R,U,i,j}\}$	Untergrundkorrektur nur bei R

Die als $(T = 0)$ bezeichnete Matrix der Tabelle 2 gilt ausschliesslich für den Auswertungsfall, bei dem an den Y-Werten keine Untergrundkorrektur vorgenommer wird ($\Delta Y_{X,R} = Y_{X,L+U} - Y_{R,L+U}$). Bei der Matrix $(T = 1)$ wird die analytische Linie auf die Untergrundintensität korrigiert ($\Delta Y = \log [I_{X,L+U} - I_{X,U}] - Y_{R,L+U}$), und die Matrix $(T = 2)$ erlaubt sogar die vollkommene Untergrundkorrektur ($\Delta Y_{X,R} = \log [I_{X,L+U} - I_{X,U}] - \log [I_{R,L+U} - I_{R,U}]$). Die Matrix $(T = 3)$ ermöglicht dagegen nur die alleinige Untergrundkorrektur bei der Bezugslinie ($\Delta Y_{X,R} = Y_{X,L+U} - \log [I_{R,L+U} - I_{R,U}]$).

Berechnung der Grundparameter der Eichgeraden

Die Berechnung der Grundparameter $A_{X,R}$ und B_X, die eindeutig den Verlauf der Eichgeraden festlegen, fusst in der Minimalisierung der Gl. (1) anhand der Methode der kleinsten Quadrate:

$$F[A_{X,R}, B_X] = \sum_{1}^{K} \sum_{1}^{M} \Delta Y_{X,R,i,j} - A_{X,R} - B_X \log c_{X,j}{}^2 = \sum_{1}^{K} \sum_{1}^{M} (eF_{i,j})^2 = \text{MIN} \quad (2)$$

Die Prozedur sieht eine konstante Zahl K für alle Eichkonzentrationen j vor. Dies ist für eine programmgesteuerte Berechnung sehr günstig. Schon bei der Eingabe der Werte der Anfangsmatrix erleichtert diese Konzeption die Organisation des ganzen Input-Systems, weiterhin erleichtert diese Auffassung auch die Durchführung der Linearitätsprüfung [5]. Die gesuchten Grundparameterwerte ergeben sich nach einer Serie von matematischen Operationen [1, 5, 9] aus Gl. (3) und (4):

$$A_{X,R} = \frac{\Sigma_1^M \log c_{X,j} \, \Sigma_1^M \Sigma_1^M \log c_{X,j} \Delta Y_{X,R,i,j}}{K[(\Sigma_1^M \log c_{X,j})^2 - M\Sigma_1^M (\log c_{X,j})^2]}$$

$$- \frac{\Sigma_1^K \Sigma_1^M Y_{X,R,i,j} \, \Sigma_1^M (\log c_{X,j})^2}{K[(\Sigma_1^M \log c_{X,j})^2 - M\Sigma_1^M (\log c_{X,j})^2]} \quad (3)$$

$$B_X = \frac{\frac{1}{M} \Sigma_1^K \Sigma_1^M \Delta Y_{X,R,i,j} \, \Sigma_1^M \log c_{X,j} - MK \, \Sigma_1^M \log c_{X,j}}{K[\frac{1}{M} \Sigma_1^M (\log c_{X,j})^2 - (\Sigma_1^M \log c_{X,j})^2]} \quad (4)$$

Weiter ist es notwendig eine Reihe von Standardabweichungen ermitteln zu lassen. Erstens ist es die Standardabweichung $s_{\Delta Y_j}$, die für die einzelnen j-

Gruppen der $\Delta Y_{X,R,i,j}$-Werte massgebend ist (Gl. 5a), und die Standardabweichung $s_{\Delta Y}$, die aus der gesamten Gruppe der $\Delta Y_{X,R,i,j}$-Werten abgeleitet wird (Gl. 5c).

$$s_{\Delta Y_j} = \left[(1/(K-1)) \sum_{1}^{K} (\Delta Y_{X,R,i,j} - \overline{\Delta Y_j})^2 \right]^{1/2} \tag{5a}$$

$$\text{wo } \overline{\Delta Y_j} = (1/K) \sum_{1}^{K} \Delta Y_{X,R,i,j} \tag{5b}$$

$$\overline{s_{\Delta Y}} = \left[(1(K-1)) \sum_{1}^{K} (1/(M-1)) \sum_{1}^{M} (\Delta Y_{X,R,i,j} - \overline{\Delta Y_j})^2 \right]^{1/2} \tag{5c}$$

Anhand dieses letztgenannten Wertes (Gl. 5c) wird die relative Präzision der Konzentrationsbestimmung (Gl. 5d) nach Prokofjevs [14] berechnet.

$$s_{c_{X,r}} = 230\, \overline{s_{\Delta Y}}\, 1/B_X \tag{5d}$$

Weiterhin ermöglicht der $\overline{s_{\Delta Y}}$-Wert die Ermittlung der Standardabweichungen $s_{AX,R}$ (Gl. 6a) und s_{BX} (Gl. 6c), die für die Beurteilung der Präzision der Aufstellung der Eichgeraden [2, 5] sowie für die Ermittlung der "totalen" Präzision der Konzentrationsbestimmung [17] notwendig ist.

$$s_{A_{X,R}} = 1/\overline{s_{\Delta Y}} \left\{ \left[\sum_{1}^{M} (\log c_{X,j})^2 \right] \Big/ \left[KM\, (\log c_{X,j} - \log \overline{c_X})^2 \right] \right\}^{1/2} \tag{6a}$$

$$\log \overline{c_X} = 1/M \sum_{1}^{M} \log c_{X,j} \tag{6b}$$

$$s_{B_X} = 1/\overline{s_{\Delta Y}} \left[K \sum_{1}^{M} (\log c_{X,j} - \log \overline{c_X})^2 \right]^{-1/2} \tag{6c}$$

Schliesslich ist es wünschenswert für die komplexe Bewertung auch den Wert der Korrelationskoeffizienten r, dessen standardabweichung s_r sowie den Wert des Bestimmtheitsmasses R zu berechnen [18].

$$r = \left\{ \frac{\Sigma_1^K \Sigma_1^M (\log c_{X,j} - \log \overline{c_X})(\Delta Y_{X,R,i,j} - \overline{\Delta Y_j})}{K[\Sigma_1^M (\log c_{X,j} - \log \overline{c_X})^2 \Sigma_1^K \Sigma_1^M (\Delta Y_{X,R,i,j} - \Delta \overline{Y_j})^2]} \right\}^{1/2} \tag{7a}$$

$$s_r = (1 - r^2)/KM \tag{7b}$$

$$R = r^2\ 100 \tag{7c}$$

Testprüfungen

Da die ermittelten Werte aus einer stochastisch zusammenhängenden Matrix der $\{\Delta_{X,R,i,j}, c_{X,j}\}$-Werte entstanden, ist es berechtigt, einige Werte durch statistische Testverfahren überprüfen zu lassen [19—21]. Erstens muss der Wert des Parameters B_X, der gleichzeitig die relative Empfindlichkeit

der Methode darstellt [22], auf die signifikante Ablehnung, der Hypothese $B_X = 1$ geprüft werden [5, 18]. Die entsprechende Formel stützt sich auf das Studentsche Testverfahren [19—21]:

$$t_c = (B_X - 1)/s_{B_X} \tag{8}$$

Diese Testprüfung wird für zwei statistische Sicherheiten (95% sowie 99%), und für den Freiheitsgrad $f = (KM) - 1$ durchgeführt. Der zuständige t_0-Wert wird entweder den Tabellen des Studenttestverfahrens (t_{tab}) entnommen, oder kann durch eine Unterprogramm STUDIN ermittelt werden, das diesen Wert aufgrund der Theorie [20, 21] berechnet. Falls $t_c \leq t_0$ findet die getestete Hypothese ihne Bestätigung, das heist B_X ist praktisch gleich Eins. Im Gegenfall, wenn $t_c > t_0$, wird die Hypothese abgelehnt da B_X von Eins signifikant unterschieden ist.

Der Wert des Korrelationskoeffizienten muss auf die Ablehnung der Hypothese $r = 0$, für den Freiheitsgrad $f = (KM - 1)$ und die statistische Sicherheit $S = 99.9\%$ geprüft werden.

$$t_c = (r(1 - r^2)^{-1/2}(KM - 2))^{1/2} \tag{9}$$

Hier gilt wierderum, dass bei $t_c > t_0$ die Hypothese als abgeleht betrachtet wird, aber wenn $t_c \leq t_0$ findet die Hypothese ihre Bestätigung.

Leider gibt die Testprüfung (Gl. 9) über den linearen Zusammenhang der Grundmatrixwerte eine ungenügende Information [3, 18] und deswegen muss diese Information auf anderem Wege ermittelt werden. Es ist dies die Prüfung der Dichte der experimentell ermittelten $\Delta Y_{X,R,i,j}$-Werte um den rechnerisch ermittelten $\widehat{\Delta Y}_j$-Wert (Abb. 2):

$$\widehat{\Delta Y}_j = A_{X,R} - B_X \log c_{X,j} \tag{10}$$

Die Berechnung des Testwertes $t_{c,LIN}$ (s.u.) verlangt die Ermittlung zweier spezieller quadratischer Abweichungswerte: der erste

$$(s_1)^2 = \left[K \sum_1^M (\overline{\Delta Y}_j - \widehat{\Delta Y}_j)^2\right] \Big/ [M - 2] \tag{11a}$$

wird für den Freiheitsgrad $f_1 = M - 2$ und der zweite

$$(s_2)^2 = \left[\frac{1}{M} \sum_1^M \sum_1^K (\Delta Y_{X,R,i,j} - \overline{\Delta Y}_j)^2\right] \Big/ [K - 1] \tag{11b}$$

für den Freiheitgrad $f_2 = M\,(K - 1)$ sowie beide für zwei statistische Sicherheitswerte $S = 95\%$ und $S = 99\%$ ermittelt.
Bei der Bildung der Quotienten $t_{c,LIN}$ wird jeweils der höhere Wert durch den kleineren dividiert, so das $t_{c,\,LIN} \geq 1$. In der Regel ist $(s_1)^2 \geq (s_2)^2$:

$$t_{c,LIN} = (s_1)^2/(s_2)^2 \tag{12}$$

Der Testwert $t_{c,LIN}$ wird im weiteren entweder mit dem aus Tabellen der F-Verteilung entommenen t_{tab}-Wert, oder mit dem durch das Unterprogram

STUDIN ermittelten t_0-Wert, für beide statistische Sicherheiten verglichen. Falls $t_c \leq t_0$ hält man die getestete Hypothese für bestätigt, und die Eichgerade entspricht den experimentallen $\Delta Y_{X,R,i,j}$-Punkten. Ist jedoch $t_c > t_0$, so muss man die Hypothese ablehnen. So eine Gerade hat keine analytische Bedeuteung; dementsprechend muss die Grundeingangsmatrix weiter optimiert werden.

Programmierte Lösung der Aufstellung von analytischen Eichgeraden

Der verallgemeinerte Ablauf des Programms CANCAL ACL-MO-78 findet sich in Abb. 3. Erstens müssen die Befehlsangaben L und T angegeben werden. Weiter werden K und M sowie die γ- und k-Werte eingespeichert. Diese letztgenannten Werte werden getrennt für die analytische Linie ($G1$, $k1$), deren Untergrund ($G2$, $k2$), sowie für die Bezugslinie ($G3$, $k3$) und deren Untergrund ($G4$, $k4$) angegeben. Der erste Teil der Eingabe (INPUT) endet mit der Eingabe der Eich-Konzentrationswerte $c_{X,j}$. Die Programmeinheit enthält noch drei weitere Eingaben. Die erste bestimmt die Informationen

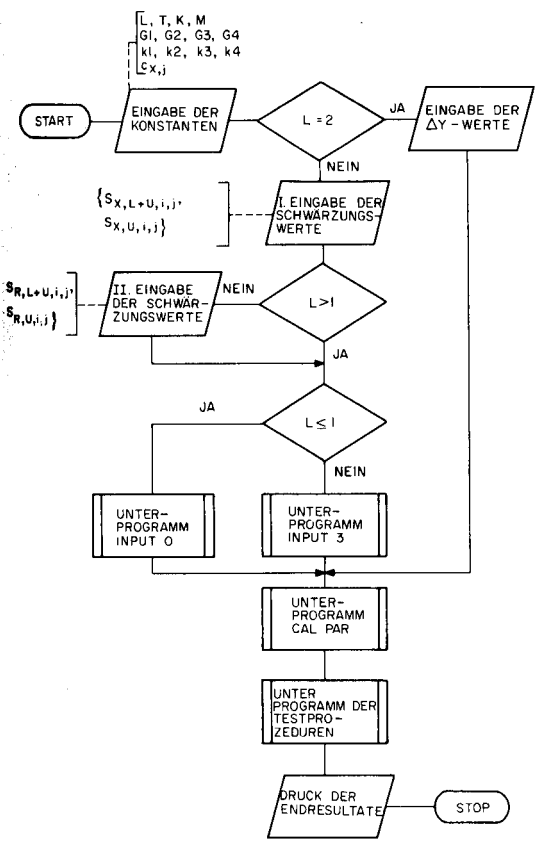

Abb. 3. Allgemeines Flussdiagramm des Programms CANCAL ACL-TIO-78.

(Transparenz- oder Schwärzungs-Werte) über die analytische Linie, inbegriffen der Untergrundwerte, und die zweite die Informationen über die Bezugslinie. Die dritte Eingabe ist für den Speziallfall bestimmt, wenn man direkt mit ΔY-Werten, die schon früher getrennt gebildet wurden, in das Programm eintreten will. Die Sequenz der Eingabe dieser Werte müssen der Reihenfolge der Eingabe der Konzentrationswerte streng entsprechen. Falls der Befehl ($L = 1$) ist, wird das Programm die Eingabedaten als Schwärzungswerte betrachten, falls ($L = 2$) ist, ist es möglich, direkt mit ΔY-Werten zu rechnen. Wenn aber ($L = 0$) ist (Abb. 4), betrachtet die Anlage die Eingabedaten als Transparenzwerte a_i und berechnet sofort die entsprechenden Schwärzungswerte ($S = \log a_0 - \log a_i$ wobei $a_0 = 1000$). Die Befehle ($L = 3$) und ($L = 4$) ermöglichen unter Anwendung des Unterprogramms INPUT 3 ohne Bezugslinienmethode zu arbeiten (Abb. 5A). Im Fall ($L = 3$) wird der ΔY-Wert wie folgt gebildet: $\Delta Y = Y_{X,L+U} - Y_{X,U}$, wobei der Untergrundwert als Bezugswert $Y_{X,U}$ angewendet wird. Der Befehl ($L = 4$) schliesslich veranlasst die folgende Bildung der ΔY-Werte: $\Delta Y = \log (I_{X,L+U} - I_{X,U}) - Y_{X,U}$. Dadurch werden die Intensitätswerte der analytischen Linien auf die Untergrundintensität korrigiert und gleichzeitig wird die Untergrundintensität als Bezugswert ($Y_{X,U} = \log I_{X,U}$) betrachtet.

Durch die T-Befehle (Abb. 4) werden die vier Berechnungsvarianten der ΔY-Werte geregelt, und deswegen ist dieser Teil als Organisations-Unterprogramm INPUT 0 zusammengefasst. Er enthält zwei weitere selbständige Unterprogramme. Das Unterprogramm TRANSL (Abb. 5B) ist für die Schwärzungstransformation bestimmt und verwendet die l-Transformation [12], die aber gegen die P-Transformation auswechselbar ist. Weiterhin

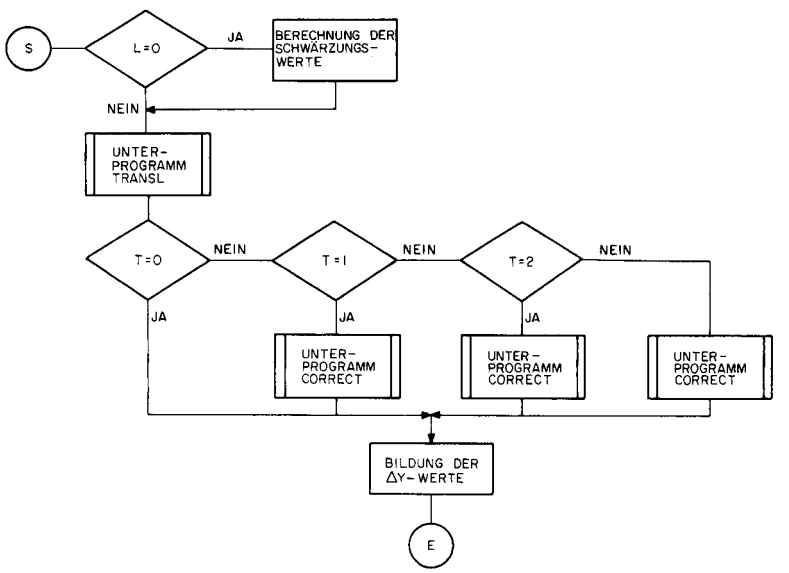

Abb. 4. Flussdiagramm des Unterprogramms INPUT 0 und Verknüpfung mit den Unterprogrammen TRANSL und CORREC.

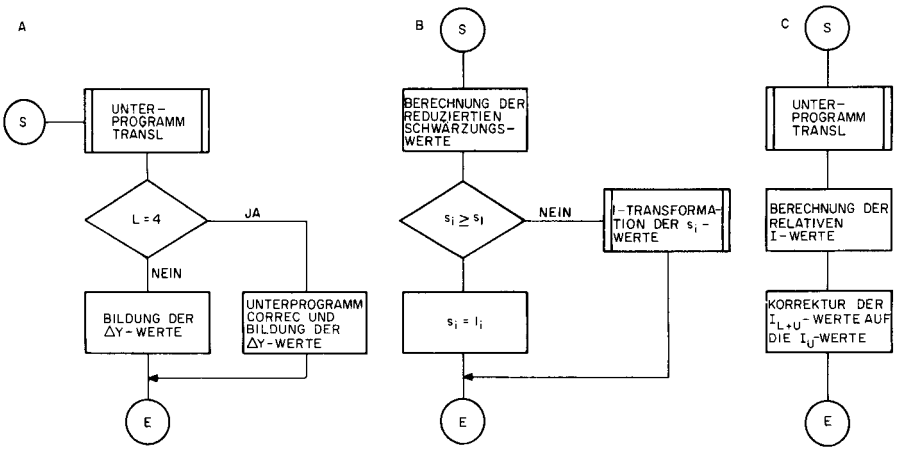

Abb. 5. Flussdiagram des Unterprogramms: (A) INPUT 3 und der Bildung der ΔY-Werte; (B) TRANSL; (C) CORREC.

beinhaltet der INPUT 0 Programmteil (Abb. 3) auch des Unterprogramm CORREC (Abb. 5C) das für die Untergrundkorrektur bestimmt ist. Schliesslich muss noch erwähnt werden, dass für die Berechnung der Parameter der Eichgeraden ein zusammengeschlossenes Unterprogramm CAL PAR aufgestellt wurde, das auf den Beziehungen des Kapitels Allgemeine Theoretische Gedankengänge beruht.

LINEARISIERUNG DER UNZUVERLÄSSIGEN EINGANGSMATRIXE

Die Linearisierung der unzuverlässigen Eingangsmatrizen richtet sich nach der folgenden Sequenz: es muss erstens der Einfluss der Untergrundkorrektur optimiert werden; weiter wird der Einfluss der eventuellen Linien- oder Band-Interferenzen (auch Blindwertkorrektur) untersucht; und schliesslich müssen manchmal von der Grundmatrix diejenigen $I_{X,L+U,i,j}$-Werte oder aber Gruppen von I-Werte entfernt werden die in der Untergrundintensität signifikant untertauchen.

Die Entscheidung über die richtigste Variante der Untergrundkorrektur [23, 24] kann nur aufgrund der Ermittlung aller erwähnten Parameterwerte der Eichgeraden getroffen werden. Der komplexeste Wertungsparameter ist dabei der $s_{cX,r}$-Wert, da dieser in gleichem Masse die Werte der Parameter B_X sowie den Standardabweichungswert $\overline{s_{\Delta Y}}$ in Betracht zieht [5].

Die Blindwertkorrektur der analytischen Linien [25] beruht auf der Subtraktion des Intensitätswertes der Blindprobe I_{bl} vom Bruttointensitätswert der analytischen Linie:

$$Y_X = \log (I_{X,L+U} - I_{bl}) \tag{13a}$$

da der interferierende Intensitätswert I_{bl} auch eine Untergrundintesität $I_{X,U}$ beinhaltet. Diese Operation, die sowieso selten zur Anwendung kommt

ist eigentlich unnötig. Falls die Bewertung der Resultate zeigt, dass eine analytische Linie durch das erwähnte Phenomen gestört ist, werden nachträglich die $Y_{X,L+U}$-Werte einer Korrektur unterworfen. Die Gl. (13a) kann aber im Fall $I_{X,U} \neq I_{bl}$ wie folgt modifiziert werden:

$$Y_X = \log (I_{X,L+U} - I_{X,U}) - \log (I_{bl} - I_{bl,U}) \tag{13b}$$

Bei der Aufstellung der analytischen Eichgeraden ist es in diesem Speziallfall möglich, anstatt der $Y_{R,L+U}$- und $Y_{R,U}$-Werte direkt die Y_{bl}- und $Y_{bl,U}$-Werte, oder aber die entsprechenden S-Werte, einzusetzen und die Berechnung auf konventionellem Weg durchzuführen.

Hauptsächlich ist es bei der Aufstellung von analytischen Eichgeraden für die Spurenelementebestimmungen empfehlenswert, ausschliesslich mit solchen Schwärzungswerten der analytischen Linien zu arbeiten, die sich signifikant von der Untergrundschwärzung abheben. Da aber die Schwärzungswerte principiell nicht addierbare Werte sind, ist es notwendig, die ganze Begrenzugsprozedur anhand der relativen Intensitätswerte und gleichzeitig unter Berücksichtigung der Bezugslinienintensitäten zu lösen [2]. Diese Prozedur verlangt zuerst in einem bestimmten i, j-Spektrum, wo $i = Z$ und $j = Q$ ist, in der unmittelbaren Nähe der analytischen Linie eine Reihe von Untergrund-Schwärzungswerten $S_{X,U,q}$ zu ermitteln, wo $q = 1,..., P$ und $P \in \langle 15, 30 \rangle$. Weiter ist es noch notwendig, im selben Z,Q-Spektrum auch die Schwärzung der Bezugslinie $S_{R,L+U,Z,Q}$ und eventuell auch deren Untergrundschwärzungswert $S_{R,U,Z,Q}$ auszumessen. Alle Schwärzungswerte müssen weiterhin aufgrund der l-Transformationsprozedur in die relativen Intensitätswerte umgerechnet werden. Aus der soeben definierten Matrix wird der Mittelwert $\bar{I}_{X,U}$ und dessen Standardabweichungswert $s_{I_{X,U}}$ berechnet:

$$\bar{I}_{X,U} = \frac{1}{P} \sum_{1}^{P} I_{X,U,q} \tag{14a}$$

$$s_{I_{X,U}} = \left[\frac{1}{P-1} \sum_{1}^{P} (I_{X,U,q} - \bar{I}_{X,U})^2 \right]^{1/2} \tag{14b}$$

Anhand dieser zwei Werte ist es möglich, einen Grenzwert zu formulieren. Dieser aber muss getrennt für die erwähnten Varianten der Untergrundkorrekturen gebildet werden.

Für die Fälle ($T = 0$) sowie ($T = 3$) wenn die analytische Linie nicht korrigiert wird, erhält man den Grenzwert Y_G: $Y_G = \log (\bar{I}_{X,U} + 6s_{IX,U})$. Der Multiplikationsfaktor 6 garantiert, ähnlich wie bei der Grantiegrenzenbestimmungen [26, 27], die 99.9%-ige statistische Sicherheit, dass das analytische Signal höher liegt als der Mittelwert $\bar{I}_{X,U}$. Falls aber $P < 30$ ist, wird es notwendig, den $s_{I_{X,U}}$ Wert nachträglich noch mit einem gewissen τ-Wert zu multiplizieren [21], der die eventuell nicht Gauss'sche Verteilung in Betracht zieht. Für die Fälle ($T = 1$) sowie ($T = 2$), wenn die analytische Linie auf der Untergrundintensität korrigiert wird, berechnet man den

Grenzwert Y_G^x: $Y_G^x = \log(6\, s_{I_{X,U}})$. Das Ausschliessungkriterium aufgrund der am Anfang der Kapitel definierten Voraussetzung lautet entweder $Y_{X,L+U,i,j} < Y_G$ (für die nichtkorrigierten analytischen Linien), oder aber $Y_{X,i,j} < Y_G^x$ (für die auf Untergrund korrigierten Linien). Die erläuterten zwei Kriterien sind besser in ΔY-Werte auszudrücken, da diese den korrigierende Einfluss der Bezugsintensität beinhalten.

Allgemein wird das Ausschliessungskriterium $Y_{X,R,i,j} < Y_{min}$ festgelegt. Der ΔY_{min}-Wert muss für die vier Auswertungsvarianten wie folgt angegeben werden:

$(T = 0)\ \Delta Y_{min} = Y_G - Y_{R,L+U,Z,Q}$; $(T = 1)\ \Delta Y_{min} = Y_G^x - Y_{R,L+U,Z,Q}$

$(T = 2)\ \Delta Y_{min} = Y_G^x - Y_{R,Z,Q}$; $(T = 3)\ \Delta Y_{min} = Y_G - Y_{R,Z,Q}$

Programmierte Lösung der Begrenzungsprozedur

Die programmierte Ausschliessung der nichtzuverlässigen ΔY-Werte sowie die Aufstellung von linearisierten analytischen Eichgeraden beginnt (Abb. 6) mit dem Programm CANCAL, wo die ganze Anfangseingabe-Matrix gespeichert werden muss. Zuerst werden mit diesem Programm die Grund-

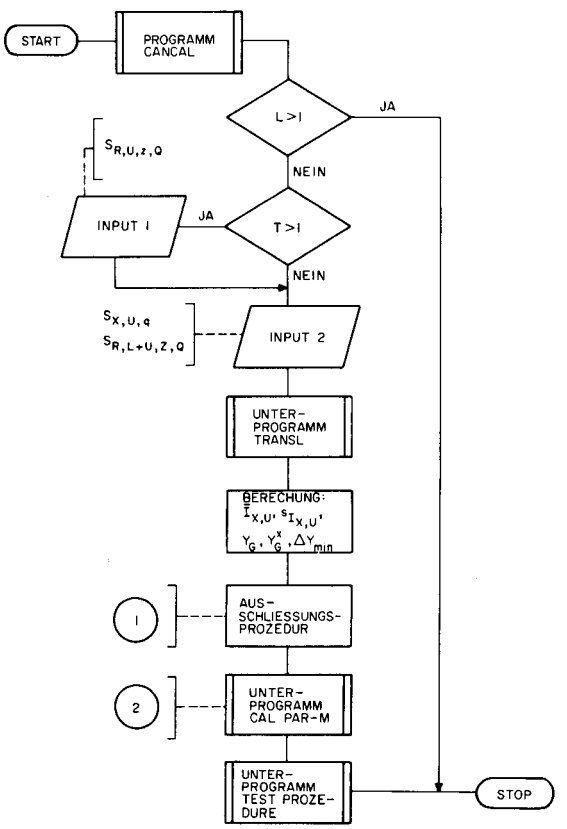

Abb. 6. Allgemeines Flussdiagramm des Programms COLINALCAL ACL-MO-78.

parameter berechnet, sowie schliesslich auch die Testwerte. Falls die Linearität nicht bestätigt wurde, müssen sukzessiv die Werte $S_{R,L+U,Z,Q}$ und $S_{R,U,Z,Q}$, die aus bestimmten (Z, Q)-Spektren zu entnehmen sind, und schliesslich auch eine Reihe von $S_{X,U,q}$-Werten die ähnlich in dem (Z, Q)-Spektrum ausgemessen wurden, eingespeichert werden. Alle Schwärzungswerte werden wiederum anhand der l-Transformation mittels Unterprogramm TRANSL in die l- sowie in relativen I-Werte umgerechnet. Aus dieser Matrix werden die Werte $\bar{I}_{X,U}$, $s_{I_{X,U}}$, Y_G, Y_G^x und ΔY_{min}-Werte ermittelt. Danach folgt die Ausschliessung (Abb. 6, Punkt 1) entsprechend den definierten Kriterien, wobei die angegebenen T-Befehle berüchsichtigt werden. Nach der Ausschliessung der ausreissenden $\Delta Y_{X,R,i,j}$-Werte werden (Abb. 6, Punkt 2) mit dem Unterprogramm CAL PAR-M die kompletten Parameter der analytischen Gerade berechnet, sowie mit dem Unterprogramm TEST PROCEDURE-M die entsprechenden Parameter getestet. Diese zwei erwähnten Unterprogramme unterscheiden sich von den Unterprogrammen des Programms CANCAL nur dadurch, dass sie nicht mit einem für alle j-Konzentrationen konstanten K-Wert der $\Delta Y_{X,R,i,j}$-Werte arbeitet.

Die Linearität der Eichgeraden kann aber auch im Gebiete höheren Konzentrationswerte durch eine einzige Gruppe der $\Delta Y_{X,R,i,j}$-Werte gestört werden (Abb. 7). Diese Störgruppe muss aber anhand eines statistischen Verfahrens festgestellt werden. Der entsprechende t_c-Testwert wird anhand der Vergleichsprozedur zweier arithmetischen Mittelwerte [19—21] berechnet:

$$t_c = |\overline{\Delta Y_j} - \widehat{\Delta Y_j}|/s_{\Delta Y_j} \qquad (15)$$

Die Glieder der Gl. (15) erhält man aus den Gleichungen (5b, 5c und 10). Da aber dieser Störeffekt nur seltener vorkommt, ist er in den angegebenen Programmen noch nicht eingebaut. Bei Eichgeraden, wo die $s_{\Delta Y}$-Werte einer

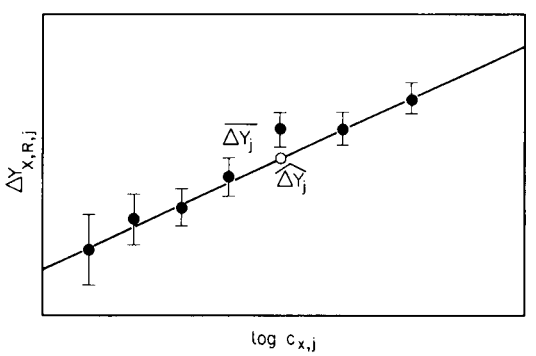

Abb. 7. Veranschaulichung eines signifikant ausreissenden $\overline{\Delta Y_j}$-Wertes.

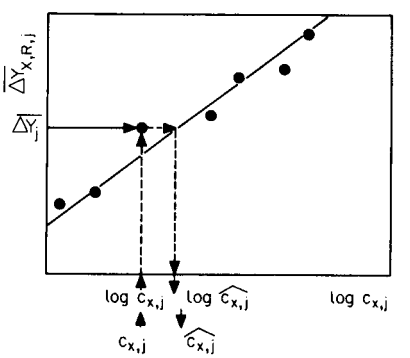

Abb. 8. Schematische Darstellung der Ermittlung des $c_{X,j}$-Wertes.

einzigen Gruppe stark streuen, ist es aber prinzipiell zu empfehlen, alle $\overline{\Delta Y_j}$-Werte anhand der gegebenen Prozedur prüfen zu lassen. Nach der Reduzierung der Glieder der $\{\Delta Y_{X,R,i,j}, c_{X,j}\}$-Matrix um jene Gruppe wo der $\overline{\Delta Y_j}$-Wert signifikant ausreisst, wird die ganze Rechenprozedur von Anfang an wiederholt.

BEWERTUNG DER VERLÄSSLICHKEIT DER EICHKONZENTRATIONSWERTE

Die Anwendung von verlässlichen Eichkonzentrationswerten ist die erste und unumstrittene Voraussetzung für die Aufstellung analytischer Eichgeraden. Bei der Anwendung von natürlichen Bezugsproben sind aber die Eichkonzentrationswerte durch die Streung der angewendeten analytischen Methoden stark belastet. Diese Ungewissheit kann anhand der eventuell vorhandenen zuverlässigen Etalons getestet werden. Leider sind solche Etalons für die breite und bunte Skala von elektrisch nichtleitenden Materialien (Erze, technische Halbprodukte, usw.) meistens nicht vorhanden. Deswegen wurde eine Ersatzprozedur erstellt die es teilweise erlaubt, das gegebene Problem zu lösen. Diese Prozedur setzt aber voraus, dass nur einige wenige Eichkonzentrationswerte falsch sind.

Anhand der laut Gl. (5b) ermittelten $\overline{\Delta Y_j}$-Werte kann durch die Gl. (16) auch ein $\hat{c}_{X,j}$-Hilfswert ermittelt werden (Abb. 8).

$$\hat{c}_{X,j} = \exp\left[(\overline{\Delta Y_j} - A_{X,R})\, B_X^{-1}\right] \tag{16}$$

Aus der Differenz der $\hat{c}_{X,j}$- und $c_{X,j}$-Werte wird weiterhin die Standardabweichung s_{c_X} berechnet:

$$s_{c_X} = \left[(1/M-1)\sum_{1}^{M}(\hat{c}_{X,j} - c_{X,j})^2\right]^{1/2} \tag{17}$$

Gleichzeitig muss man aber anhand der Gl. (16) und (17) auch für die einzelnen $\Delta Y_{X,R,i,j}$-Gruppen, die zu einem gewissen $c_{X,j}$-Konzentrationswert gehören, die Standardabweichungswerte $s_{c_{X,j}}$ ermittel lassen. Bei diesem Rechengang werden aber in der Gl. (16) anstatt der $\overline{\Delta Y_j}$-Wert die einzelnen $\Delta Y_{X,R,i,j}$-Werte und bei der Gl. (17) anstatt der $\hat{c}_{X,j}$-Wert, die ermittelten $\hat{c}_{X,i,j}$-Werte angewendet.

Falls ein $s_{c_{X,j}}$-Wert signifikant vom s_{c_X}-Wert abweicht, kann der entsprechende $c_{X,j}$-Eichkonzentrationswert als nichtzuverlässiger Wert betrachtet werden. Für die Testprüfungen werden die Gleichungen (11a), (11b) und (12) angewendet, Selbstverständlich müssen dabei nicht die Standardabweichungen sondern die quadratischen Abweichungswerte angewendet werden. Die Unterprogramme CAL PAR und CAL PAR-M beinhalten diese Rechengänge, aber die endgültige Entscheidung bei der Reduzierung der Zahl von Eichkonzentrationen muss von Hand gemacht werden. Danach wird die ganze Rechenprozedur wiederholt.

Schlussbemerkung

Die Aufstellung von analytischen Eichgeraden für die Emissionsspektrochemie, die für eine im voraus definierte Konzentrationsspannweite $\langle c_{X,\min}, c_{X,\max} \rangle$ erfolgt, muss auf die Linearität geprüft werden. Die zuständige statistische Methode fusst in der Prüfung der Dichte der durch experimentelle Messung gewonnenen ΔY-Werte um die durch Rechnung ermittelten Gerade. Falls die Linearität bei der ersten Aufstellung nicht erreichbar ist, müssen weitere Bemühungen unternommen werden. Es sind dies die Auswahl die wirksamste Art der Untergrundkorrektur, die eventuelle Blindwertkorrektur, sowie eine Begrenzung der Zahl der Glieder des ursprünglichen Eingangsmatrix $\{\Delta Y_{X,R,i,j}, c_{X,j}\}$.

Für die Berechnung der Grundparameter der analytischen Eichgeraden, inbegriffen deren statistischen Bewertungen, wurde das Grund-Programm CANCAL entworfen, und für die weitere Linearisierung wurde dieses Programm mit einer Ausschliessungsprozedur der nichtzuverlässigen, $\Delta Y_{X,R,i,j}$-Werte ergänzt. Das Programm COLINANCAL sowie das Grundprogramm CANCAL sind in FORTRAN IV geschrieben.

LITERATUR

1 K. Flórián, A. Lavrin und M. Matherny, Chem. Zvesti, 27 (1973) 623.
2 M. Matherny, Wiss. Z. Karl-Marx-Univ. Leipzig, Math.-Naturwiss. R., 28 (1979) 449.
3 H. Kaiser, Optica, 21 (1964) 309.
4 M. Matherny, Chem. Anal. (Warszawa), 21 (1976) 339.
5 M. Matherny, Kém. Közlemények, 52 (1979) 49.
6 B. A. Lomakin, Z. Anorg. Chem., 187 (1930) 75.
7 G. Scheibe und O. Schnettler, Naturwissenschaften, 19 (1931).
8 J. T. M. Malpica, Gen. Elec. Rev., 43 (1940) 288.
9 E. Gegeus und A. Dombi, Acta Chim. (Budapest), 94 (1977) 295.
10 H. Hohnerjäger-Sohn und H. Kaiser, Spectrochim. Acta, 2 (1944) 396.
11 M. Matherny, Anal. Chim. Acta, 112 (1979) 277.
12 T. Török und K. Zimmer, Quantitative Evaluation of Spectrograms by Means of *l*-Transformation, Akadémiai Kiadó, Budapest; Heyden, London, 1972.
13 H. Kaiser, Spectrochim. Acta, 3 (1947) 159.
14 V. K. Prokofjev, Spektralní analysa kovů a slitin, SNTL, Praha, 1954.
15 M. Matherny, Chem. Zvesti, 24 (1970) 112.
16 M. Matherny, Spectrosc. Lett., 6 (1973) 711.
17 M. Matherny, Spectrosc. Lett., 5 (1972) 227.
18 K. Flórián, V. Juričková und M. Matherny, Chem. Zvesti, 25 (1971) 421.
19 J. Swietoslawska, in Spektralna analiza emisyjna: Kap. VII, PAW, Warszawa, 1957.
20 R. S. Burrington und D. C. May, Handbook of Probability and Statistics, 2nd edn., McGraw-Hill, New York, 1970.
21 A. Hald, Statistical Theory with Engineering Applications, Wiley, New York, 1962.
22 IUPAC Compendium of Analytical Nomenclature, Pergamon, Oxford, 1978.
23 E. Krakovská und M. Matherny, Chem. Zvesti, 29 (1975) 177.
24 M. Matherny, Chem. Zvesti, 30 (1976) 153.
25 T. Török, J. Mika und E. Gegus, Spectrochemical Analysis, Akadémiai Kiadó, Budapest; Heyden, London, 1978.
26 H. Kaiser, Fresenius Z. Anal. Chem., 209 (1965) 1.
27 M. Matherny, Fresenius Z. Anal. Chem., 271 (1974) 101.

Analytica Chimica Acta, 133 (1981) 151—168
Computer Techniques and Optimization
Elsevier Scientific Publishing Company, Amsterdam — Printed in The Netherlands

ASSESSMENT OF OIL CONTAMINATION IN THE MARINE ENVIRONMENT BY PATTERN RECOGNITION ANALYSIS OF PARAFFINIC HYDROCARBON CONTENT OF MUSSELS

PETER W. KWAN*

Laboratory for Chemometrics, Chemistry Department, University of Washington, Seattle, Washington 98195 (U.S.A.)

ROBERT C. CLARK, Jr.

Environmental Conservation Division, Northwest and Alaska Fisheries Center, National Marine Fisheries Service, National Oceanic and Atmospheric Administration, 2725 Montlake Boulevard East, Seattle, Washington 98112 (U.S.A.)

(Received 20th July 1980)

SUMMARY

Data on the paraffinic hydrocarbon content of mussels (*Mytilus edulis* and *M. californianus*) were analyzed statistically in an attempt to assess oil contamination of several aquatic areas of the greater Puget Sound basin in the State of Washington. The mussels were collected quarterly over a period of two years from ten locations. Fundamental statistical treatment of the data did not reveal meaningful trends. Application of pattern recognition techniques to the hydrocarbon data set allowed the mussel samples to be successfully classified into groups, from areas near known sources of potential pollution or from areas remote from known pollution. Several samples however, could not be grouped consistently as either from contaminated or uncontaminated sites. In addition, the mussels from a particular area could be separated as to season of sampling. Seasonal variation in levels of individual paraffinic hydrocarbons were greater than annual changes. The n-C_{16} hydrocarbon concentration was the most useful of the 34 features studied for establishing possible oil contamination of the areas. The n-C_{16} hydrocarbon content was also used successfully to detect oil spills and to define uncontaminated locations in Puget Sound.

Aquatic plants and animals can accumulate petroleum hydrocarbons from the environment even when the pollutants are present at very low concentrations [1]. The levels of paraffinic hydrocarbons (C_xH_{2x+2}), one of the major groups of compounds in crude oil and refined petroleum products, in certain aquatic animals can serve as indicators of petroleum pollution in the marine environment [2—4]. With the advent of automated gas chromatography and mass spectrometry, a considerable amount of data on the hydrocarbon content of marine organisms and environmental materials has been published. A recent approach in discerning significant environmental trends in the

*Present address (and author for correspondence): Ameron Corporate Research, 4813 Firestone Blvd., South Gate, California 90280, U.S.A.

0378—4304/81/0000—0000/$02.50

massive tables of newly acquired data, is to apply a family of computer-assisted mathematical analysis techniques, collectively known as pattern recognition analysis.

Pattern recognition techniques have been successfully applied in a wide variety of analytical chemical studies involving, for example, spectrophotometric and forensic investigations [5—9]. Application to petroleum pollution research was first undertaken by Duewer et al. [10] to identify sources of oil spills. In the present study, pattern recognition techniques were applied to the analysis of paraffinic hydrocarbon data from mussels collected in the greater Puget Sound basin of Washington. The principal objective was to apply pattern recognition to a suite of mussel hydrocarbon values to determine if it was possible to relate different areas in Puget Sound to nearby potential sources of petroleum pollution. The combination of pattern recognition and paraffinic hydrocarbon analyses was chosen to examine the trends in pollutant content in mussels from the Puget Sound area which has not yet experienced serious water quality degradation.

TABLE 1

Sampling sites

Site code	Site name	Number of mussel samples	Pollution characteristics of the site
Baseline sampling program			
1	Armeni	8	Seattle's harbor; commercial/industrial
2	Mukilteo	8	Marine transportation; fuel depot
3	Cherry Point	8	Refinery area
4	Manchester	8	Marine transportation; fuel depot
5	March Point	8	Refinery area
6	Sequim	8	Remote; oil pollution research lab.
7	Seabeck	8	Remote
8	South Puget Sound	8	Remote
9	Fauntleroy	8	Remote
10	Freshwater Bay	8	Remote
Oil spill study programs			
Anacortes spill 1971			
11	Guemes Island Central	1	Fuel oil spill
12	Saddlebag Island	1	Fuel oil spill
13	Guemes Island Southwest	1	Reference area
14	Decatur Island	1	Reference area
General M.C. Meigs spill 1972			
15	Orange Rock — 1	1	Unknown exposure, 1 month after spill
	— 2	1	Unknown exposure, 2 months after spil
Manchester spill 1974			
16	Exposed rock	1	Unknown oil spill
	Reference rock	1	Reference area

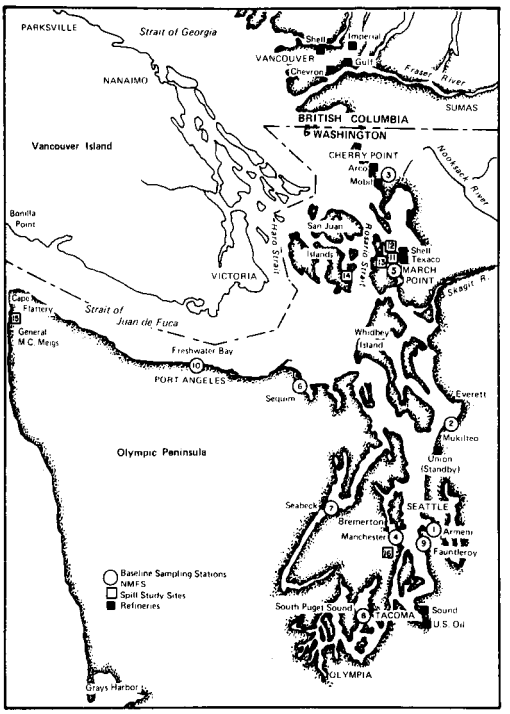

Fig. 1. Map of the greater Puget Sound basin showing hydrocarbon baseline sampling stations and oil refineries.

EXPERIMENTAL

Samples

Mussels (*Mytilus edulis* and *M. californianus*) were collected quarterly over a period of two years (1971 and 1972) at 10 sites in the greater Puget Sound basin of Washington (Table 1). Locations of these sites are shown in Fig. 1. The two-year sampling program was designed to provide data on existing or baseline levels of paraffinic hydrocarbons in mussels from a variety of environmental locations. The ten sites included regions containing refineries (Cherry Point and March Point), industrial and commercial waterways (Armeni, Mukilteo, and Manchester), and areas remote from known sources of petroleum pollution (South Puget Sound, Seabeck, Fauntleroy, Freshwater Bay, and Sequim). Three additional locations previously exposed to oil spills (Guemes Island [11], the "General M. C. Meigs" grounding site [12–14], and Manchester), were selected to evaluate how data from spill-exposed areas would fit into pattern recognition analysis. One sample consisting usually of 6–14 individuals was collected at each site during each of four seasons giving a total of 80 samples for the two-year study. Concentrations of 26 paraffinic hydrocarbons (n-$C_{14}H_{30}$ through n-$C_{37}H_{76}$ plus pristane and phytane) in mussels were determined by gas chromatography

[15, 16]. Eight additional parameters derived from these measurements were generated.

Pattern recognition analysis

Pattern recognition was applied to the biological data without reference to environmental conditions or restraints on the data, i.e., the pattern recognition was conducted blind. Once the pattern recognition analysis was completed, the results were assessed with regard to sample location, oceanographic conditions, proximity to potential petroleum sources, seasonal variations, and actual spill events.

In the pattern recognition terminology, each individual mussel sample is an "object" and each of the 34 variables is used to generate "features" which may be simple measurements, some mathematical transformations of the measurements, or combinations of both. The features define a data vector for each of the objects. Defined groups of data vectors, such as sampling sites, are called categories.

The data were analyzed using a batch-process version of ARTHUR [17, 18] which contains more than 40 statistical and pattern recognition methods in FORTRAN. All processing was done on the CDC 6400 computer at the University of Washington Academic Computer Center. The techniques used were largely nonparametric, making no or only minimal assumptions about the underlying statistics of the data. Brief descriptions of the series of operations performed on the data set are as follows.

Autoscale. The effect of the differing measurement magnitudes was compensated by normalizing the measurements. Thirty-four features with uniform means of zero and variances of unity are formed by first subtracting the measurement mean from the individual values, then dividing by the total measurement variance [19].

Correlation matrix. The interdependence of the 34 measurements was investigated by using the standard statistical intermeasurement correlation matrix.

Weight. Weight is a preprocessing method that weights each feature on the basis of its individual importance to the solution of a pattern recognition problem. Once the various measurements have been autoscaled to allow comparison, weighting methods determine which of these new features are useful for separation of the categories and should be enhanced or weighted, and which new features are not useful and can be de-emphasized, or even eliminated. The utility of each feature in separating the various mussel samples is assessed by calculating for each feature the multicategory variance and Fisher weights which are the geometric and arithmetic averages, respectively, of the inter—intra category weights [19].

Select. This method is an iterative feature selection procedure that generates orthogonal features based on their importance to classification [20]. The criterion for importance of categorized data is the variance weight. The feature with the highest weight is selected as the first feature. The

remaining features are then decorrelated from it. The decorrelated features are reweighted and the feature now with the highest weight becomes the second selected feature. The process continues until either a specified number of features has been chosen or the weight of the last selected falls below a preset limit.

Karlov (Karhunen—Loeve Transform). The K—L transform consists of a combination of subroutines essentially performing a principal component analysis. It is often used as a method of reducing the dimensionality of a data set [19]. It was used here to project data from higher dimensional space onto two dimensions for display.

Least. This approach utilizes the least-squares multi-linear regression method to calculate weight vectors which are used for property prediction or category classification [17].

K-nearest neighbor analysis (KNN). KNN classifies unknown data vectors using their interpattern distances to data vectors in the training set as the decision criterion [21]. Generalized Euclidean n-space distance was used here. A data vector is classified into the category which contributes the greatest number of the k nearest data vectors in the training set. For this study, the results of the 1-nearest neighbor are presented.

Statistical isolinear multiple component analysis (SIMCA). SIMCA is a classification method made up of five independent routines to facilitate disjoint principal component analysis of categorized data [22]. A specified number of principal components is extracted from each category in turn. These components are then classified on the basis of Euclidean distance from each data vector to the function defined by the components of each category.

Although this data set does not include any information about experimental errors, it should be noted that ARTHUR is also designed to handle data sets with known uncertainties in the measurements. The uncertainties form a matrix which corresponds to, and is of the same dimensions as the data matrix. Therefore, each measurement in the data matrix is treated as a mean value with a probability distribution defined by its error.

RESULTS AND DISCUSSION

Typical results for the paraffinic hydrocarbon content of mussels from two locations are given in Table 2. The 34 features used in the pattern recognition analysis are denoted in the first column. Differences between the two data sets based solely on a visual examination of the 34 features did not unequivocally demonstrate that these samples were the same or different. When such tabulated displays are increased by a factor of 40 for the total of 80 samples used here, conclusions based on visual examination of the data become difficult if not impossible, because of the small differences between the values of the 34 features (26 independently varying measurements) and the large numbers of samples.

TABLE 2

Paraffinic hydrocarbon data sheet

Used in pattern recognition	Feature[a]	Mussel sample	Mussel sample
—[b]	Location	Armeni	Fauntleroy
—[b]	Date collected	Fall '72 (10/22/72)	Fall '72 (10/22/72)
—	No. of individuals	41	11
—	Wet weight (g)	62.20	55.06
—	Dry shell wt. (g)	46.27	46.89
—	Dry residue wt. (g)	2.9443	3.3326
—	Organic extract wt. (g)	0.5120	0.5715
—	Dry extracted wt. (g)	3.4563	3.9041
	Carbon no.	ng g^{-1} (dry wt.)	ng g^{-1} (dry wt.)
—	10	<20	48.7
—	11	48.1	3.10
—	12	1,070	21.8
—	13	494	6.19
X	14	449	39.2
X	15	252	206
X	16	415	126
X	17	540	157
X	Pristane[c]	1,990	1,820
X	18	664	2.55
X	Phytane[d]	<40	5.11
X	19	145	237
X	20	390	37.2
X	21	794	445
X	22	163	100
X	23	524	124
X	24	207	115
X	25	703	312
X	26	<20	391
X	27	128	1,050
X	28	119	1,950
X	29	399	3,050
X	30	806	2,940
X	31	1,660	2,920
X	32	1,450	1,390
X	33	259	1,100
X	34	155	360
X	35	186	289
X	36	823	22.8
X	37	487	6.08
X	Total HCs (ppb)	15,300	19,300
X	n-C_{17-37}	11,700	17,400
X	CPI_{14-20}[e]	0.63	3.65
X	CPI_{20-36}	1.33	1.28
X	n-C_{17}/pristane ratio	0.27	0.068

TABLE 2 (continued)

Used in pattern recognition	Feature[a]	Mussel sample	Mussel sample
—	n-C_{18}/phytane ratio	—	0.50
X	C_{17}/baseline (g.c.) ratio	1.38	2.12
X	C_{16} ratio	28.2	138
X	Solvent extractables[f]	148,100	146,500 ppm
—	Major HC (all)	pristane: 13%	n-C_{29}: 16%
—	Major n-C_{14-37}	n-C_{31}: 14%	n-C_{29}: 18%

[a]For description of features, see Clark and Finley [15]. [b]Used to identify each sample geographically and seasonally. [c]2, 6, 10, 14-Tetramethylpentadecane. [d]2, 6, 10, 14-Tetramethylhexadecane. [e]Carbon preference index. [f]Total solvent extractables by Soxhlet (ppm).

A correlation matrix of the 34 features is shown in Table 3. Values greater than ±0.7 are underlined and considered highly correlated. This matrix shows the correlation for all 34 paraffinic hydrocarbon features based on patterns occurring in all 80 mussel samples. For instance, at all sampling sites, n-C_{16} correlates highly with n-C_{15}, phytane, n-C_{19}, and n-C_{20} (0.722, 0.723, 0.718, and 0.765, respectively) but less well with n-C_{14}, n-C_{17}, pristane, and n-C_{18} (0.445, 0.589, 0.343, and 0.645, respectively) and poorly with such features as n-C_{37} (0.062), Carbon Preference Index over the range of C_{20}—C_{36} (CPI_{20-36}) (−0.051), n-C_{17}/pristane ratio (−0.016), or total solvent extractables (−0.178). Negative values denote an inverse relationship between features being compared.

The levels of n-C_{24} to n-C_{35} paraffinic hydrocarbons were highly correlated and, in some cases, correlations of over 0.9 occurred. As expected, total hydrocarbons and total n-paraffins over the range C_{14}—C_{37} showed positive correlations with the levels of parafffinic hydrocarbons from which these two features were derived. In contrast, the last six features of Table 3 were mostly negatively correlated to the rest of the features.

An attempt was made to distinguish the 10 sampling sites by classifying the characteristic levels of paraffinic hydrocarbons in mussels from each site. There are 34 features for each sample, thus each can be described as a point in a 34-dimensional space where each axis represents one feature. Distributions and variances of these samples can be examined visually by K—L projection of these data points from the original 34-dimensional space onto a 2-dimensional plot. The projection is done in such a way as to preserve the maximum variance among these data points. Classification of these 10 sampling sites simultaneously could not be achieved. Even though there were differences in the 10 sites as reflected by the concentration of paraffinic hydrocarbons in the mussel samples, seasonal and annual variations in hydrocarbon levels in mussels made characterization of the sites difficult.

TABLE 3

Correlation matrix

	n-C_{14}	n-C_{15}	n-C_{16}	n-C_{17}	Pris.	n-C_{18}	Phyt.	n-C_{19}	n-C_{20}	n-C_{21}	n-C_{22}	n-C_{23}	n-C_{24}	n-C_{25}	n-C_{26}	n-C_{27}	n-C_{28}
n-C_{14}	1.000																
n-C_{15}	.556	1.000															
n-C_{16}	.445	.722	1.000														
n-C_{17}	.220	.364	.589	1.000													
Pris.	.165	.330	.343	.126	1.000												
n-C_{18}	.265	.455	.645	.464	.453	1.000											
Phyt.	.368	.586	.723	.241	.176	.208	1.000										
n-C_{19}	.306	.491	.718	.554	.287	.488	.431	1.000									
n-C_{20}	.242	.505	.765	.689	.245	.643	.459	.588	1.000								
n-C_{21}	.080	.234	.359	.209	.230	.463	.179	.424	.447	1.000							
n-C_{22}	.099	.217	.370	.355	.198	.384	.144	.325	.441	.340	1.000						
n-C_{23}	.091	.205	.255	.096	.221	.527	.080	.179	.403	.466	.451	1.000					
n-C_{24}	.027	.095	.197	.230	.097	.328	.066	.090	.299	.232	.536	.649	1.000				
n-C_{25}	—.005	.116	.208	.301	.073	.280	.091	.032	.250	.004	.364	.449	.861	1.000			
n-C_{26}	.017	.090	.150	.163	—.018	.164	.110	.036	.188	.043	.437	.474	.897	.796	1.000		
n-C_{27}	.061	.157	.227	.154	—.012	.241	.198	.117	.257	.180	.464	.521	.850	.745	.942	1.000	
n-C_{28}	—.013	.084	.137	.063	—.033	.089	.201	.020	.110	.011	.350	.416	.762	.737	.846	.890	1.000
n-C_{29}	.034	.225	.261	.082	.027	.185	.319	.158	.240	.171	.367	.398	.622	.566	.675	.794	.881
n-C_{30}	.066	.296	.295	.063	.164	.384	.268	.162	.308	.153	.300	.552	.630	.582	.621	.704	.786
n-C_{31}	.131	.361	.332	.144	.206	.458	.231	.164	.332	.072	.333	.431	.550	.571	.535	.590	.658
n-C_{32}	.011	.285	.168	.031	.171	.310	.122	.057	.182	—.033	.196	.364	.410	.451	.363	.367	.485
n-C_{33}	—.020	.272	.129	.023	.287	.309	.058	.047	.149	—.061	.105	.349	.368	.412	.288	.272	.408
n-C_{34}	.077	.270	.153	.009	.360	.455	—.011	.076	.198	—.004	.082	.461	.277	.316	.139	.095	.172
n-C_{35}	.118	.257	.229	.080	.314	.506	.037	.099	.228	—.019	.255	.399	.382	.422	.245	.193	.253
n-C_{36}	.091	.189	.135	—.001	.297	.368	—.007	.066	.128	.117	.336	.474	.583	.653	.450	.427	.443
n-C_{37}	.007	.191	.062	—.015	.379	.351	.016	.050	.115	.059	.138	.265	.146	.181	—.002	—.031	.019
Total HC	.487	.644	.675	.405	.501	.685	.460	.517	.606	.382	.471	.610	.613	.551	.506	.573	.532
n-C_{14-37}	.374	.546	.606	.432	.305	.641	.394	.434	.586	.294	.504	.596	.716	.669	.631	.688	.672
CPI_{14-20}	—.219	—.074	—.315	.010	—.256	—.358	—.205	—.214	—.255	—.252	—.241	—.293	—.249	—.265	—.168	—.206	—.169
CPI_{20-36}	.023	—.041	—.051	—.093	.328	—.039	—.064	—.037	—.136	.125	—.197	—.117	—.211	—.123	—.172	—.163	—.247
n-C_{17}/Pris.	—.071	—.038	—.016	.393	—.350	—.120	—.106	—.003	.165	—.104	.035	—.017	—.002	.042	—.007	—.066	—.075
n-C_{17}/BL	—.179	—.089	—.238	—.044	.218	—.286	—.164	—.213	—.192	—.213	—.188	—.245	—.257	—.287	—.216	—.262	—.055
n-C_{16} ratio	—.153	—.251	—.271	—.198	—.253	—.221	—.155	—.190	—.205	—.159	.098	.071	—.024	—.143	—.052	—.057	.016
Extractables	—.181	—.181	—.178	—.098	.169	.026	—.170	—.223	—.219	.002	.186	.008	.134	.124	.182	.121	.174

TABLE 3 (continued)

	n-C_{29}	n-C_{30}	n-C_{31}	n-C_{32}	n-C_{33}	n-C_{34}	n-C_{35}	n-C_{36}	n-C_{37}	Total HC	n-C_{14}-C_{37}	CPI $_{14-20}$	CPI $_{20-36}$	n-C_{17} pris.	n-C_{17} BL	n-C_{16} ratio	Extract-ables
n-C_{29}	1.000																
n-C_{30}	.903	1.000															
n-C_{31}	.803	.918	1.000														
n-C_{32}	.636	.784	.909	1.000													
n-C_{33}	.514	.696	.808	.913	1.000												
n-C_{34}	.271	.574	.679	.760	.872	1.000											
n-C_{35}	.365	.601	.746	.777	.826	.914	1.000										
n-C_{36}	.380	.528	.609	.589	.553	.568	.635	1.000									
n-C_{37}	.124	.306	.469	.631	.628	.621	.628	.547	1.000								
Total HC	.630	.740	.758	.592	.567	.554	.605	.584	.371	1.000							
n-C_{14-37}	.752	.839	.864	.703	.643	.571	.653	.611	.367	.948	1.000						
CPI_{14-20}	—.193	—.250	—.260	—.185	—.184	—.208	—.235	—.268	—.226	—.377	—.332	1.000					
CPI_{20-36}	—.235	—.290	—.225	—.235	—.193	—.155	—.131	—.043	—.048	—.100	—.224	—.074	1.000				
n-C_{17}/Pris.	—.099	—.146	—.085	.008	.026	—.017	—.055	—.139	—.119	—.132	—.044	.222	—.150	1.000			
n-C_{17}/BL	—.282	—.305	—.306	—.226	—.086	—.097	—.213	—.220	—.151	—.279	—.343	.489	.083	.078	1.000		
n-C_{16} ratio	—.027	—.063	—.058	.024	—.012	—.053	—.081	—.129	.047	—.218	—.151	.229	—.214	.160	.100	1.000	
Extractables	.003	—.007	—.020	—.059	—.029	—.030	.035	.152	—.050	—.040	—.046	.036	.115	—.188	.228	—.052	1.000

Nevertheless, this preliminary study of the data set provided some insight into the properties of these samples. Data on samples from some sites clustered, whereas data from samples from other sites had large scatter. This suggested that mussels from some sampling sites showed similar paraffinic hydrocarbon compositions and could be grouped together as a category. Two categories were formed; category A consisted of data for samples from Armeni, Mukilteo, and Cherry Point, and category B consisted of data from mussel samples from Seabeck, South Puget Sound, Fauntleroy, and Freshwater Bay. Data from samples from other sites (Manchester, March Point and Sequim) were distributed between categories A and B so that no distinct group could be formed.

The data sets in Table 2 for two mussel samples are without distinguishable qualities. However, when taken in context with data from the remaining 78 samples, the two sets could be separated into different categories by use of pattern recognition.

Table 4 shows the means and ranges of values for the hydrocarbons in the mussels arranged by categories A and B, and unclassified. Values for individual features in all three groups show considerable overlap. The following discussion focuses on samples from the two distinct groups, categories A and B.

Geographic variations

K—L projection of data vectors of mussel samples from categories A and B from 34-dimensional space onto a 2-dimensional plot preserving 49% of total variance is shown in Fig. 2. Even though 51% of the total variance was lost during the transformation, 49 data vectors could be separated into clusters of the two categories with only 7 data vectors misclassified (i.e. not fitting the dominant pattern of the figure). The data were also classified by using the LEAST, SIMCA, and KNN techniques (Table 5). Completely correct classification of samples of category A from those of category B was achieved by LEAST using all 34 features. Some reservations concerning the result necessarily exist when all 34 features are used, because the data vector: feature ratio (56:34) was low. For the result to be statistically valid, this ratio should be greater than 4:1 and preferably over 10:1. The data vector: feature ratio can be increased by selecting fewer features.

The second column (all four seasons) of Table 6 shows the three most distinctive features and their respective variance weights for the SELECT method. When these three features were used, at least 87% accuracy of classification was achieved by use of the LEAST and SIMCA methods (Table 5). The n-C_{16} paraffinic hydrocarbon feature was first selected in the seasonal groups; it also showed the greatest variance weight among the six most important features in Table 6. Thus, the n-C_{16} ratio is the most diagnostic feature in distinguishing between mussels collected at sites in category A and those collected at sites in category B. This result was based on the results of the pattern recognition analysis where the n-C_{16} ratio was just one of 34 equally-weighted parameters analyzed (Table 2). Clark and Finley [15]

TABLE 4

Ranges and means of features for mussels collected at different sites

Feature	Category A			Category B			Other sites		
	Armeni, Mukilteo, Cherry Point			Seabeck, South Puget Sound, Fauntleroy, Freshwater Bay			Manchester, March Point, Sequim		
	Max.	Min.	Mean[a]	Max.	Min.	Mean	Max.	Min.	Mean
n-C_{14}	11,000	21.8	1,600	673	0.24	42.4	632	0.73	1.08
n-C_{15}	1,710	42.1	496	1,590	<4	170	1,800	1.25	201
n-C_{16}	1,500	49.5	528	435	1.1	90	3,100	1.70	262
n-C_{17}	4,840	133	1,570	2,690	5.2	551	4,710	19.1	920
Pristane	7,260	756	2,690	9,880	39.7	1,450	5,760	55.6	1,550
n-C_{18}	2,750	17.4	667	596	2.55	77.2	1,540	3.63	280
Phytane	613	<10	116	481	<1	22.2	1,210	<1	90
n-C_{19}	2,590	<10	467	187	<4	67.8	1,980	<4	207
n-C_{20}	1,560	26.1	460	1,770	0.26	149	1,760	0.01	245
n-C_{21}	3,230	6.9	534	681	6.79	165	1,200	29.9	316
n-C_{22}	1,260	<5	233	758	<2	138	519	0.09	130
n-C_{23}	1,770	34.9	423	641	<2	181	1,400	6.02	251
n-C_{24}	1,170	6.8	398	2,020	<1	232	2,170	<4	254
n-C_{25}	1,890	112	709	3,660	10	327	2,740	14.6	431
n-C_{26}	986	<2	242	2,220	3.81	236	3,270	<5	285
n-C_{27}	1,440	<2	330	2,320	0.3	240	3,420	1.04	350
n-C_{28}	2,030	<2	355	3,070	<1	376	3,650	14.0	471
n-C_{29}	3,340	<2	615	3,050	0.6	480	3,010	<5	475
n-C_{30}	3,260	13.3	884	2,940	<1	583	2,530	<5	537
n-C_{31}	4,650	103	1,100	3,210	<1	599	1,900	<5	492
n-C_{32}	3,960	<2	551	1,430	0.93	336	818	<6	224
n-C_{33}	3,810	<5	458	1,100	<1	226	763	3.09	230
n-C_{34}	2,770	<10	414	561	<1	130	371	4.80	84.5
n-C_{35}	2,210	<10	416	738	<1	120	681	<6	103
n-C_{36}	848	4.6	238	1,240	<1	103	573	0.49	77.1
n-C_{37}	892	<10	147	399	<1	61.8	535	4.59	67.7
Total HC	41,800	2,810	18,800	34,100	495	7,200	33,500	919	8,470
n-C_{14-37}	33,700	1,920	13,900	32,300	410	5,700	27,900	771	6,690
CPI_{14-20}	9.91	0.22	1.91	19.8	1.27	5.22	8.40	0.26	2.95
CPI_{20-36}	7.17	0.97	1.75	4.3	0.75	1.34	3.14	0.84	1.56
n-C_{17}/Pris.	3.72	0.03	0.85	7.9	0.01	1.42	8.95	<0.01	1.25
n-C_{17}/BL	6.18	1.04	1.83	14.1	1.43	3.88	6.59	1.27	2.38
n-C_{16} ratio	74.3	10.1	34.3	1,270	15.7	206	795	8.54	109
Extractables	193,600	47,700	130,000	225,800	102,300	142,900	272,000	112,600	159,800

[a]Arithmetic mean.

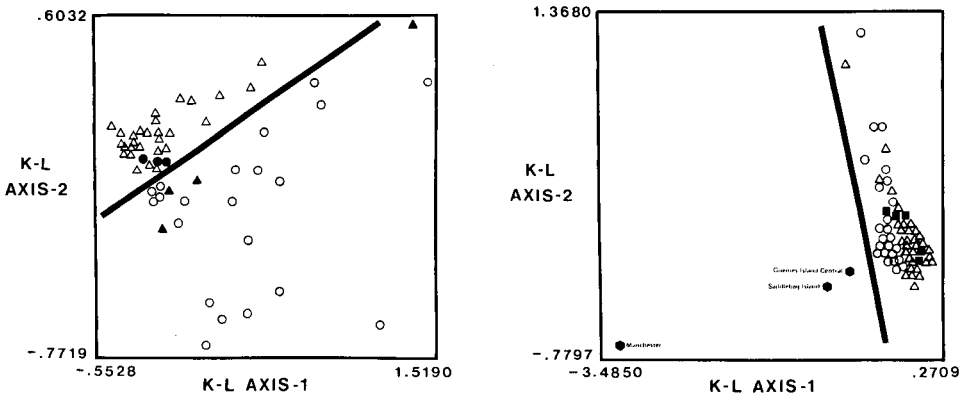

Fig. 2. K—L projection of the data vectors of 56 mussel samples representing 7 locations from 34-dimensional space onto a 2-dimensional plot preserving 49% of the total variance. (○) Category A; (△) category B; (●, ▲) misclassified samples.

Fig. 3. K—L projection of the data vectors of 56 mussel samples representing 7 locations plus 5 reference and three spill samples from 34-dimensional space onto a 2-dimensional plot preserving 66% of the total variance. (○) Category A; (△) category B; (◆) spill mussel samples; (■) reference samples.

suggested that the n-C_{16} ratio might be a useful diagnostic parameter for interpreting oil pollution in marine organisms; the present evaluation of the paraffinic hydrocarbon data from mussels supports this earlier contention.

LEAST gave an 86% accuracy of classification, utilizing only the n-C_{16} ratio. This result is slightly lower than the values of 100 and 91% which were obtained by LEAST when 34 and 3 features were used respectively (Table 5).

TABLE 5

Classification results for category A and category B, based on samples collected during different seasons

Numbers of features	Classification method	Samples correctly classified into category A[a] or B[b] (%)		
		56 samples from spring, summer, fall, winter (%)	28 samples from spring, summer (%)	28 samples from fall, winter (%)
34	LEAST	100	100	100
	SIMCA	79	83	84
	KNN	77	75	64
3	LEAST	91	93	93
	SIMCA	87	92	89
	KNN	77	86	79
1	LEAST	86	93	89

[a]Armeni, Mukilteo, Cherry Point.
[b]Seabeck, South Puget Sound, Fauntleroy, Freshwater Bay.

TABLE 6

SELECT results for seasonal and spill cases[a]

Feature rank	Category A Category B			Category A and category B Category C
	Spring, summer, fall and winter	Spring and summer	Fall and winter	Spring, summer, fall and winter
1	n-C_{16} (2.12)[b]	n-C_{16} (2.48)	n-C_{16} (2.22)	n-C_{16} (1.49)
2	CPI [c] C_{20-36} (1.12)	n-C_{28} (1.28)	CPI C_{20-36} (1.19)	n-C_{16} ratio (1.41)
3	n-C_{17}/Baseline (g.c.) (1.10)	n-C_{19} (1.24)	n-C_{17}/Baseline (g.c.) (1.13)	n-C_{17}/Baseline (g.c.) (1.23)

[a]Categories A and B as in Table 5. Category C includes spill and reference samples.
[b]Variance weight. [c]Carbon Preference Index.

The concentrations of the n-C_{16} hydrocarbon were on average higher in mussels collected at Armeni, Mukilteo, and Cherry Point (category A). These sites are subject to heavier marine traffic and are closer to sources of potential petroleum pollution than category B sites. Accumulation from the aquatic environment could account for the higher level of total n-C_{16} paraffinic hydrocarbons. Based on the results from over a thousand analyses of a variety of aquatic organisms from a wide number of locations as well as literature searches (e.g., [1]), the n-C_{16} content is a minimum compared to n-C_{15} or n-C_{17} content in uncontaminated marine organisms. However, most hydrocarbon patterns in petroleum materials (including those of contaminated organisms), contain all three hydrocarbons at about the same level [15].

An additional group of 1,156 features (all possible ratios of the 34 features) was also investigated. Because these ratios are nonlinear combinations of the measurements, the ratio features usually bear a higher discriminatory power for classification. Only two of the ratio features, n-C_{16}/n-C_{17} BL (n-C_{16} content compared with the gas chromatographic baseline measured at n-C_{17}) and the pristane/n-C_{17} BL showed variance weights (2.16 and 2.15, respectively) slightly higher than that of n-C_{16} (2.12). Therefore, classification results achieved using these two ratio features did not show any significant improvement over those obtained when n-C_{16} alone was used. Under these circumstances, n-C_{16} continues to be preferred over the two ratio features as the key feature. The use of ratio features may bring more information to bear on some problems but can lead to difficulties in applying the results to environmental situations since they may be difficult to interpret.

Nevertheless, the use of ratio features should not be overlooked in future studies especially if their variance weights are considerably higher than those of features which are formed from measurements or linear combinations of

measurements. The data set available here was internally consistent so that it was possible to employ absolute concentrations of paraffinic hydrocarbons as well as normalized parameters (i.e. CPIs, n-C_{17}/pristane, n-C_{17}/BL, n-C_{16} ratio); however, under other circumstances it may be desirable to use only normalized or relative values, especially when comparing data obtained by different laboratories or analytical procedures.

By use of the various pattern recognition methods, the mussel samples could be grouped into two distinct categories. Quarterly-collected samples from three sites (Manchester, March Point, and Sequim) fell into both categories. An environmental evaluation of the ten sites strongly supports the statistical results.

Category A mussels came from areas which could be exposed to petroleum pollutants. Armeni is adjacent to a boat launching ramp in Elliot Bay, the major commercial harbor of the Pacific Northwest. Mukilteo is located near a military fuel depot, a marine state park having boat launching facilities, marinas, a ferry landing, and a turning point for a major navigation route to the port of Everett. Cherry Point is near two large oil refineries and an aluminium-reduction facility, all of which are dependent on waterborne transport of raw materials.

Category B mussels came from areas generally remote from known sources of recurring petroleum pollution (land runoff from industrial, urban and populated areas, sewage, downwind airborne fallout, commercial and recreational boating, etc.). These samples contained the lowest levels of n-C_{16} content and the highest n-C_{17}/baseline ratio; both of these indicate lack of petroleum contamination [15]. These samples also displayed the largest odd-carbon predominance over the range n-C_{20} to n-C_{36} (CPI_{20-36}) which is indicative of biogenic terrestrial hydrocarbon input [23].

Samples of mussels that fell into both categories at various times are subject to intermittent petroleum pollution. Manchester is located near one of the largest U.S. Navy fuel depots on the West Coast and is on the edge of a narrow passage leading to the port of Bremerton, where incidences of oil pollution had been reported. The March Point site is adjacent to two major oil refineries and is also subject to seasonal boat traffic. Sequim is remote from sources of pollutants, but midway through the two-year sampling period it was subjected to oil pollutants introduced during a carefully controlled experimental study on the biological effects of oil pollution. Apparently, the present paraffinic hydrocarbon baseline sampling program was sufficiently sensitive to detect the uptake of very low levels of petroleum hydrocarbons in mussels during certain periods corresponding to the local oil exposure study. Thus, the samples from these three sites would fall into category A or B, depending on the conditions of the environment just prior to the time of sampling.

Seasonal variations

In order to gain some understanding of seasonal variations in levels of paraffinic hydrocarbons, classification to categories A and B was performed

on data from each season and for all possible combinations of the four seasons. The best correlation resulted (Table 5) when samples collected in spring and summer were combined for comparison with fall and winter. The results indicated that hydrocarbon levels in mussels collected during the first half of a year at a particular site were similar, and the same was true for mussels collected in the second half of the year. Moreover, the concentrations of paraffinic hydrocarbons in samples collected during the first half of a year were different from those collected during the latter half at the same site. This may be explained by the change in food sources and by maturation of the mussels as the year progressed [24]. The difference is illustrated by the SELECT results (Table 6). Even though the level of n-C_{16} paraffinic hydrocarbon was still the most important feature for classifying samples into categories A or B during both periods, the second and third ranked features were different.

Annual variations in levels of paraffinic hydrocarbons in mussels were also examined by a similar approach. Data from samples collected during the same season in 1971 and 1972 were classified into categories A and B. No significant differences in selected features nor in classification results were observed. Apparently annual variations in hydrocarbon levels in mussel samples collected at the same sampling site were small during the two-year period.

Oil spill studies

Three mussel samples collected after oil spills along with three unexposed (reference) and two unknown condition samples from Orange Rock were compared with those in categories A and B (Table 1). Visual examination of the data revealed significantly higher levels of most paraffinic hydrocarbons in the spill-exposed samples. No obvious differences existed between reference samples and those in baseline categories A and B. K—L projection of the entire data set is shown in Fig. 3. The projections of the three spill samples were separated from the rest; the three reference and two unknown condition samples were clustered together among the baseline mussel data vectors. The spill samples were then removed from the data set and the remaining data vectors were projected from 34-dimensional space onto a 2-dimensional plot (Fig. 4). The two unknown samples from Orange Rock and the reference sample from Manchester were classified as category A while two other reference samples from Guemes Island Southwest and Decatur Island were classified as category B. Classification by LEAST, SIMCA and KNN gave the same results.

Orange Rock sample 1 was collected in the vicinity of the wreck of the troopship "General M. C. Meigs" within the first month of the grounding; Orange Rock sample 2 was collected one month later. On the K—L projection (Fig. 4) these samples fell into the group of baseline samples exposed to suspected pollution (category A); hence, both Orange Rock mussel samples were contaminated but not to the degree of the Anacortes or

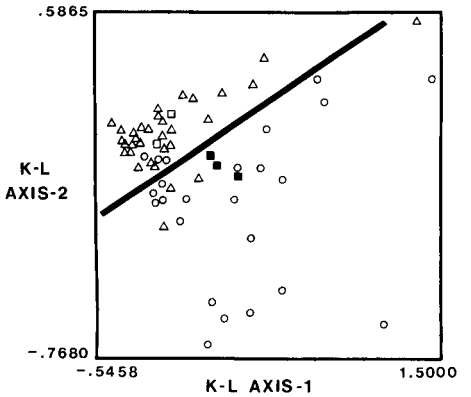

Fig. 4. K—L projection of the data vectors of 56 mussel samples representing 7 locations plus 5 reference samples from 34-dimensional space onto a 2-dimensional plot preserving 49% of the total variance. (○) Category A; (△) category B; (■) reference samples (exposed; Orange Rock 1 and 2 and Manchester); (□) reference samples (remote; Guemes Island SW and Decatur Island).

Manchester spill samples. The Manchester reference sample was, similarly, from an area susceptible to occasional minor oil spills and was grouped with the more polluted category A baseline samples. The reference samples from Guemes Island Southwest and Decatur Island were from areas normally remote from known sources of recurring pollution and so grouped with category B baseline samples.

Applications

The examples described above demonstrate the usefulness of pattern recognition analysis applied to a large set of data (over 2,700 individual values). The original data showed a relatively small range of values and could not be classified by simple correlative or visual evaluation. By pattern recognition, it was possible to establish several categories (i.e. remote uncontaminated sites, contaminated sites, low-level or intermediate sites, and spill case sites). These groups represented locations that could be described by environmental parameters relating to possible petroleum exposure. These examples showed how a number of subtle differences between locations can be quantified and combined mathematically to obtain an overview of the baseline conditions within a geographic area generally regarded as only lightly affected by petroleum development [25, 26].

This pattern recognition analysis serves as a suitable example of the usefulness of the technique. However, a cautionary note must be made: as we understand more about the metabolism of petroleum hydrocarbons, it becomes clear that many marine organisms have an ability to convert petroleum hydrocarbons to metabolites which are not detected by conventional analytical methods for hydrocarbons. While mussels may be suitable for some studies [4], other marine organisms may not be. For example,

the conversion of aromatic hydrocarbons to oxygenated derivatives occurs through the action of mixed function oxygenase systems in many marine organisms, through microbial activity, or through non-enzymatic chemical reactions in the environment. When marine animals are placed in clean sea water, most of the accumulated hydrocarbons are eventually discharged [27, 28]. Hence, it is valid to query the value of trying to assess petroleum pollution of an ecosystem based solely on routine low-level (ng g^{-1}) paraffinic and aromatic petroleum hydrocarbon analysis of marine organisms [29].

While this approach using one species in a limited geographic area was successful, the real potential for such computer-based analyses lies in the evaluation of data from large-scale environmental assessment and monitoring programs now being undertaken by some government agencies. Computer programs, such as those used in this study, can be used to analyze existing tables of biological, chemical and environmental data at small expense compared with the large investment involved in obtaining the original information. Besides application to existing environmental data sets, pattern recognition can also be used as an aid in the design of future environmental studies, so that the data generated are in formats suitable for pattern recognition analysis.

Pattern recognition is no panacea for every problem, but it can serve as a powerful tool in reducing massive amounts of data to meaningful information. The interdisciplinary approach of applying pattern recognition analysis to biological and chemical baseline data is especially valuable for interpreting subtle changes, whether they are environmental, spatial, or temporal.

The authors express their gratitude to B. R. Kowalski, J. I. Hedges, and G. Snyder for their counsel and criticism, to Maynarhs da Koven for his valuable observations, and to J. S. Finley for his analysis of the hydrocarbon content of the samples.

REFERENCES

1 D. C. Malins (Ed.), Effects of Petroleum on Arctic and Subarctic Marine Environments and Organisms, Vols. I and II, Academic Press, New York, 1977.
2 M. Blumer, in D. P. Hoult (Ed.), Oil on the Sea, Plenum, New York, 1969, p. 5.
3 J. W. Farrington, J. M. Teal, and P. L. Parker, in E. D. Goldberg (Ed.), Strategies for Marine Pollution Monitoring, Wiley-Interscience, New York, 1976, p. 3.
4 E. D. Goldberg, V. T. Bowen, J. W. Farrington, G. Harvey, J. H. Martin, P. L. Parker, R. W. Risebrough, W. Robertson, E. Schneider, and E. Gamble, Environ. Conserv., 5 (1978) 101.
5 B. R. Kowalski, P. C. Jurs, T. L. Isenhour, and C. N. Reilley, Anal. Chem., 41 (1969) 1945.
6 B. R. Kowalski, T. F. Schatzki, and F. H. Stross, Anal. Chem., 44 (1972) 2176.
7 B. R. Kowalski, Chem. Technol., 5 (1974) 300.
8 B. R. Kowalski, Anal. Chem., 47 (1975) 1152A.
9 D. L. Duewer and B. R. Kowalski, Anal. Chem., 47 (1975) 526.
10 D. L. Duewer, B. R. Kowalski and T. F. Schatzki, Anal. Chem., 47 (1975) 1573.
11 R. C. Clark, Jr. and J. S. Finley, Mar. Pollut. Bull., 4 (1973) 172.

12 R. C. Clark, Jr., J. S. Finley, B. G. Patten, D. F. Stefani, and E. E. DeNike, Proc. of the 1973 Joint Conf. on Prevention and Control of Oil Spills, Am. Pet. Inst., Washington, D.C., 1973, 793.
13 R. C. Clark, Jr., J. S. Finley, B. G. Patten, and E. E. DeNike, Proc. of the 1975 Conf. on the Prevention and Control of Oil Pollut., Am. Pet. Inst., Washington, D.C., 1975, p. 479.
14 R. C. Clark, Jr., B. G. Patten, and E. E. DeNike, J. Fish. Res. Board. Can., 35 (1978) 754.
15 R. C. Clark, Jr. and J. S. Finley, Proc. of the 1973 Joint Conf. on Prevention and Control of Oil Spills, Am. Pet. Inst., Washington, D.C., 1973, 161.
16 R. C. Clark, Jr. and J. S. Finley, NBS Special Publ. No. 409, National Bureau of Standards, Washington, D.C., 1974, p. 302.
17 A. M. Harper, D. L. Duewer, B. R. Kowalski, and J. L. Fasching, ACS Symp. No. 52, Am. Chem. Soc., Washington, D.C., 1977.
18 D. L. Duewer, J. R. Koskinen, and B. R. Kowalski, ARTHUR, available from B. R. Kowalski, Lab. for Chemometrics, Dept. of Chemistry, University of Washington, Seattle, WA 98195.
19 B. R. Kowalski and C. F. Bender, J. Am. Chem. Soc., 94 (1972) 5632.
20 B. R. Kowalski and C. F. Bender, Pattern Recognition, 8 (1976) 1.
21 T. M. Cover and P. E. Hart, IEEE Trans. Inform. Theory, IT-13 (1967) 21.
22 S. Wold, Pattern Recognition, 8 (1976) 127.
23 B. P. Tissot and D. H. Welte, Petroleum Formation and Occurrence, Springer—Verlag, Berlin, 1978.
24 P. A. Gabbott, in B. L. Bayne (Ed.), Marine Mussels. Their Ecology and Physiology, Cambridge University Press, Cambridge, 1976, 293.
25 R. C. Clark, Jr. and J. S. Finley, Proc. of the 1971 Joint Conf. on the Prevention and Control of Oil Spills, Am. Pet. Inst., Washington, D.C., 1971, p. 139.
26 R. C. Clark, Jr., Mar. Fish. Rev., 38 (1976) 20.
27 J. W. Anderson, R. C. Clark, Jr., and J. Stegeman, Marine Bioassays Workship Proc., Mar. Technol. Soc., Washington, D.C., 1974, p. 36.
28 U. Varanasi and D. C. Malins, in D. C. Malins (Ed.), Effects of Petroleum on Arctic and Subarctic Marine Environments and Organisms, Academic Press, New York, 1977, Vol. II, p. 175.
29 D. C. Malins, unpublished report, Northwest and Alaska Fisheries Center, NMFS, NOAA, U.S. Dept. of Commerce, Seattle, WA 98112. Presented at Int. Conf. and Exhibition on Petroleum and the Mar. Environ., Monaco, May, 1980.

Analytica Chimica Acta, 133 (1981) 169—182
Computer Techniques and Optimization
Elsevier Scientific Publishing Company, Amsterdam — Printed in The Netherlands

CHARACTERIZATION OF AN ENZYMATIC DETERMINATION OF ARSENIC(V) BASED ON RESPONSE SURFACE METHODOLOGY

RAY J. MATTHEWS**, SCOTT R. GOODE, and STEPHEN L. MORGAN*
Department of Chemistry, University of South Carolina, Columbia, SC 29208 (U.S.A.)
(Received 14th January 1980)

SUMMARY

Response surface methodology was used to characterize a new enzymatic method for the determination of arsenic in aqueous solutions. A Box—Behnken three-level fractional factorial experimental design was employed to characterize the reaction-rate response surface as a function of five experimental factors. Interpretation of the results of regression analysis provides an operational description of the analytical method as well as information that can be correlated with the mechanism of the chemical reaction.

The development of an analytical method is usually considered complete when the optimum experimental conditions have been found. The achievement of best performance from an analytical method, however, is often a difficult task to define in terms of a single optimization goal. The analyst must consider possible tradeoffs between multiple responses (such as sensitivity and selectivity) in relation to the needs of the analysis. Another concept of major importance in analytical methods development in Youden's idea of "ruggedness" [1, 2]. Ideally, an analytical method should be rugged against potential uncontrolled changes in the experimental factors. Factors which cause large changes in the response when their levels are varied must be controlled carefully to minimize variations within and between laboratories. Other factors may be controlled less rigorously. Often the speed of manual analytical procedures can be increased, without sacrificing the overall performance simply by controlling carefully only those factors which have a significant effect on the response. Factor tolerances are important in the description of methods of measurement, not only to obtain good reproducibility, but also to avoid wasting resources on unnecessarily fine control of insignificant factors [3—5].

The development and characterization of an analytical method typically requires interpretation of experiments in which three or more experimental factors are varied. The major difficulty encountered is that the effects of the experimental factors can no longer be easily visualized. Response surface methodology (r.s.m.) consists of a group of empirical techniques for investigating relationships between several experimental variables and one or

**Present address: Brockway Glass Co., Brockway, PA, U.S.A.

0378—4304/81/0000—0000/$02.50

more responses [6—8]. These techniques involve the design of experiments to characterize the response(s) as a function of the several factors, the fitting of empirical or theoretical models to the experimental data, the interpretation of the nature of the fitted response, and the judgement of the adequacy of the model. In this paper, the characterization of a method for ultra-trace levels of arsenic [9] in water is presented. With the aid of r.s.m., the ruggedness of this analytical method can be evaluated quantitatively and viewed objectively as a function of five experimental factors. Interpretation of these results provides a clear description of the analytical utility of the method as well as providing information that can be correlated with the mechanism of the chemical reaction.

The analytical method [9] is based on measuring the rate of reaction of D-glyceraldehyde-3-phosphate (G3P) with arsenate to form 1-arseno-3-phosphoglycerate. For each mole of G3P consumed, one mole of the coenzyme, nicotinamide adenine dinucleotide (NAD) is reduced to NADH in the presence of the enzyme glyceraldehyde-3-phosphate dehydrogenase.

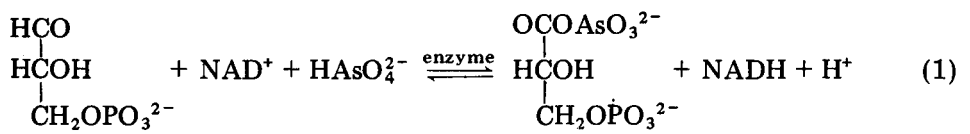

$$\begin{array}{l} HCO \\ | \\ HCOH \\ | \\ CH_2OPO_3^{2-} \end{array} + NAD^+ + HAsO_4^{2-} \overset{\text{enzyme}}{\rightleftharpoons} \begin{array}{l} OCOAsO_3^{2-} \\ | \\ HCOH \\ | \\ CH_2OPO_3^{2-} \end{array} + NADH + H^+ \qquad (1)$$

EXPERIMENTAL

Procedure

Measured volumes of β-mercaptoethanol (BME), G3P, sodium fluoride, and Tris buffer (pH 8.5, 0.2M) were added to a 2.0-ml portion of an aqueous solution of arsenic(V). After mixing, NAD and enzyme were added. With excitation at 360 nm, the increase in fluorescence at 460 nm was monitored using a spectrofluorimeter (Model 430, Turner Associates, Palo Alto, CA) and strip-chart recorder. The initial rate of reaction was determined by drawing a tangent to the fluorescence—time curve and recording the slope in arbitrary units.

Experimental design

Five experimental factors (BME, G3P, NaF, NAD, and enzyme) were included in an initial study to improve the reaction rate response using a modified sequential simplex method [5, 10]. In each of these experiments, sufficient Tris buffer was added to the sample so that the total volume of sample plus reagents was 3.75 ml. The volumes of each of the five other reagents were varied by the simplex algorithm within the boundaries shown in Table 1. The simplex optimization was started with a large initial simplex in order to explore a large extent of the factor space [11].

The reaction rate response surface was mapped using a five-factor Box—Behnken design [12], centered on the vertex of highest response from the simplex optimization. The Box—Behnken design is a three-level fractional

TABLE 1

Boundaries and experimental design levels of factors

Factor	Conc.	Simplex lower boundary (ml)	Levels in Box—Behnken design (ml)[a]			Simplex upper boundary (ml)
			Low(−1)	Middle(0)	High(+1)	
BME	0.25 M	0	0.109	0.209	0.309	0.5
Enzyme	750 μg ml^{-1}	0	0.029	0.039	0.049	0.05
G3P	0.001 M	0	0.013	0.026	0.039	0.1
NaF	0.27 M	0	0.128	0.282	0.382	1.0
NAD	0.02 M	0	0.040	0.065	0.090	0.1

[a]Centered on the location of the vertex of highest response from the sequential simplex optimization.

factorial design consisting of a full 2^2 factorial seeded into a balanced incomplete block design [12]. For example, the Box—Behnken design in three factors (Fig. 1) consists of 12 points all lying on the surface of a sphere surrounding the center of the design, which is replicated three times. The five-factor Box—Behnken design similarly is composed of a replicated center point surrounded by a number of points distributed on the surface of a hypersphere in five-factor space. The spacings between levels (Table 1) were chosen to insure that the design covered a broad region of factor space within the factor limits. Table 2 gives the 46 experiments required for the five-factor design. The experiments were blocked into two groups of 23 experiments each with three replicates of the center point (all factors at the zero level) in each block. A computer program was employed to generate the full design, to randomize the time order of the experiments within each block, and to calculate the volumes of the reagents needed for each experiment. All 46 experiments were performed on a single day, the first block of 23 in the morning and the second block of 23 in the afternoon. The six

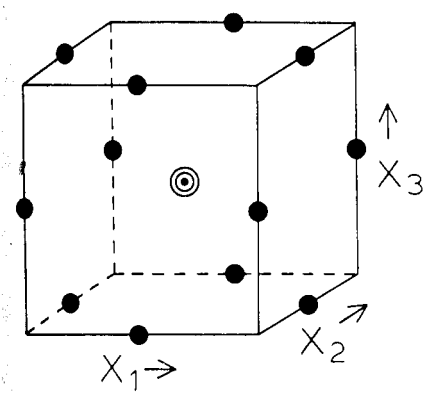

Fig. 1. The Box—Behnken design in three factors.

TABLE 2

Results of Box–Behnken design in five factors

Exp. no.	Time order	Coded factor levels[a]					Measured response
		BME	Enzyme	G3P	NaF	NAD	
A. BLOCK 1							
1	7	0	0	0	0	0	8.4
2	14	0	0	0	0	0	8.2
3	21	0	0	0	0	0	8.5
4	15	1	1	0	0	0	9.0
5	13	1	−1	0	0	0	7.3
6	3	−1	1	0	0	0	8.3
7	4	−1	−1	0	0	0	8.0
8	1	0	0	1	1	0	8.0
9	9	0	0	1	−1	0	8.0
10	16	0	0	−1	1	0	7.7
11	22	0	0	−1	−1	0	7.5
12	19	0	1	0	0	1	9.5
13	18	0	1	0	0	−1	9.1
14	2	0	−1	0	0	1	7.8
15	5	0	−1	0	0	−1	9.0
16	6	1	0	1	0	0	9.0
17	17	1	0	−1	0	0	6.5
18	12	−1	0	1	0	0	7.5
19	8	−1	0	−1	0	0	8.4
20	23	0	0	0	1	1	7.5
21	11	0	0	0	1	−1	9.1
22	10	0	0	0	−1	1	8.5
23	20	0	0	0	−1	−1	7.8
B. BLOCK 2							
24	28	0	0	0	0	0	8.4
25	35	0	0	0	0	0	8.4
26	42	0	0	0	0	0	8.1
27	24	0	1	1	0	0	9.4
28	44	0	1	−1	0	0	9.0
29	33	0	−1	1	0	0	7.2
30	31	0	−1	−1	0	0	7.2
31	29	1	0	0	1	0	8.0
32	39	1	0	0	−1	0	9.0
33	38	−1	0	0	1	0	9.3
34	27	−1	0	0	−1	0	8.5
35	30	0	0	1	0	1	9.2
36	34	0	0	1	0	−1	8.1
37	45	0	0	−1	0	1	6.8
38	41	0	0	−1	0	−1	9.7
39	36	1	0	0	0	1	9.1
40	46	1	0	0	0	−1	10.6
41	25	−1	0	0	0	1	10.2
42	40	−1	0	0	0	−1	9.7
43	32	0	1	0	1	0	8.0
44	37	0	1	0	−1	0	10.0
45	43	0	−1	0	1	0	8.1
46	26	0	−1	0	−1	0	7.1

[a]See Table 1.

replicates of the center points were spaced equally throughout the series of experiments so that time trends could be easily detected.

RESULTS AND DISCUSSION

The sequential simplex algorithm [13, 14] was first employed by analytical chemists in 1968 and 1969 [15, 16]. Recently, applications in analytical chemistry have been critically reviewed [17, 18]. In the work presented here, the optimization study was terminated after 31 vertexes had been evaluated. At that point, the differences in response among the vertexes approached the level of experimental uncertainty and no further substantial improvement in response was expected. The reaction rate response at the conditions specified by the vertex of highest response was approximately six times that originally achieved.

Response surface mapping and modelling

The reaction rate response measured at each of the 46 experimental conditions specified by the five-factor Box—Behnken design are given in the right-hand column of Table 2. The rate response was fit to a full second-order polynomial model of the general form:

$$R = \beta_0 + \sum_{i=1}^{k} \beta_i x_i + \sum_{i=1}^{k} \beta_{ii} x_i^2 + \sum_{\substack{ij \\ i<j}} \beta_{ij} x_i x_j \qquad (2)$$

where R represents the estimated response, β_0 is an intercept parameter, the β_i terms are linear parameters, the β_{ii} terms are quadratic parameters, the β_{ij} are interaction parameters, and x_i represents the ith of k experimental factors. With five factors, the full second-order model involves 21 parameters: an intercept, 5 linear terms, 5 quadratic terms, and 10 two-factor inter-

TABLE 3

Regression analysis

Factor	Parameter[a]	Estimate	Level of significance[b] at which null hypothesis can be rejected (%)	Factor	Parameter[a]	Estimate	Level of significance[b] at which null hypothesis can be rejected (%)
(intercept)	β_0	8.33[c]	100.00	Inter-	$\beta_1\beta_2$	0.350	81.50
BME	β_1	−0.0875	49.79	action	$\beta_1\beta_3$	0.850[c]	99.72
	β_{11}	0.331	93.17	terms	$\beta_1\beta_4$	−0.450	90.80
Enzyme	β_2	0.662[c]	100.00		$\beta_1\beta_5$	−0.500	93.70
	β_{22}	−0.0354	16.00		$\beta_2\beta_3$	0.100	29.94
G3P	β_3	0.225	90.80		$\beta_2\beta_4$	−0.750[c]	99.27
	β_{33}	−0.435[c]	98.08		$\beta_2\beta_5$	0.400	86.80
NaF	β_4	−0.0438	26.40		$\beta_3\beta_4$	−0.0500	15.30
	β_{44}	−0.194	72.41		$\beta_3\beta_5$	1.00[c]	99.93
NAD	β_5	−0.281[c]	96.19		$\beta_4\beta_5$	−0.575[c]	96.56
	β_{55}	0.606[c]	99.82				

[a]See eqn. 2. [b]Based on variance of residuals. [c]Parameter estimate significantly different from zero at 95% confidence level[b].

TABLE 4

Analysis of variance

Source of variation	Sum of squares	Degrees of freedom	Mean square
Total	3305	46	71.85
Due to the mean	3268	1	3268
Corrected for the mean	37.65	45	0.8367
Due to the factors	31.05	20	1.553
Residuals	6.598	25	0.2639
Due to blocks	2.397	1	2.397
Due to lack of fit	4.088	19	0.2152
Due to pure experimental uncertainty	0.1133	5	0.02267

Significance of regression:
$F_{20,25} = 5.88$, based on variance of residuals. Level of significance = 100.00%.
$F_{20,5} = 68.5$, based on pure experimental variance. Level of significance = 99.99%.
Significance of lack of fit:
$F_{19,5} = 9.49$. Level of significance = 98.98%.
Coefficient of multiple determination: $R^2 = 0.825$.

actions. Table 3 gives the 21 parameters estimates obtained by matrix least squares [19]. The parameter estimates have been rounded off to three significant figures for ease of presentation. The level of significance at which the null hypothesis for each parameter (H_0: $\beta_i = 0$) can be rejected is also shown in Table 3. The standard deviations of the parameter estimates were based on the standard deviation of the residuals [20].

Judging the adequacy of the model

An analysis of variance of the regression results is given in Table 4. As indicated by the R^2 value, the source of variation attributed to the factors (linear, quadratic, and interaction terms) accounts for 82.5% of the variation in the sum of squares corrected for the mean. The significance of the regression, tested by the F-ratio of the mean square due to the factors divided by the mean square due to residuals, is highly significant (100.0%). Despite this apparent goodness of fit, the model shows a significant lack of fit, as tested by the F-ratio of the mean square due to lack of fit divided by the mean square due to pure experimental uncertainty. This apparent paradox is discussed further below.

The separation of the experimental design into two blocks of 23 experiments is arranged so that the differences between blocks (i.e., any time trend) is uncorrelated with the estimates of all other parameters in the full second-order model [12]. In Table 4, the block effect is split from the residual sum of squares so that the lack of fit test is not biased [12]. Although there is not a large difference between the mean responses of the two blocks, the sum of squares that can be attributed to the block difference does contribute

substantially to the residual sum of squares. A plot of residuals against time order of experiment shows a slight positive correlation due to the block effect. No definite trends are seen in the residuals within each block or in the time order of the replicated center points. The size of the largest residual is 0.80 (approximately 10% of measured response); the standard deviation of the residuals is 0.514 (approximately 6% of the measured response). In summary, although the lack of fit of the model is statistically significant, the lack of fit is not practically significant. The residuals are small enough for the simple polynomial approximation to be tentatively entertained as an adequate description of the system.

Cell mean plots

The Box—Behnken design for five factors is a fractional three-level experimental design consisting of 40 experiments distributed on the surface of a hypersphere. Each of these 40 experiments is equidistant from the center point, which is replicated six times. Although the Box—Behnken design allows the efficient estimation, by regression techniques, of the parameters in a full second-order model, it suffers from the disadvantage that factor effects can not be easily assessed by visual comparison of the raw data. One classical statistical approach, developed originally for the analysis of effects from full factorial designs, is the cell mean plot [21, 22]. The cell mean plot used to illustrate the main effects (linear and quadratic effects) of a factor is simply a graph of the measured response at each level of that factor averaged over all levels of the other factors. The relative importance of each factor can be inferred from the shape of its cell mean plot without reference to fitting a model to the data. Conclusions from the cell mean plots, however, can be compared with the results of the regression analysis.

Figures 2—4 show cell mean plots illustrating the main effects of the first three factors (BME, enzyme, and G3P) on the reaction rate response for the determination of arsenic. In each case, the three points plotted are the average at low (−1), middle (0), and high (+1) levels of the factor, regardless of the levels of the other factors (see Table 2). The level of experimental uncertainty is indicated by a bracketed line centered on the response at the midpoint in each plot ($\pm 1s$, where $s = 0.30$ from the six replicate center points).

The change in response produced by variations in the level of the first factor, BME, is illustrated by the cell mean plot of Fig. 2. This effect is seen to be not very large in comparison to the experimental uncertainty. This conclusion regarding the main effects of BME is supported by the significance levels associated with the linear and quadratic parameters for BME (see Table 3). Another interpretation of the low significance of the main effects for BME might be that BME is not necessary to the procedure. As will be seen later, this interpretation is not justified.

The change in response produced by variations in the level of the second factor, enzyme, is shown in Fig. 3. As expected, the reaction rate is directly

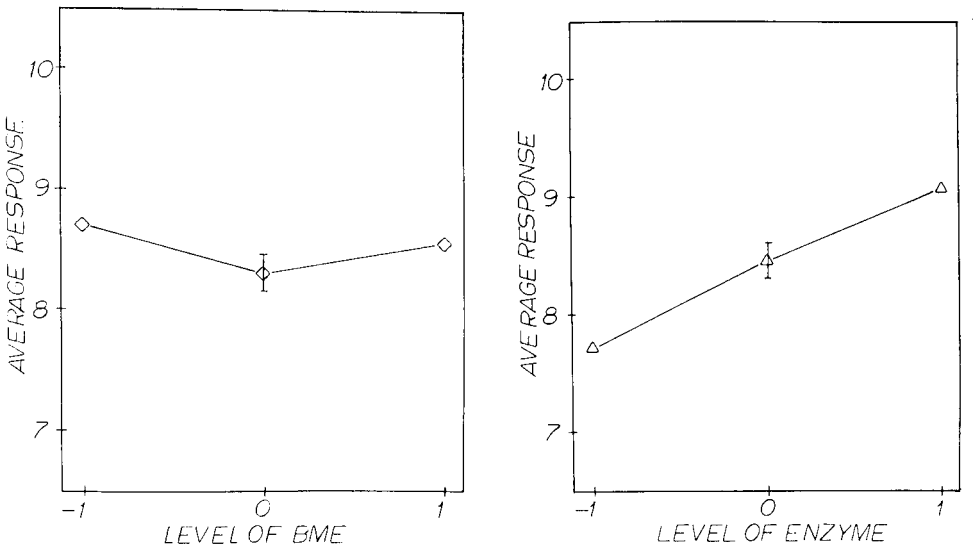

Fig. 2. Cell mean plot showing the main effects of β-mercaptoethanol (BME) averaged over all levels of the other factors.

Fig. 3. Cell mean plot showing the main effects of the enzyme, GAPDH, averaged over all levels of the other factors.

proportional to the concentration of the enzyme in the reagent mixture. Table 2 shows the linear parameter for this factor to be highly significant. For this reason, the enzyme concentration in the reagent mixture must be controlled carefully to maintain adequate precision in routine analysis.

Figure 4 shows the change in response produced by variations in the level of the third factor, G3P. The reaction rate goes through a local optimum at the middle level of the factor. The high significance of the β_{33} parameter in Table 3 confirms that the curvature in this plot is significant in comparison with the experimental uncertainty.

In summary, these three cell mean plots indicate that the reaction rate is fairly rugged with respect to BME, is quite sensitive to the level of enzyme, and shows a local maximum at the middle level of G3P. These tentative conclusions ignore possible interactions between the factors [21]. The effect of any single factor may depend upon the level of one or more other factors. Figures 2—4 only display the effect of single factors averaged over all levels of other factors and thus tend to average any factor interaction that is present.

For example, a significant interaction between G3P and NAD would mean that the effect of G3P on the reaction rate depends on the level of NAD. This information, although available in the raw data, has been eliminated in the averaging process leading to the main effect cell mean plot. To investigate the possible presence of a G3P-NAD interaction requires, in this case, three cell mean plots showing the effect of G3P at the low, middle, and high

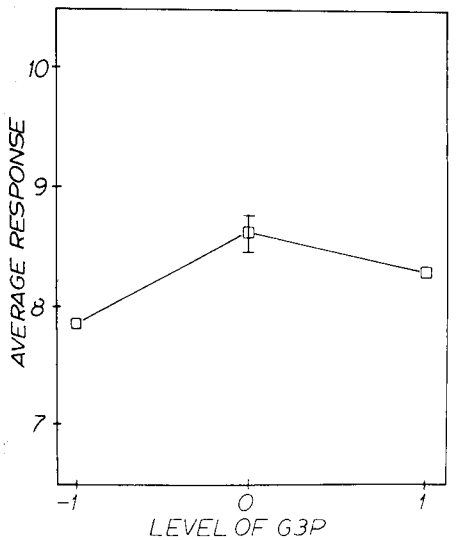

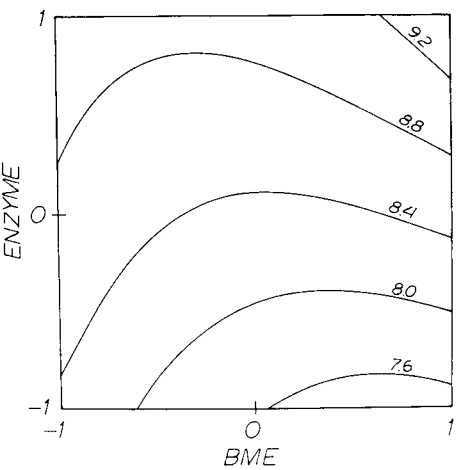

Fig. 4. Cell mean plot showing the main effects of D-glyceraldehyde-3-phosphate (G3P) averaged over all levels of the other factors.

Fig. 5. Reaction rate response surface contours as a function of BME and enzyme levels with all other factors at the zero level.

levels of NAD (averaged over all other factors). To examine all possible two-factor interactions in this manner would require ten sets of such plots, a total of 30 graphs.

The usefulness of main effect cell mean plots depends greatly on whether or not interaction is present. If no interaction between factors is present, the general trend with increasing the level of a factor will be the same for all levels of other factors. Olansky et al. [23] have employed main effect cell mean plots to summarize the information from a six-factor Box—Behnken design investigating six different responses affecting the determination of calcium. The amount of data to be assimilated and the small number of significant interactions between factors justified the use of the main effect plots in that study. When interaction between two factors is significant, cell mean plots showing the effect of one factor at several different levels of the second factor may be used [24, 25].

Cell mean plots (not shown here) for the main effects of NaF and NAD indicate little dependence of reaction rate on the level of NaF and a significant amount of curvature for NAD. Both of these observations are supported by the results in Table 3 but, as before, the cell mean plots are not sufficient by themselves to describe the factor effects if interactions are present.

Response surface interpretation from contour plots

When dealing with a multifactor system, the examination of the raw data from an experimental design or the inspection of the approximating equation

often provides little direct understanding of the response surface. The visualization of the model as a response surface over the factor space is an extremely useful approach which leads to a characterization of the surface by means of contours of equal response. Contour plots of the response surface as a function of two factors at a time, holding all other factors at fixed levels, are helpful in understanding both the main effects of the factors and their interaction effects in combination with one another. Contour plots for each of the 10 two-factor combinations were generated on the graphics screen of a minicomputer. Because some of the factor effects and interactions do not appear to be highly significant, only a selected number of these plots will be discussed.

Figure 5 shows the iso-response contours for the response surface as a function of the first two factors, BME and enzyme concentrations. The ranges of the two factor levels in the plot enclose the region within which the experimental design was performed. In agreement with the low significance of the BME main effects (β_1 and β_{11} in Table 3) the contours run nearly parallel to the BME axis, indicating that BME has little effect on the reaction rate in this region of factor space. This also agrees with the BME cell mean plot in Fig. 2. As the enzyme concentration is varied from low to high levels, the response increases steeply. Figure 5 confirms the highly significant linear effect of enzyme concentration previously noted in the cell mean plot of Fig. 3 and in the regression analysis. The effect of enzyme concentration is similar at all levels of BME, with the exception of decreased sensitivity to enzyme concentration at the lower level of BME. Although the BME-enzyme interaction is not highly significant (see Table 3), the decreased sensitivity to enzyme at low levels of BME can be explained by the chemistry. The active site of the enzyme GAPDH is known to contain sulfhydryl groups [26]. The β-mercaptoethanol is used as a reducing agent to protect these groups from oxidation. The importance of having BME present in the reagent has been confirmed by additional experiments either leaving BME out or adding hydrogen peroxide to the reagent.

Figure 6 shows a contour plot of the reaction rate as a function of the first and third factors, BME and G3P. As in Fig. 5, BME by itself does not appear to have a large effect on the response. The effect of increasing G3P at the low level of BME is to decrease the response from above 8.6 to below 8.2; at the high level of BME, increasing the rate from 7.4 to over 9.0. This change in the effect of G3P at different levels of BME is the reason for the highly significant BME-G3P interaction in the response surface model (see Table 3). In view of the role that BME plays in the chemistry of the method, it is not surprising that BME has a significant effect on the reaction rate only in combination with a second factor. Finally, regarding Figure 6, the contours shown do not depict a response surface with a simple maximum or minimum. The contour depicts a saddle point [6, 8] with a broad near-stationary region in the middle of the plot. The analytical method is insensitive to small changes in both factors near the region of the stationary point.

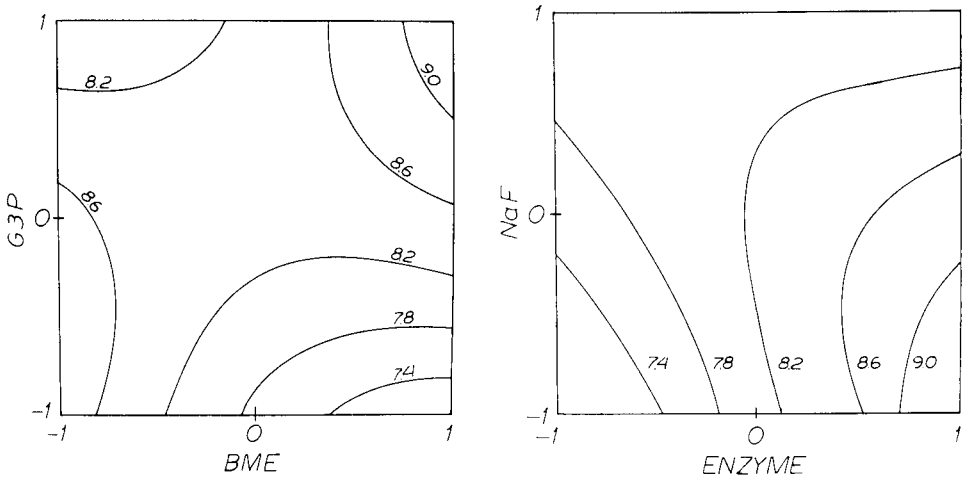

Fig. 6. Reaction rate response surface contours as a function of BME and G3P levels with all other factors at the zero level.

Fig. 7. Reaction rate response surface contours as a function of enzyme and NaF levels with all other factors at the zero level.

Figure 7 shows response surface contours as a function of enzyme and NaF concentrations with all other factors held at the zero level. The main effect of the enzyme level is seen to be highly significant only at low levels of NaF, whereas NaF has little effect on the reaction at all. The interaction parameter for these two factors is highly significant (β_{24} in Table 3). A possible explanation is that sodium fluoride inhibits the action of several enzymes [27], including some which are probably co-crystallized along with GAPDH in the commercial preparation. At high concentrations of sodium fluoride, only the analytical reaction is important. Since the reaction is pseudo-first-order in arsenic, the other reagents, including the enzyme, are always in excess. Changes in the enzyme levels influence the rate of reaction, but certainly not as much as do changes in arsenic(V) concentration. When NaF is low, it is no longer reasonable to assume that the analytical reaction is the only significant reaction. Increasing the enzyme concentration probably increases the response to the same degree when NaF is low as when it is high. The side-reactions proceed to a more significant extent when NaF is low. The rate of these side-reactions can be expected to be directly proportional to enzyme concentration.

Figure 8 gives contours of the response surface model versus levels of G3P and NAD, with all other factors held at zero levels. The regression analysis indicated a significant interaction between these two factors (β_{35} in Table 3). The rate of reaction is high when the levels of G3P and NAD are both high, or both low. This phenomenon, known as negative cooperativity, is well documented for this enzyme system [27]. To catalyze the reaction, the enzyme requires both G3P and NAD at the active site. If either reagent

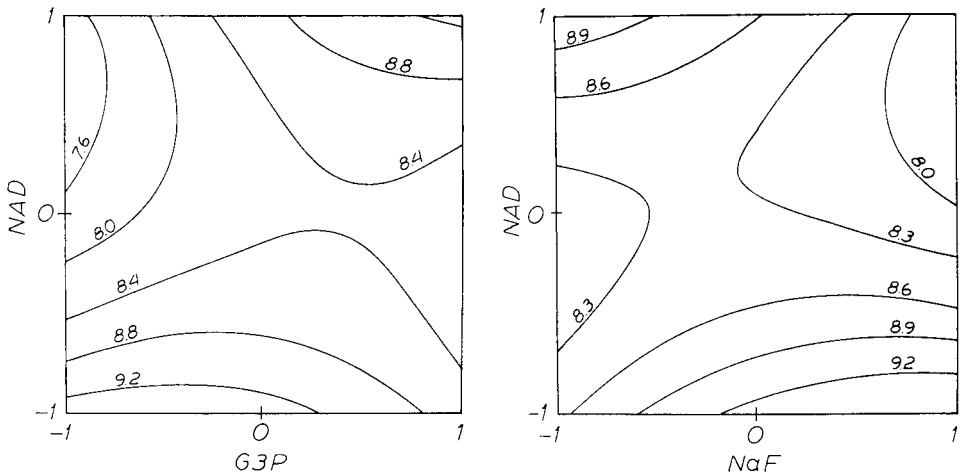

Fig. 8. Reaction rate response surface contours as a function of G3P and NAD levels with all other factors at the zero level.

Fig. 9. Reaction rate response surface contours as a function of NaF and NAD levels with all other factors at the zero level.

is present in excess, the active site of many of the enzyme molecules will lack the two necessary reagents. These enzyme-substrate groups cannot react with arsenic, thus the overall rate of reaction is decreased.

Figure 9 shows a contour plot for the final two factors which exhibit a significant interaction effect, NaF and NAD (see β_{45} in Table 3). This plot illustrates another saddle region with high response when one of the two factors is low and the other is high. The chemical interpretation of this effect is not simple and is largely unknown. Figures 8 and 9 both display a significant NAD effect on the reaction rate; in both cases, however, the effect of NAD depends dramatically on the level of the second factor.

The five contour plots illustrating the more significant of the two-factor interactions are presented here. These reaction-rate contours illustrate graphically the effect of each of these factors singly and in combination with one another. The contours for each set of factors involved setting all other factors at the zero, or middle, levels as designated by the experimental design. Successive contour plots can be generated to illustrate how any of these contour plots change as a third factor is varied.

The interpretation of a response surface model from contour plots is restricted in two respects. First, the response contours plotted using the full second-order response surface model are only estimates of the true contours. Knowledge of the true contours is limited by experimental uncertainties and possible lack of fit of the model to the data. Secondly, the response surface model should not be extrapolated outside the region of experimentation. The hazards of extrapolating regression models beyond the range of the experimental data have been described by Hahn [28]. The full second-order

model is utilized to approximate the true response surface over a limited region; higher-order or nonlinear effects have been assumed to be negligible and, if present, contribute to the lack of fit of the model.

A final interpretative technique of response surface methodology is the characterization of the model with the aid of analytical geometry and calculus. The stationary point of a response surface is located at that point in factor space where the first partial derivatives of the regression equation (in this case, the 21 parameter version of eqn. 2) with respect to each factor are simultaneously equal to zero. For our particular model, the stationary point is located at the coordinates, BME = 1.75, Enzyme = —4.05, G3P = 2.93, NaF = 3.22, NAD = 1.40 (coded levels). This point is located outside the region of the Box—Behnken design. Further canonical analysis [6, 8, 29] of the full second-order model indicates four canonical directions of significance. Two of these canonical directions are associated with local maxima and two are associated with local minima. The reduced conic form of the full model may be described as a saddle point. The predicted response at the stationary point at the center of the conic is actually less than at some points in the experimental region.

In conclusion, the use of response surface methodology has aided the development of this method for arsenic in water. The initial simplex optimization produced improved reaction rate response and located a region of near-stationary response. This region, in which further response surface experiments were performed, has been shown to be fairly insensitive to changes in the experimental factors. The characterization of the reaction rate response in this region has facilitated an understanding of the factor effects and interactions that can be correlated with fundamental chemical knowledge.

This work was supported in part by the Clemson University Water Resources Research Institute grant B-121-SC.

REFERENCES

1 W. J. Youden, Mat. Res. and Stand., 1 (1961) 862.
2 W. J. Youden and E. H. Steiner, Statistical Manual of the Association of Official Analytical Chemists, AOAC, Washington, DC, 1975.
3 J. Mandel, The Statistical Analysis of Experimental Data, John Wiley, New York, 1964.
4 A. L. Wilson, Talanta, 17 (1970) 21.
5 S. L. Morgan and S. N. Deming, Anal. Chem., 46 (1974) 1170.
6 G. E. P. Box, Biometrics, 10 (1954) 16.
7 R. H. Myers, Response Surface Methodology, Allyn and Bacon, Boston, 1971.
8 G. E. P. Box, W. G. Hunter and J. S. Hunter, Statistics for Experimenters, John Wiley, New York, 1978.
9 S. R. Goode and R. J. Matthews, Anal. Chem., 50 (1978) 1608.
10 S. N. Deming and S. L. Morgan, Anal. Chem., 45 (1973) 278A.
11 L. A. Yarbro and S. N. Deming, Anal. Chim. Acta, 73 (1974) 391.
12 G. E. P. Box and D. W. Behnken, Technometrics, 2 (1960) 455.

13 W. Spendley, G. R. Hext and F. R. Himsworth, Technometrics, 4 (1962) 441.
14 J. A. Nelder and R. Mead, Comput. J., 7 (1965) 308.
15 R. R. Ernst, Rev. Sci. Instrum., 39 (1968) 988.
16 D. E. Long, Anal. Chim. Acta, 46 (1969) 193.
17 S. N. Deming and L. R. Parker, Jr., CRC Crit. Rev. Anal. Chem., 7 (1978) 187.
18 D. L. Massart, A. Dijkstra and L. Kaufman, Evaluation and Optimization of Laboratory Methods and Analytical Procedures, Elsevier, Amsterdam, 1978.
19 S. N. Deming and S. L. Morgan, Clin. Chem., 25 (1979) 840.
20 N. R. Draper and H. Smith, Applied Regression Analysis, John Wiley, New York, 1966.
21 D. R. Cox, Planning of Experiments, John Wiley, New York, 1958.
22 J. L. Myers, Fundamentals of Experimental Design, 3rd edn., Allyn and Bacon, Boston, 1979.
23 A. S. Olansky, L. R. Parker, Jr., S. L. Morgan and S. N. Deming, Anal. Chim. Acta, 95 (1977) 107.
24 L. R. Parker, Jr., S. L. Morgan and S. N. Deming, Appl. Spectrosc., 29 (1975) 429.
25 A. S. Olansky and S. N. Deming, Anal. Chim. Acta, 83 (1976) 241.
26 J. I. Harris and M. Waters, Glyceraldehyde-3-phosphate Dehydrogenase in P. D. Bayer (Ed.), The Enzymes, Vol. XIII, part C, 3rd edn., Academic Press, New York, 1976.
27 J. J. M. De Vijlder, W. Boers, A. G. Hivers, B. J. Harmsen and E. C. Slater, in H. Sund (Ed.), Pyridine Nucleotide Dependent Dehydrogenases, Springer Verlag, New York, 1970, p. 233.
28 G. J. Hahn, CHEMTECH, 8 (1978) 699; 9 (1979) 46.
29 O. L. Davies (Ed.), The Design and Analysis of Industrial Experiments, Hafner, New York, 1963.

Analytica Chimica Acta, 133 (1981) 183—190
Computer Techniques and Optimization
Elsevier Scientific Publishing Company, Amsterdam — Printed in The Netherlands

DISCREPANCIES IN CURVE FITTING FOR DIRECT AND LINEARIZED FUNCTIONS, ILLUSTRATED WITH TRANSIENT ELECTRODE POTENTIALS

ADAM SHATKAY* and MEIR AZOR
Israel Institute for Biological Research, Ness-Ziona (Israel)

(Received 14th March 1980)

SUMMARY

The discrepancies arising from curve-fitting with direct equations or with linearized equations are discussed. The argument is illustrated with three equations purporting to represent transient potentials in ion-selective electrodes. The advantages and the disadvantages of using direct equations instead of linearized ones are considered in detail. It is shown that the use of "pseudo-linearized" equations is inferior in all respects, and can yield significantly wrong results.

Fitting an analytic equation to a set of experimental data (curve-fitting) is a basic procedure in physical chemistry, as well as in other experimental sciences. The theory of curve-fitting has been studied very thoroughly, ranging from abstract treatment [1] to practical applied mathematics [2, 3]. However, a number of points remain unclear and deserve further attention.

Any mathematical equation may be written in several equivalent forms, obtained by algebraic manipulations one from the other. If the theoretical model leading to the equation is correct, and if there are no approximations or experimental errors, then no matter what form the equation takes, any curve-fitting procedure will yield the same, completely accurate, results.

In practice, several possible approximate equations are usually available, and the measurements are subject to experimental errors. It will be shown here that under such conditions the results of curve-fitting can depend heavily upon the form in which the equation has been cast. Thus it is essential to choose properly the form in which the equation is to be treated. The statistical aspects of curve-fitting (regression) will not be discussed, as the subject is dealt with in most statistical texts [4]. However, it should be noted that if the form and the related assumptions of the equations allow statistical treatment, it is possible to obtain from the equations important additional information, such as confidence regions for parameters and for similar future experiments. In this paper, a specific practical example, which is of considerable intrinsic interest, is considered. The conclusions reached apply to curve-fitting in general.

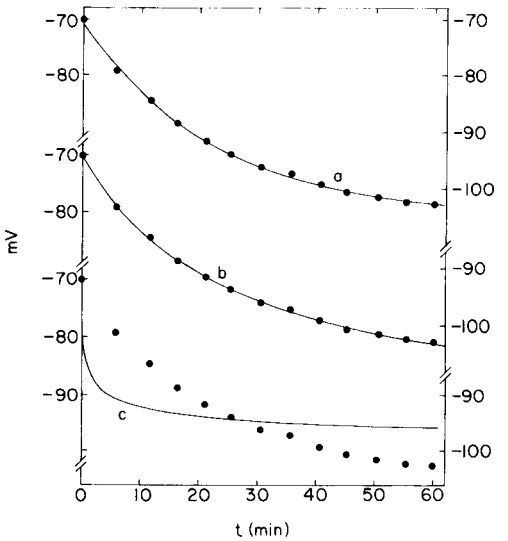

Fig. 1. Transient e.m.f. from the data of Savage and Isard [5]. Points: experimental. Curves: theoretical. Curves: (a) best fit to eqn. (1); (b) best fit to eqn. (2); (c) best fit to eqn. (3).

EQUATIONS FOR TRANSIENTS AND THEIR LINEARIZED FORM

When an ion-selective electrode (coupled with a reference electrode) is introduced into a solution containing a concentration C of the appropriate ion, a steady e.m.f. of E_0 mV is reached after some time. On changing abruptly the concentration from C to C' the e.m.f. changes from E_0 to a final steady-state value of E_∞. The change from E_0 to E_∞ with time is a "transient". A typical transient is illustrated by the experimental points in Fig. 1, based on the data of Savage and Isard [5].

The function E_t is intuitively expected to be well behaved, and to change monotonically and asymptotically from the initial value E_0 to the final value E_∞. Some mechanisms of the transient potential [6] lead us to expect a relation:

$$E_t = E_0 + (E_\infty - E_0)[1 - \exp(-Kt)] \tag{1}$$

Other mechanisms [6—8] lead to an equation of a hyperbolic form, e.g.:

$$E_t = E_0 + (E_\infty - E_0)\, Kt/(1 + Kt) \tag{2}$$

In a previous paper [6], eqn. (3) was suggested, among others:

$$E_t = E_0 + (E_\infty - E_0)\, t^K/(1 + t^K) \tag{3}$$

This equation has no theoretical basis, but is of the general form of eqns. (1) and (2), and has the same number of adjustable parameters.

The aim here is to choose the model which is in the best agreement with the experimental data, and to estimate the parameters E_∞ and K (E_0 is measured experimentally).

Equations (1)—(3) can be cast in many alternative forms. Mertens et al. [7] suggested the following form for eqn. (1):

$$\ln [(E_\infty - E_t)/(E_\infty - E_0)] = -Kt \tag{4}$$

Rechnitz and Hameka [9] also suggested the use of eqn. (4); however, since their graphs did not pass through zero, evidently they used another equivalent form of eqns. (1) and (4), such as:

$$\ln (E_t - E_\infty) = \ln (E_0 - E_\infty) - Kt \tag{5}$$

Equation (2) has been presented by Mertens et al. [7] in the form:

$$t/(E_t - E_0) = 1/K(E_\infty - E_0) + t/(E_\infty - E_0) \tag{6}$$

Finally, eqn. (3) can also be written as:

$$\exp (-A_t/K) = t \tag{7}$$

$$\text{where } A_t = \ln[(E_\infty - E_0)/(E_t - E_0) - 1] \tag{8}$$

Equations (4)—(7) might all be considered as "linearized" forms of eqns. (1)—(3), since the graphs of the lefthand function versus t yield straight lines. However, proper linearization (as used in curve-fitting) consists of obtaining an equation of the form:

$$y = ax + b \tag{9}$$

where y and x are measurable quantities, and do not contain any unknown adjustable parameters, while a and b are the quantities to be estimated. Since E_∞ and K appear in the left hand sides of eqns. (4), (5) and (7), these equations should not be considered as a strict linearization of the respective original eqns. (1) and (3); we shall refer to such equations as "pseudo-linear" equations.

Equation (2) can be linearized also to the form

$$1/(E_t - E_0) = 1/[(E_\infty - E_0)Kt] + 1/(E_\infty - E_0) \tag{10}$$

Since E_0 is an experimentally measurable quantity, eqns. (6) and (10) correspond to eqn. (9) and fulfil all the conditions stated with it. However, one should note that in eqn. (6) the variables are $t/(E_t - E_0)$ vs. t, while in eqn. (10) the variables were $1/(E_t - E_0)$ vs. $1/t$. Thus eqn. (6) uses the independent variable t on both sides of the equation. Such a procedure is inadvisable, as discussed by Sherwood [10].

TESTS FOR GOODNESS OF FIT

To test the "goodness of fit" of equations to experimental data, a number of procedures and measures is available. The most direct one is to obtain

from the experimental data estimates for the unknown parameters (such as E_∞ and K), and then for each observed value (say O_i) to compute the expected value (say X_i), using the appropriate equation. The set of the n observed values is then compared with the set of the expected values. A measure for the fit might be the average absolute deviation, the maximum absolute deviation etc. The commonest measure of fit is the root-mean-square deviation, S:

$$S = \left[\frac{1}{n} \sum_i (O_i - X_i)^2 \right]^{1/2} \tag{11}$$

Usually the estimates are chosen to minimize S; they are then called "least-squares estimates". The quantity S is also the estimate of the standard error of the measurement, provided that the model is correct.

Equation (11) is used to obtain best fit in conjunction with any of the eqns. (1)—(10). The differences in the results obtained are pointed out in the following paragraphs.

Comparison of the original equations with the transformed ones

The advantages of using linearized forms of equations are threefold. First, there are exact closed solutions for the values of a and b in eqn. (9), which yield directly the unknown parameters of the original equations (e.g. E_∞ and K). Thus the treatment of eqns. (6) and (10) is much easier than that of the equivalent eqn. (2). With the advent of computers and numerical methods, the above argument has lost much of its force. It should also be noted that the "pseudo-linearized" eqns. (4), (5) and (7) lack this advantage of the correctly linear form.

Secondly, a fit to a straight line is easily tested graphically. Thus one plots a set of purely experimental data, and tests the "straightness" of the curve (e.g. in eqn. 10, one plots $1/(E_t - E_0)$ vs. $1/t$). Again it should be noted that the "pseudo-linear" eqns. (4), (5) and (7) do not allow this procedure to be used, since one has to estimate some adjustable parameter in order to plot the points (e.g. on using eqn. 5, the ordinate is $\ln (E_t - E_\infty)$, which contains the unknown parameter E_∞). The results of such procedures are illustrated in Fig. 2. Actually, such graphical procedures could be carried out for the original eqns. (1)—(3) just as well as for eqns. (4), (5) and (7): on plotting the l.h.s. versus the r.h.s. a straight line should be obtained, with a slope of 45°, passing through the origin.

Thirdly, if certain conditions (such as normality and homogeneity) are met by the deviations from the linear curve, one can conveniently use the data for statistical inference about the mathematical model. On linearization (to the form of eqn. 9 only) these conditions are often met, and in such cases linearization is usually advisable.

However, despite the advantages of the linearized equations, there are also good reasons for the use of the direct equations, such as eqns. (1)—(3). To begin with, the presentation of E_t vs. t has a direct bearing on our experience. The time is measured directly in units of time, and the corresponding

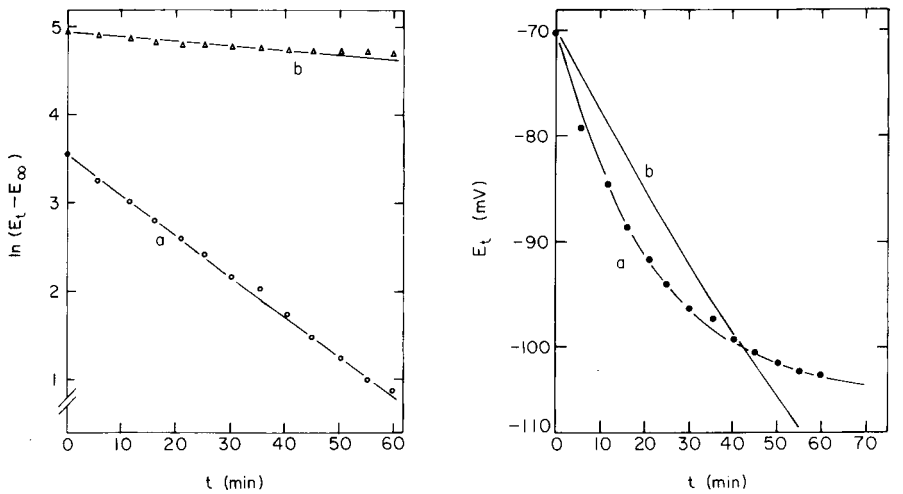

Fig. 2. Best fit to eqn. (5). Experimental values of E_t and t as in Fig. 1. Curves: (a) using $E_\infty = -105$ and $K = 4.4 \times 10^{-2}$; (b) using $E_\infty = -213$ and $K = 5.5 \times 10^{-3}$.

Fig. 3. Best fit to eqn. (1). All data as in Fig. 2.

e.m.f. in millivolts. It may be argued that "directly" is an ambiguous word, for what is really measured is at best the angle between the hands of a clock, or the flickerings on the dials of a potentiometer. Such objections are difficult to refute [11, 12]. It would, however, be widely agreed that in general a plot of E_t vs. t (as in Fig. 1) represents experience more directly than a plot of ln $(E_t - E_\infty)$ vs. t, or of $t/(E_t - E_\infty)$ vs. t.

Next, when the direct equations are employed in conjunction with eqn. (11), a value of S is obtained where O_i is the i'th observed e.m.f., while X_i is the corresponding expected e.m.f., computed from the direct equation. Thus S is in units of the e.m.f. (mV), and so its value can be compared directly with the known experimental error (say ± 0.5 mV). Thus the goodness of fit can be directly roughly evaluated.

The fact that S is always expressed in mV also makes it possible to compare directly the goodness of fit obtained by using the different mathematical models (eqns. 1—3), while on using the transformed equations (eqns. 4—10) such direct comparison is in general impossible.

It is possible to compare the goodness of fit for the various models even when the transformed equations are used, by introducing the estimators of K and E_∞ obtained from these equations into the direct equations. This procedure yields S^*, representing in mV the average difference between the observed and the computed e.m.f. However, it should be noted that the S^* computed from any transformed equation will always be greater than the S^* computed with the estimates obtained from the direct equation (in which case $S^* = S$).

The above objection can be removed in principle by suitably weighting each term $O_i - X_i$ in eqn. (11). However, this requires the calculation of

suitable weights for each set of the original and the transformed functions, and thus offsets the advantages of the linear functions for the "goodness of fit" [13, 14]. It should also be noted that correct weighting depends on full knowledge of the model, which often is not available.

The arguments above are illustrated by using the experimental data of Savage and Isard [5], presented in Fig. 1. The results of the various calculations are summarized in Table 1.

It was pointed out above that the different results obtained on using different forms of any equation stem from two causes: the experimental error and the approximation to the physical model. Obviously the effect of linearization on the "goodness of fit" depends also on the form of the direct and the linearized functions, on the possibilities of additive errors, on the distribution of the random variable, etc. It can be seen from the data illustrated in Fig. 1 that in this case the measurements were carried out competently, and that the experimental error is slight. In fact, judging from the "state of the art", one would expect an error of less than 0.5 mV in any measurement. Furthermore, curves a and b in Fig. 1 indicate that the mathematical models of eqns. (1) and (2) are both a good approximation of the physical behaviour of the transient. Thus one is led to expect that the use of eqns. (1), (4) and (5) should yield similar results. In particular, eqns. (4) and (5), which have nearly the same form, should be almost equivalent. Table 1 bears this out.

Similarly, the results of eqns. (2), (6) and (10) should be almost equal. Again, this is true.

However, eqn. (3) was chosen to illustrate the case where the mathematical model is only a poor approximation. In such a case, different results would be expected from the equivalent eqns. (3) and (7). In fact the E_∞ *is* -100

TABLE 1

Goodness of fit for the data of Savage and Isard [5] by employing eqn. (11) with the various mathematical models

Model	Employing equation	E_∞ (mV)	K	S	S^* (mV)
Exponential	(1)	−105	4.7×10^{-2} min^{-1}	0.40 mV	0.40
	(4)	−105	4.4×10^{-2} min^{-1}	4.0×10^{-2} [a]	0.53
	(5)	−105	4.4×10^{-2} min^{-1}	3.7×10^{-2} [a]	0.53
Hyperbolic	(2)	−117	4.1×10^{-2} min^{-1}	0.30 mV	0.30
	(6)	−116	4.1×10^{-2} min^{-1}	1.6×10^{-2} min mV^{-1}	0.30
	(10)	−115	4.3×10^{-2} min^{-1}	1.08×10^{-3} mV^{-1}	0.41
Power	(3)	−100	0.45[a]	5.50 mV	5.50
	(7)	−109	0.38[a]	17.2 min	7.3

[a]Dimensionless.

for eqn. (3), while it becomes −109 for eqn. (7). Similarly, K is 0.45 when obtained from eqn. (3), and 0.38 from eqn. (7). In both cases S^* is well outside the experimental error.

Despite the fact that the model represented by eqns. (3) and (7) is obviously much poorer than the two other models, eqns. (4), (6) and (7) cannot be directly compared by considering the respective values of S, since it is measured in different units. Such comparison can be carried out on considering S^*, which employs the same units. However, as already stated, S^* is minimized upon use of the direct eqns. (1)—(3). Therefore when alternative models are to be compared it is advisable to use the direct equations, and not the transformed ones.

Another point against transformations is more technical, but still deserves attention as it may cause difficulties during calculations. Manipulation of the original equations may introduce expressions that require caution. Thus in eqn. (5), E_∞ cannot be assumed greater than any value of E_t, otherwise a negative argument is obtained for the logarithm. Moreover, when the measured quantities appear in reciprocals, as in eqns. (6) and (10), then for small values of these quantities even small experimental errors may cause large deviations, and thus yield incorrect results.

Finally, an injudicious choice of the transformed form, especially when the adjustable parameters appear on both sides of the equation, can yield completely wrong values for these parameters, despite the fact that the S obtained will be lower than that of the correct estimates. For instance, in eqn. (5), by choosing very large values for E_∞ one can decrease S below any arbitrary value. Figure 2 shows two plots of eqn. (5), based on the same experimental values of t and E_t. In curve a the values quoted in Table 1 for this equation are used ($E_\infty = -105$, $K = 4.4 \times 10^{-2}$), while in curve b the values used are $E_\infty = -213$ and $K = 5.5 \times 10^{-3}$. It can be seen that the fit in curve b is better than that in curve a. However, when these two sets of E_∞ and K are plotted using eqn. (1) (cf. Fig. 3), it is obvious that curve b gives a much poorer fit than curve a.

The linearization of a direct function can also affect other statistics, such as scaling, or confidence regions. However, this subject is not considered in detail, since our main point is sufficiently clear.

Conclusions

When a set of experimental data has to be expressed by a mathematical model, one can use either a direct equation relating explicitly one measurement as a function of the other, or a transformed form of such an equation. The advantages of using a direct equation are that the equation expresses actual experience, corresponding to intuitive expectations, and that the values of S obtained have the dimensions of the experimental variable, so that they can be compared directly with the known experimental error. The goodness of fit can be assessed directly, and the goodness of fit of alternative models can be directly compared.

The advantages of using the linearized form of an equation are that calculations are easier, that a convenient graphical presentation (straight line) is possible so that the goodness of fit can be examined even without calculation of the adjustable parameters, and that, if certain conditions are met, a statistical analysis can be conveniently carried out.

Transformation to a "pseudo-linear" form, where the adjustable parameters appear on both sides of the equation, is undesirable in all cases, because the calculations remain complicated, plotting of the data as a straight line is possible only after computation of the adjustable parameters, and the values obtained for these parameters can be significantly incorrect.

REFERENCES

1 I. P. Natanson, Constructive Function Theory, Frederik Unger, New York, 1964.
2 I. S. Sokolnikoff and R. M. Redheffer, Mathematics of Physics and Modern Engineering, 2nd edn., McGraw-Hill, New York, 1966.
3 L. A. Pipes and L. R. Havrill, Applied Mathematics for Engineers and Physicists, 3rd edn., McGraw-Hill, New York, 1970.
4 W. J. Youden, Statistical Methods for Chemists, Wiley, New York, 1951, Chap. 5.
5 J. A. Savage and J. O. Isard, Phys. Chem. Glasses, 3 (1962) 147.
6 A. Shatkay, Anal. Chem., 48 (1976) 1039.
7 J. Mertens, P. Van den Winkel and D. L. Massart, Anal. Chem., 48 (1976) 272.
8 J. Buffle and N. Parthasarathy, Anal. Chim. Acta, 93 (1977) 111.
9 G. A. Rechnitz and H. F. Hameka, Fresenius Z. Anal. Chem., 214 (1965) 252.
10 T. K. Sherwood, Chem. Tech., 4 (1974) 736.
11 K. Pearson, The Grammar of Science, Everyman's Library, Vol. 939, J. M. Dent, London, 1937.
12 C. E. M. Joad, Guide to Philosophy, V. Gollancz, London, 1948.
13 B. R. Kowalski and T. L. Isenhour, Anal. Chem., 40 (1968) 1186.
14 P. C. Jurs, Anal. Chem., 42 (1970) 747.

Analytica Chimica Acta, 183 (1981) 191—201
Computer Techniques and Optimization
Elsevier Scientific Publishing Company, Amsterdam — Printed in The Netherlands

THE USE OF A MINICOMPUTER FOR DATA COLLECTION AND TREATMENT IN THE STUDY OF ELECTROCHEMICAL SURFACE PROCESSES

J. MOZOTA**, B. BARNETT, D. TESSIER, H. ANGERSTEIN-KOZLOWSKA and B. E. CONWAY*

Chemistry Department, University of Ottawa, Ottawa, Ontario K1N 6N5 (Canada)

(Received 2nd June 1980)

SUMMARY

Procedures for on-line acquisition and processing of data from controlled-potential (linear potential sweep and cyclic voltammetric) experiments on electrode surface processes by means of a PDP 11/34 minicomputer are described. Advantages of this procedure over regular recording of current—potential or current—time traces on an oscilloscope are discussed.

The electrochemistry of surface processes in monolayers studied by non-steady-state techniques has excited recent interest [1]. Special advantages can be realized through the use of an on-line computer system in the study of these processes by linear-sweep or cyclic voltammetry. Computers are especially suitable for recording fast events and thus may be used to process current—potential profiles which arise from application of linear voltage sweeps at high rates. In this role, the computer system functions advantageously as a fast-recording "digital oscilloscope". The development of relatively cheap micro- and mini-computers with reasonable capacity has led to innumerable applications involving data acquisition, storage and processing, as well as automatic monitoring and process simulation. With regard to electrochemistry, however, the emphasis in software development and hardware interfacing has tended towards data handling, though considerable attention has been given to on-line control of experiments.

As early as 1965, Breiter [2] described the use of a computer for on-line collection of cyclic voltammetric data with a paper-tape encoding system. Since then, other publications in this area have appeared [3—5]. However, more detailed information is needed, especially with regard to the practical details of how a minicomputer can be used for acquisition and treatment of data obtained in non-steady-state studies of surface processes at electrodes. Provision of such information can greatly facilitate the initial steps involved in establishing an on-line data acquisition and processing system.

In this paper, the advantages of a PDP 11/34-based minicomputer system

**Present address: Universidad Simon Bolivar, Dpto. de Quimica, Apdo 80659, Caracas, Venezuela.

0378—4304/81/0000—0000/$02.50

in various cyclic voltammetric experiments employed in the study of monolayer surface processes, are described. While general applications of computers in electrochemistry are well known, the purpose of this article is to provide details of a system designed for electrochemical studies on surface films for workers intending to set up or develop an on-line minicomputer system for thin-film evaluation. Hence some elementary details as well as operational principles will be described.

EXPERIMENTAL

A block diagram of the experimental and computing set-up is shown in Fig. 1. The computer consists of a PDP-11/34 mainframe with 32K words of random access memory (RAM), a dual RX-01 floppy disc unit, an RL-01 hard disc and a magnetic tape unit. Two types of software were used, namely the Digital RT11 extensions package and a supplementary software library designed in this laboratory and tailored to our special requirements, i.e., the sampling of two or more channels alternately at very fast rates. Programs were written in FORTRAN IV and MACRO 11 (PDP Assembly Language); an excellent introduction to MACRO 11 programming with respect to laboratory applications of a minicomputer has been given by Cooper [6]. FORTRAN sections of the program handled the input of parameters and the creation of data files while the data acquisition, display and interface control were performed by FORTRAN-callable MACRO subroutines because of the need to manipulate the bits in the status register of the interfacing modules. Figure 2 shows a program which performs the data collection and storage. In Fig. 3 a typical data-acquisition and data-plotting flow chart is shown, illustrating the logical stages of program flow.

A PAR 173 potentiostat coupled with a TACUSSEL type GSATP signal generator was used to achieve potentiostatic control and the derived potential–time programs, respectively.

The potential (V) of the working electrode vs. the reference electrode and the resulting current (I) in the working/counter electrode circuit, transformed to a potential difference in the usual way by means of a standard resistance, were passed through operational amplifiers (Tektronix type AM 501), acting as non-inverting amplifiers of variable gain. Appropriate gains were determined by the maximum input range of the A/D converter, which

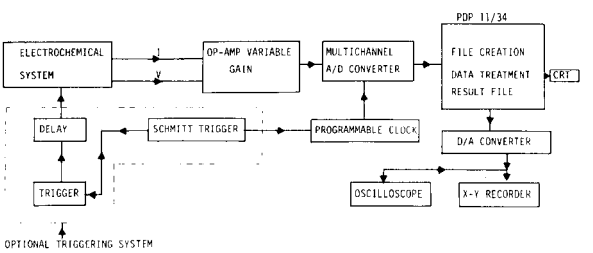

Fig. 1. Block diagram of experimental and computer hardware.

FORTRAN PROGRAM

```
C       DECLARATION OF COMMON BLOCK TO BE
C       SHARED WITH MACRO SUBROUTINE
        INTEGER DATBUF
        COMMON /DATA/ L,M,ICODE,ICOUNT,DATBUF(4096)
C       INPUT PARAMETERS
        TYPE*,'INPUT I AND V CHANNELS'
        ACCEPT*,L,M
        TYPE*,'INPUT SAMPLING TIME INTERVAL'
        ACCEPT*,T
C       DETERMINATION OF CLOCK CODE AND COUNT FOR
C       THE REQUIRED SAMPLING TIME
        CALL TIMER(T,ICODE,ICOUNT)
C       GOTO MACRO COLLECTION SUBROUTINE
        CALL DATAC
C       STORE DATA IN A FILE
        CALL ASSIGN(2,,-1,'NEW',,)
        DEFINE FILE 2(1,4096,U,NREC)
        NREC=1
        WRITE(2'NREC) DATBUF
        CALL CLOSE(2)
        CALL EXIT
        END
```

MACRO PROGRAM

```
        ADSTAT=170400    ;DEFINITION OF ADDRESSES FOR THE
        ADBUF=ADSTAT+2   ;STATUS AND BUFFER REGISTERS OF THE A/D
        CLSTAT=170404    ;AND THE STATUS AND COUNTER REGISTERS
        CLKBUF=CLSTAT+2  ;OF THE KW11-K
DATAC:: MOV ICOUNT,CLKBUF
        MOV ICODE,CLSTAT
        MOV #2048.,R1    ;SET UP A DATA COUNTER
        MOV #DATBUF,R0   ;SET UP A POINTER TO THE DATA BUFFER
        MOV L,ADSTAT     ;SELECT CHANNEL L TO BE SAMPLED
ALOOP:  TSTB ADSTAT      ;IS SAMPLE DONE?
        BPL ALOOP        ;LOOP IF NOT
        MOV ADBUF,(R0)+  ;MOVE DATA INTO STORAGE LOCATION
        MOV M,ADSTAT     ;SELECT CHANNEL M TO BE SAMPLED
BLOOP:  TSTB ADSTAT
        BPL BLOOP
        MOV ADBUF,(R0)+
        MOV L,ADSTAT     ;RETURN TO SAMPLE CHANNEL L
        DEC R1           ;DECREMENT DATA COUNTER
        BNE ALOOP        ;LOOP IF SAMPLING NOT FINISHED
        RTS PC           ;RETURN TO MAIN PROGRAM
        .PSECT DATA,GBL,OVR
L:      .BLKW 1
M:      .BLKW 1
ICODE:  .BLKW 1
ICOUNT: .BLKW 1
DATBUF: .BLKW 4096.
        .END DATAC
```

Fig. 2. FORTRAN and MACRO programs for data acquisition.

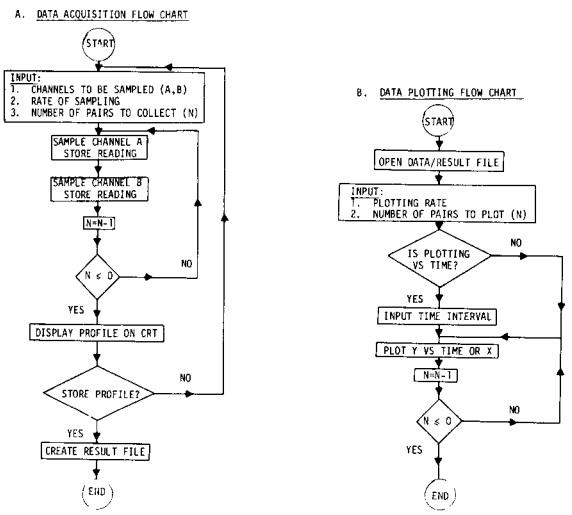

Fig. 3. Flow charts for (A) data acquisition; (B) data plotting.

here was +5V to −5V. The resulting amplified signals were then fed through an H322 distribution panel to a multichannel, 12-bit A/D converter (Digital AD11-K) in a differential input mode, by means of shielded cable to minimize noise pick-up. The sampling rate was determined by software programming of the built-in Digital KW11-K clock, which had fixed crystal-controlled frequencies of 60 Hz, 100 Hz, 1 kHz, 100 kHz, 1 MHz, and provision for obtaining, through software, any desired intermediate frequency. Current and potential values were sampled alternately (at rates discussed below) and the resulting digitized data were stored as (I, V) pairs in the computer.

Once the data had been stored, plotting by means of a 12-bit D/A analog converter (Digital AA11-K) was made on an x—y recorder with software control of the plotting speed, chosen sufficiently low that writing errors were avoided. Normally I vs. V or I vs. time (t) was plotted.

The stored data could be further treated by means of appropriate software. Typical applications include; optimization of the data by signal averaging, IR correction, determination of peak parameters [7], integration and deconvolution of I vs. V profiles for electrochemical adsorption, e.g., underpotential deposition processes, in multiple states within monolayer coverage.

In the present work, integration of I vs. V or I vs. t data at various sweep rates (S) was performed by means of the FORTRAN Subroutine QSF from the FORTRAN Scientific Subroutine Package provided by Digital. This subroutine utilizes Simpson's Rule, together with Newton's 3/8 Rule [8, 9], to integrate equidistant data values (in the present experiments, collected at constant intervals ΔV or Δt).

In order to provide illustrative results reflecting current research interests in this laboratory [10, 11], applications of minicomputer procedures to cyclic voltammetric experiments on surface processes at gold and iridium in 1.0 M $HClO_4$ and 0.5 M H_2SO_4 will be described. The experimental results were obtained by using standard techniques and equipment [12, 13].

RESULTS AND DISCUSSION

The results obtained are discussed in terms of optimization of input parameters, exemplification of treatment of various types of transient profiles derived from electrochemical experiments, noise level problems, and the advantages of a computer-based system over conventional methods of data recording and analysis [14].

Input parameters

Four input parameters must be optimized as outlined below in order to utilize fully the capabilities of the A/D converter without degrading the data.

Rate of sampling. Theoretically this should be determined by the rate at which the event takes place but in practice it is limited by hardware and software capabilities. On the hardware side, it has to be recognized that the A/D converter has a finite throughput time which includes sample-and-hold, interchannel settling and A/D conversion time, typically 20 μs. This couples with software delays such as flag testing and loading of status registers which in the present case adds another 20 μs, to give a maximum sampling rate (m.s.r.) given by m.s.r. (Hz) = 1/time delays (s) = $1/40 \times 10^{-6}$ s $\equiv 25 \times 10^3$ Hz.

The practical sampling rate used depends on the resolution of the A/D converter and the sweep rate at which the experiment is being conducted. Since the A/D converter has a data register of 12 bits, it can store only 2^{12} values (4096). Then the resolution (r) of the converter is given by r = voltage range (mV)/2^{12} = +5V—(−5V)/4096 = 10000 mV/4096 $\simeq$ 2.5 mV. In sampling a linear potential ramp, the change in potential, δV, accompanying the passage of an increment of time, δt, is given by δV (mV) = sweep rate (mV s^{-1}) $\times$ δt (s). Thus, by combining the resolution of the A/D converter

and the fastest sampling time, it follows that the limit of sweep rate that can be handled for potential sampling at increments of 2.5 mV is given by 2.5 mV/40 × 10^{-6} s = 60 V s^{-1}. Therefore, any linear potential ramp with a sweep rate exceeding 60 V s^{-1} will be sampled at potential intervals greater than 2.5 mV. If two channels are sampled, which is the case when I vs. V profiles are to be recorded, the highest sweep rate that can be handled, when sampling is to be made every 2.5 mV, will be halved.

It is possible to improve the resolution by means of amplification of the voltage signal, so that consecutive voltage points that would normally be separated by only 1 mV, and thus would be below the resolution of the A/D converter, are in practice separated by 1 mV multiplied by the amplification factor. However, this improvement in resolution reduces the limit of sweep rate that can be handled for potential sampling at increments of 1 mV, as indicated above.

Mode of sampling. Sampling can be performed in several modes determined chiefly by individual preference with regard to the desired display of data and type of information required. For cyclic voltammetric results, however, a method of sampling alternate values of I and V is convenient so that the profile can be later displayed in the same way that it is normally recorded, i.e., I vs. V.

A problem arises in the sampling of I—V data pairs: after a sample V_i has been taken, the current I_i sampled next does not correspond to V_i but to [V_i + (sampling time × sweep rate)]. Thus, a correction has to be introduced by means of software instructions before the data are treated further.

In sampling I vs. t relations, triggering of the collection routine at an accurately known potential value on the potential ramp is necessary in order to assign correct values of potential corresponding to those of time on the time axis, as determined by the sweep rate. I vs. V sampling simplifies the circuit and does not require any knowledge of the ramp slope. Nevertheless, in some cases, such as IR drop determination or recording of current or potential decay curves, it is obvious that sampling in time is required.

Synchronization of sampling. In the study of a current response which is stable repetitively in time with respect to a periodic potential program, triggering the initiation of I vs. V sampling is not necessary; and only the time interval between samples need be controlled. The AD11-K sampling was timed by means of overflow pulses from the clock. In the repetitive mode, the clock counts at a predetermined rate until the previously-loaded clock counter goes to zero. Then an overflow pulse triggers the AD11-K which collects a sample, and the initial value of the counter is reloaded and the process repeated.

For collection of one-shot I vs. t or V vs. t transients, the necessary triggering of the initiation of sampling can be conveniently achieved by means of Schmitt trigger (ST) circuits on the KW11-K which start the clock when the input potential to the ST crosses a predetermined threshold in a specified direction. A delay circuit may be needed for the ST to be triggered slightly

before the transient signal is presented, so that the initial part of the transient may be obtained. Once sampling has been initiated, timing proceeds as outlined above.

Number of samples. This depends primarily on: (a) the type of experiment, e.g. continuous sweeping contrasted with holding the potential constant at the end of a sweep (anodic or cathodic) for programmed periods of time; (b) the number of sweeps to be recorded, in the event of optimization through signal averaging; and (c) memory limitations of the storage device. Typically, approximately 4000 points is a convenient sample number, with the data being stored as integers to minimize file size.

Typical profiles

Figures 4—11 show sets of results obtained for several different types of experiments which serve to illustrate the usefulness and capabilities of the computer-based method. The salient features of these *I*—*V* profiles will be briefly discussed below, as each illustrates a different advantage or capability of the computer, and underlines the versatility of the technique. Where possible, directly photographed oscilloscope traces are displayed for comparative purposes together with the *I* vs. *V* profiles recorded and played back by means of the computer on large-scale graphs at a low writing speed. Different types of experiments are considered in the following paragraphs.

Work at various sweep rates. Figure 4 shows results of a typical study of the effect of varying the sweep rate (*S*) on the surface oxide formation and reduction behaviour of gold in aqueous 1 M $HClO_4$ [11], keeping *I/S* (which gives the capacitance [7]) constant in the *S* range 0.5—10 V s^{-1}. The behaviour

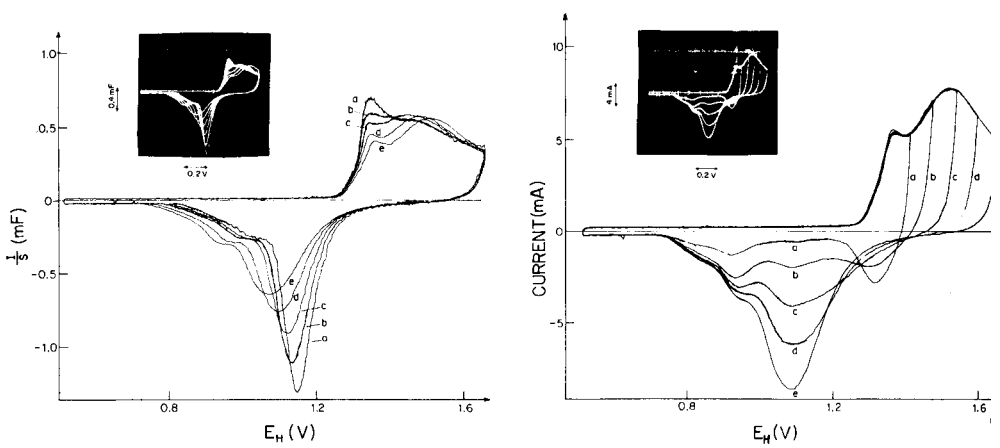

Fig. 4. Comparison of cyclic voltammetry *I/S* vs. *V* profiles for gold in 1 M $HClO_4$ at 298 K collected and plotted through the computer, with directly recorded oscilloscope traces: (a) 0.5 V s^{-1}; (b) 1 V s^{-1}; (c) 2 V s^{-1}; (d) 5 V s^{-1}; (e) 10 V s^{-1}.

Fig. 5. Comparison of cyclic voltammetry *I* vs. *V* profiles for gold in 1 M $HClO_4$ at 15 V s^{-1} and 298 K, with variable anodic end potential, collected and plotted through the computer, with directly recorded oscilloscope traces: (a) 1.415 V; (b) 1.475 V; (c) 1.540 V; (d) 1.600 V; (e) 1.665 V.

at high sweep rates was not included here because of the relatively large *IR* drop which then arises at appreciable surface oxide coverages ($\theta_0 \sim 0.5$). The behaviour at lower sweep rates is discussed later with regard to background noise.

Systematic variation of the positive end-potential of successive anodic sweeps. Figure 5 shows the results of an experiment of this type carried out at 10 V s^{-1} on gold in 1 M $HClO_4$. The resolution obtained here on the x—y recorder output is strikingly superior to that obtainable on the oscilloscope trace. Note that the trace thickness on the storage oscilloscope used (Tektronix type 5115) routinely obliterates detail in crowded regions of the

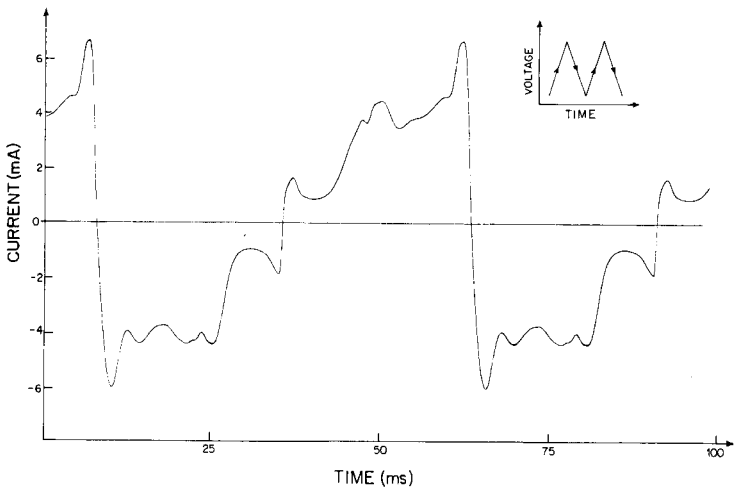

Fig. 6. Computer-collected and plotted I vs. t profiles for gold in 0.2 M $Ba(OH)_2$ at 50 V s^{-1} and 298 K, obtained in cyclic voltammetry between potentials V_A = 1.252 and V_C = 0.040 V E_H.

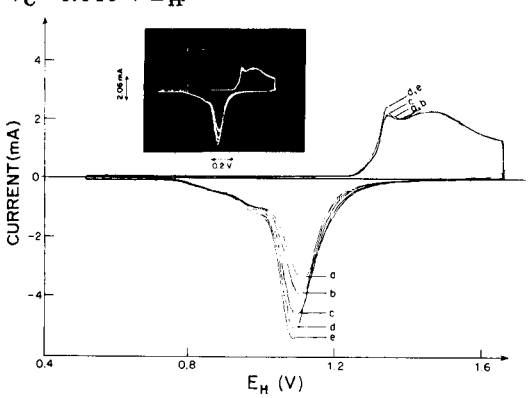

Fig. 7. Comparison of successive anodic and cathodic linear potential sweep I vs. V profiles for gold in 1 M $HClO_4$ at 2 V s^{-1} and 298 K, collected and plotted through the computer, with directly recorded oscilloscope traces, with arrest (τ, s) of potential at 1.662 V E_H for (a) 0.0 s; (b) 0.1 s; (c) 0.5 s; (d) 1.0 s; (e) 2 s.

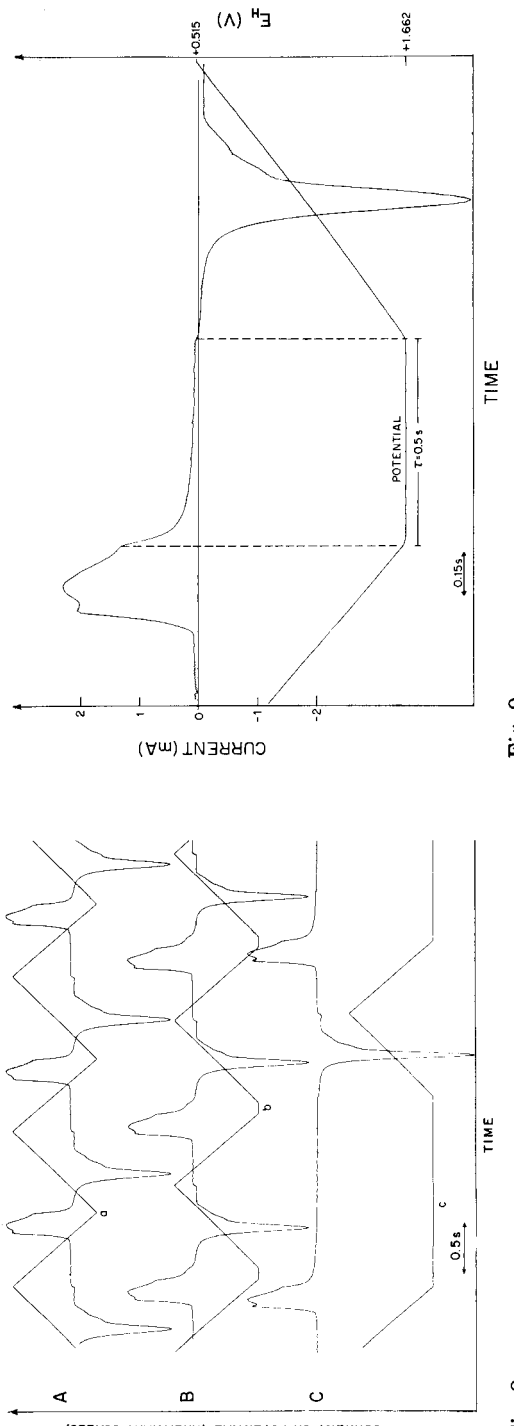
CURRENT OR POTENTIAL (ARBITRARY SCALES)
A
B
C
a
b
c
0.5s
TIME

Fig. 8.

CURRENT (mA)
2
1
0
-1
-2
POTENTIAL
T=0.5s
0.15s
TIME
E_H (V)
+0.515
+1.662

Fig. 9.

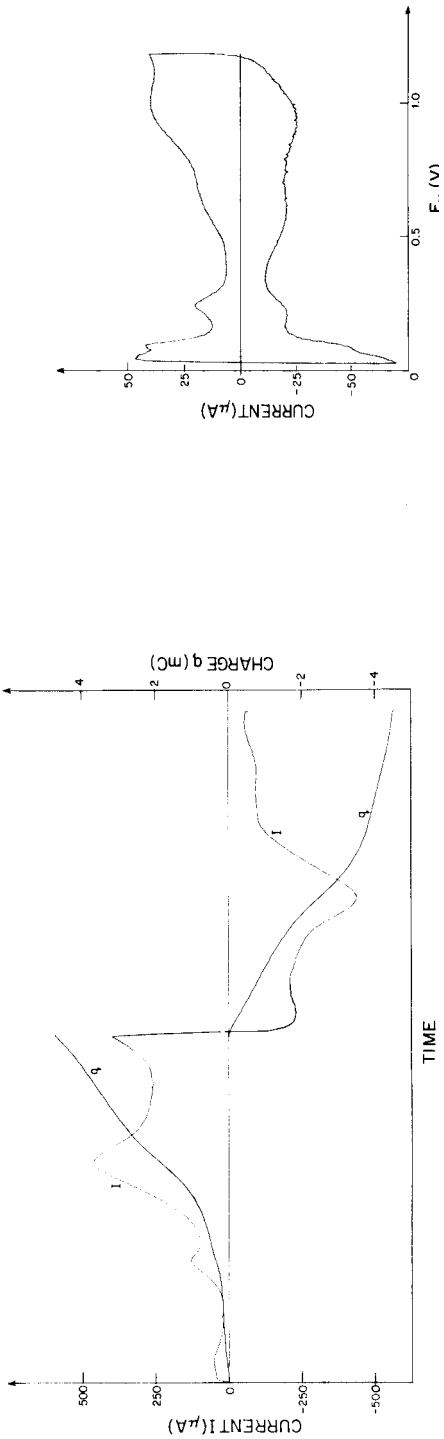
CURRENT I(μA)
500
250
0
-250
-500
CHARGE q (mC)
4
2
0
-2
-4
I
q
TIME
CURRENT(μA)
50
25
0
-25
-50
0
0.5
1.0
E (V)

plots; it is evident from Fig. 5 that this is not a problem at all on the recorded computer output of I vs. V data.

Fast sweep work. Figure 6 shows an I vs. t profile for the double-layer charging region of the I vs. V profile on gold in 0.2 M $Ba(OH)_2$ at 50 V s^{-1}, where only a small amount of surface oxide is allowed to form. This example illustrates the applicability of the method to experiments at higher sweep rates.

Holding experiments. These include experiments where the end-potential of the anodic sweep is maintained for programmed periods of time. Figure 7 shows the I vs. V profiles obtained for gold in 1 M $HClO_4$ at 2 V s^{-1} where the anodic potential limit was maintained for 0 (multisweep), 0.1, 0.5, 1 and 2 s. Again the resolution obtained on the x—y recorder output is seen to be substantially superior to that on the oscilloscope, especially in detecting small, but significant changes in relatively crowded regions of the profile which are not distinguishable on the concomitant oscilloscope trace. The 0_{A2} and 0_{C2} regions are especially notable (cf. [13]).

Figure 8 illustrates I and V vs. t profiles, again for gold in 1 M $HClO_4$ at 2 V s^{-1}. Of particular interest is the good stability of the readings which are free of noise, especially in the V vs. t plot. Figure 9 presents an expanded view of the computer-plotted profile with a holding time of 0.5 s and shows how the I vs. t decay curve can be easily observed.

Data treatment. Figure 10 shows an I vs. t profile for iridium in 0.5 M H_2SO_4 at 0.05 V s^{-1}; because the thick, reversibly formed and reduced oxide [15] is present on the surface of this electrode, the current signal in this case is high enough not to be disturbed by the noise problems discussed below. The corresponding charge isotherm, determined by computer integration of the I vs. $V(t)$ profile, is plotted together with the latter profile with appropriate software-determined scales for each of the plots. The charges for the anodic and cathodic profiles were obtained separately by the integration procedure above.

Noise level

Experiments at $S<0.5$ V s^{-1} tend to have a higher noise level than those

Fig. 8. Series of I vs. t curves in response to successive anodic and cathodic linear potential sweeps (V vs. t) with and without arrest (τ, s) for various times at the end of anodic sweeps, for gold in 1 M $HClO_4$ at 2 V s^{-1} and 298 K. (A) τ = 0.0 s, arrest at a; (B) τ = 0.1 s, arrest at b; (C) τ = 2.0 s, arrest at c. Curves were computer-collected and plotted.

Fig. 9. Computer-collected and plotted I vs. t response to anodic and cathodic linear potential sweeps for gold in 1 M $HClO_4$ at 2 V s^{-1} and 298 K, with an arrest for 0.5 s at 1.662 V E_H. This plot also shows the current decay on holding the potential at 1.662 V.

Fig. 10. Computer-collected and plotted I vs. t anodic and cathodic profiles for iridium in 0.5 M H_2SO_4 at 0.050 V s^{-1} and 298 K, and the computer-calculated and plotted charge isotherm (q) for these profiles.

Fig. 11. Computer-collected and plotted I vs. V profile for iridium in 0.5 M H_2SO_4 at 0.050 V s^{-1} and 298 K.

done at higher S values because of the relation between I and S. Thus, at lower S, the I signal is relatively smaller and amplification does not help because the signal-to-noise ratio is low and fixed, so that the noise becomes amplified with the signal, unless a signal-averaging procedure is applied to a repeated set of sweeps.

For $S \leqslant 0.05$ V s^{-1}, as applies in Fig. 11 for iridium in 0.5 M H_2SO_4 at 0.05 V s^{-1}, a 60-cycle filter can be effectively used to record an excellent, undistorted, noise-free I vs. V profile of the monolayer stage of surface oxidation at iridium. For values of S beyond 0.1 V s^{-1} however, it is known that such a filter distorts the I vs. V profile to an unacceptable extent. While an x—y recorder can be used without a filter because some damping of noise is achieved on account of mechanical inertia, the computer samples both the signal and the noise, giving profiles that are unacceptable, if a filter cannot be used in this range of S values.

Some approach to a solution of this problem can be made by design of alternate filters as well as by multiple sweep collection, followed by signal averaging, as is done in reflectance work [16].

Conclusions

It is apparent that a computer-based system can be utilized with advantage in routine experimental cyclic voltammetry work over the traditional methods employing analogue or digital oscilloscope recording, or the use of transient recorders.

Some of the advantages of the computer-based data collection and treatment system are as follows. First, high resolution of transient or repetitive non-steady signals allows small but significant differences in various I vs. V profiles to be detected better than is possible on storage oscilloscopes. Secondly, computer calculation of derived quantities, such as the charge isotherm for an electrochemical surface process and treatment of data in general, can be done accurately and rapidly. Thirdly, output of the collected data at low, error-free writing speeds on to an x—y recorder allows manual calculation of diagnostic parameters [17], superposition of experimental data and calculated results, as well as scaling up of data obtained under various conditions for comparison or publication purposes. Fourthly, safe storage of results in the short and long term, e.g., on magnetic tape, can be easily realized.

Other possibilities include automatic IR correction, multistate [1] curve deconvolution or simulation procedures and applications to the study of diffusion-controlled processes by means of cyclic voltammetry. For the latter type of application, the data processing programs will, of course, be different from those for treatment of surface processes.

Grateful acknowledgement is made to the Natural Sciences and Engineering Research Council of Canada for award of funds for acquisition of a PDP 11/34 minicomputer for electrochemical energy conversion studies. One of

us (J. M.) acknowledges the award of a CONICIT (Venezuela) scholarship and another (B. B.) of a Noranda Research Scholarship. D. T. acknowledges the award of a Province of Ontario and later an N.S.E.R.C.C. Graduate Scholarship.

REFERENCES

1 D. M. Kolb, Adv. Electrochem. Electrochem. Eng., 11 (1978) 125; see also B. E. Conway, F. C. Ho and H. Angerstein-Kozlowska, J. Vacuum Sci. Technol., 14 (1977) 351.
2 M. W. Breiter, J. Electrochem. Soc., 112 (1965) 845.
3 P. E. Whitson, H. W. Vandenborh and D. H. Evans, Anal. Chem., 45 (1973) 1298.
4 D. Gosden, M. Hayes, A. T. Kuhn and D. Whitehouse, J. Appl. Electrochem., 8 (1978) 437.
5 K. F. Drake, R. P. van Duyne and A. M. Bond, J. Electroanal. Chem., 89 (1978) 231.
6 J. W. Cooper, The Minicomputer in the Laboratory with Examples using the PDP-11, Wiley, New York, 1977.
7 H. Angerstein-Kozlowska, J. Klinger and B. E. Conway, J. Electroanal. Chem., 75 (1977) 45; 75 (1977) 61; 87 (1978) 301; 87 (1978) 321.
8 F. B. Hildebran, Introduction to Numerical Analysis, McGraw-Hill, New York, 1956, p. 71.
9 R. Zurmuehl, Praktische Mathematik für Ingenieure und Physiker, Springer, Berlin, 1963, p. 214.
10 B. E. Conway and H. Angerstein-Kozlowska, Acc. Chem. Res., (1981) in press.
11 H. Angerstein-Kozlowska, B. E. Conway, B. Barnett and J. Mozota, J. Electroanal. Chem., 100 (1979) 417.
12 F. G. Will and C. A. Knorr, Z. Elektrochem., 64 (1968) 270.
13 H. Angerstein-Kozlowska, B. E. Conway and W. B. A. Sharp, J. Electroanal. Chem., 43 (1973) 9.
14 S. P. Perone and D. O. Jones, Digital Computers in Scientific Instrumentation. Applications to Chemistry. McGraw-Hill, New York, 1973.
15 P. A. J. Rand and R. Woods, J. Electroanal. Chem., 55 (1974) 375.
16 F. C. Ho, B. E. Conway and H. Angerstein-Kozlowska, Surf. Sci., 81 (1979) 125.
17 H. Angerstein-Kozlowska and B. E. Conway, J. Electroanal. Chem., 95 (1979) 1.

Analytica Chimica Acta, 133 (1981) 203–208
Computer Techniques and Optimization
Elsevier Scientific Publishing Company, Amsterdam — Printed in The Netherlands

A MODIFIED GRAN METHOD FOR DETERMINATION OF EQUIVALENCE POINTS IN POTENTIOMETRIC PRECIPITATION TITRATIONS

JORGE F. MAGALLANES and AURORA F. CARIDI

Departamento Química, Gerencia Procesos Quimicos, Comision Nacional de Energia Atomica, 1429 Buenos Aires (Argentina)

(Received 28th January 1980)

SUMMARY

Gran's method is frequently applied in potentiometric titration to obtain a more precise estimate of the equivalence point, particularly when the analyte concentration is too low to give well defined end-points. With precipitation reactions, however, when the analyte concentration is comparable to the solubility of the precipitate, even the use of Gran's method will not avoid significant errors. A correction term is introduced and a computer program outlined to overcome this problem. Titrations of 10^{-4} M chloride are used for illustration.

Gran [1] utilized algebraic manipulation of the Nernst equation and the stoichiometry to obtain various expressions which describe all cases of potentiometric titrations.

In precipitation titrations of the general type $xA + yB \rightarrow A_xB_y$, the expression is

$$(V_0 + V)\, 10^{16.9\, nA\,(E-K_1)} = K_2\,(V_e - V) \qquad (1)$$

where V_0 is the initial volume, V the volume added, and V_e the volume added at the equivalence point; nA or nB is the number of electrons involved in the electrode reaction of A or B, respectively; K_1 and K_2 are arbitrary constants; $F\,(2.30\,RT)^{-1} = 16.9\ V^{-1}$ (at 25°C). Equation (1) is applicable for an electrode which is sensitive to ion A before the equivalence point is reached. After the equivalence point, the expression is

$$(V_0 + V)\, 10^{16.9\, nA\,(K_3-E)}\, x/y = K_4\,(V - V_e) \qquad (2)$$

The analogous expressions when the electrode is sensitive to ion B are

$$(V_0 + V)\, 10^{16.9\, nB\,(K_5-E)}\, y/x = K_6\,(V_e - V) \qquad (3)$$

$$(V_0 + V)\, 10^{16.9\, nB\,(E-K_7)} = K_8\,(V - V_e) \qquad (4)$$

before and after the equivalence point. In all cases it is assumed that A is the analyte and B the titrant added.

The plots of the left-hand sides of eqns. (1)—(4) vs. V are straight lines. Figure 1 shows the plots obtained for eqns. (3) and (4) applied to chloride titration with silver(I) standard solutions and the Orion model 94-16 Ag_2S indicator electrode. When the initial concentration of chloride is 10^{-3} M (or more), the V_e results are exact, but when this is decreased to 10^{-4} M the values are considerably different from the theoretical values. With 10^{-4} M solutions, the straight lines do not intersect on the abscissa as predicted by the equations. Further, the intersection point does not indicate the true value of V_e, as would be expected if the errors of both lines were compensated.

Various workers have described improvements of the method of calculation to determine V_e. McCallum and Midgley [2] developed a more general expression than Gran's equations. They took into account the solubility of the ionic species precipitated and the activity coefficients. In the present paper, Gran's general development is retained and the solubility effect is considered as a correction term. The calculations are then the same as in Gran's method and the correction term can be included or not, depending on the error expected, which can be estimated in advance. Isbell and Pecsok [3] used a method based on a rigorous non-linear least-squares adjustment to fit experimental variables. They considered theoretically a solubility term but it was neglected during derivation of the equations.

Another method of data handling in the evaluation of low concentrations is the standard addition method. Still [4] compared this method to Gran's

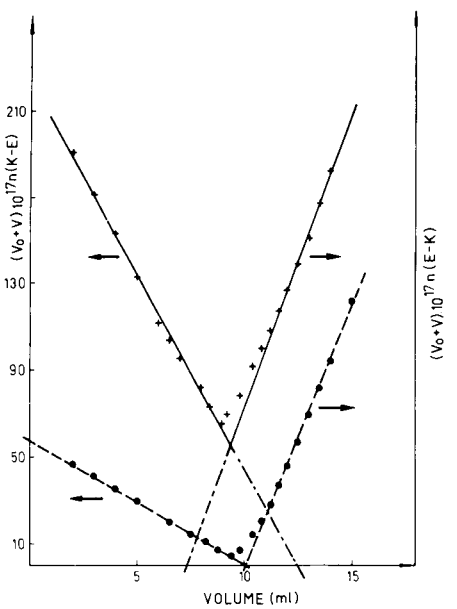

Fig. 1. Gran plots based on eqns. (1—4). (•) Titration of 10 ml of 10^{-3} M chloride with 10^{-3} M silver nitrate in 1 M HNO_3; (+) titration of 100 ml of 10^{-4} M chloride with 10^{-3} M silver nitrate in 1 M HNO_3.

method for complexation reactions. Horvai et al. [5] used a different method of data handling for the standard addition calculation. Although this technique is simpler and faster than others, standard addition still gives less reliable results than titration methods.

THEORY

The same general precipitation reaction as used by Gran and as cited above is considered. In all cases, species A is active at the electrode, exchanging n electrons, while B is electrochemically inert.

First, the case where A is the analyte and B the standard is considered. Before the equivalence point, the concentration of B (C_B) is equal to the concentration (S_B) predicted by the solubility product. $C_{A'}$ becomes the excess with respect to C_B. Thus $C_B = S_B$ and

$$C_A = C_{A'} + S_B\, x/y \tag{5}$$

Two other equations related to the solubility product and the stoichiometry of the reaction are well known:

$$K_{so} = C_A^x C_B^y = S_B^y\ (C_{A'} + S_B x/y)^x \tag{6}$$

$$C_A^0 V_0 = C_B^0 V_e x/y \tag{7}$$

where C_A^0 and C_B^0 are the original concentrations of the reactants. From here, the development of the theory proceeds similarly to Gran, but with some modifications. The value of $C_{A'}$ for V ml of standard added is

$$C_{A'} = (C_A^0 V_0 - C_B^0 V x/y)/(V_0 + V) = C_B^0 (x/y)\ (V_e - V)/(V_0 + V) \tag{8}$$

Substitution of eqn. (8) in eqn. (5) gives

$$C_A = (x/y)\ \{[C_B^0 (V_e - V)/(V_0 - V)] - S_B\} \tag{9}$$

Another expression for C_A can be obtained from the Nernst equation:

$$E = E' + f\, RT(nF)^{-1} \ln C_A \tag{10}$$

where $E' = E_0' + E_j - E_r + f\, RT(\mathrm{nF})^{-1} \ln \gamma$. Here E is the electrode potential, E' is the electrode formal potential, E_0' is a function which depends on electrode construction, E_j is the junction potential, E_r the reference electrode potential, γ is the activity coefficient of A and $f = S_L nF(RT)^{-1}$ is the fraction of the ideal Nernstian response of the electrode (S_L = slope). It is assumed that E' will remain constant during the titration and then E' can be expressed as $E' = f\, RT(nF)^{-1} \ln K_A^0$, where K_A^0 is a constant.

Together with eqn. (10), this expression for E' gives

$$E = f\, RT(nF)^{-1} \ln (C_A^0 K_A^0) \tag{11}$$

Changing to decimal logarithms and replacing $F(2.30\, RT)^{-1}$ by its value 16.9 V^{-1} (at 25°C) gives

$$C_A = (K_A^0)^{-1}\ 10^{16.9nE/f} \tag{12}$$

Comparison of eqn. (12) with the second term of eqn. (9) and rearrangement gives

$$(V_0 + V)\,[10^{16.9nE} - K_A\,(x/y)\,S_B] = K_A^0\,(x/y)\,C_B^0\,(V_e - V) \tag{13}$$

To express eqn. (13) in a form similar to that of Gran's equation, the following substitutions are made: $K_A^0\ (x/y)\ C_B^0 = K_1\ 10^{16.9nK_2}$, where K_1 and K_2 are arbitrary constants, and $K_A^0 = 10^{16.9nE'/f}$ (from $E' = f\,RT(nF)^{-1}\ln K_A^0$). With these substitutions, and division by $10^{16.9nK_2}$, eqn. (13) becomes

$$(V_0 + V)\,[10^{16.9n(E-K_2)/f} - (x/y)S_B\ 10^{16.9n(E'-K_2)/f}] = K_1\,(V_e - V) \tag{14}$$

which can be compared with eqn. (1) obtained by Gran. The main term on the left-hand side of eqn. (14) is the same as in eqn. (1), but there is a Gran term. On the same side there is a less significant correction term which is a function of solubility. In eqn. (1) $f = 1$ is assumed, i.e. exactly Nernstian response of the electrode; if this is not the case, the correct value can be introduced in eqn. (14). A critical test for eqn. (14) is that it reduces to eqn. (1) when the solubility becomes negligible, i.e., when S_B approaches zero.

In the reverse case, when A is the standard and B the analyte (similar to Gran's eqn. 3), $C_A = S_A$, $C_B = C_{B'} + S_A\ y/x$, $K_{so} = S_A{}^x\,(S_A\ y/x + C_{B'})^y$, $C_B^0\ V_0 = C_A^0\,V_e y/x$, and

$$C_{B'} = (C_B^0 V_0 - C_A^0 V y/x)/(V_0 + V) = C_A^0\,(y/x)\,(V_e - V)/(V_0 + V) \tag{15}$$

Substitution of eqn. (15) in the preceding equation for K_{so} followed by substitution in the expression for C_B, gives an expression equivalent to eqn. (9). Thereafter the development continues in the same way as the previous one giving:

$$(V_0 + V)\,[10^{16.9n(x/y)(K_2-E)/f} - (y/x)\,(S_A/K_{so}^{1/y})\,10^{16.9n(x/y)(K_2-E')/f}]$$
$$= K_1\,(V_e - V) \tag{16}$$

This expression cannot be directly compared with the corresponding Gran equation because of differences in its development. However, the similarities are evident and the considerations are the same as those made for eqn. (14).

When the corresponding derivations are applied to the range in which the equivalence point has been overshot (i.e., $V > V_e$), it is found that for A = analyte and B = standard, eqn. (16) is valid if the sign of the right-hand side is changed. And for A = standard and B = analyte, eqn. (14) is valid with the same change of sign. In the first case, direct comparison with eqn. (2) is possible.

CALCULATIONS

To obtain V_e from eqns. (14) or (16), it is necessary to plot the left side of those equations against V. A problem in resolving the equations arises

from the calculation of S_A or S_B (S generally). This is not a constant but, because of the common ion effect, depends on the excess of reagent present in each aggregate, as is obvious from the equations for K_{so}. However, to calculate $C_{B'}$ or $C_{A'}$ from eqns. (15) or (8), V_e must be known, and so an iterative procedure is required. First, V_e is estimated without taking the correction term into account. With this value S is calculated, and a corrected value of V_e is obtained. Iteration is continued until the desired approximation is reached. Convergence is fast: 3—5 cycles were enough to bring V_e with the required titration error.

Calculations were done with a FORTRAN IV program. The main routine uses two subroutines, one of which calculates the linear regression for successive estimates of V_e; the other carries out the Newton—Raphson iteration method to calculate S from the relevant expression for K_{so} and was taken from IBM FORTRAN SUBROUTINES. Figure 2 shows the program flow chart; a program listing can be obtained on request from the authors.

The values of E' and f were calculated by plotting electrode potential E vs. pAg. The K_2 value (arbitrary) was taken around the average of the measured potential range of the titration. The K_{so} value taken from the literature was corrected for ionic strength (1 M HNO_3 medium) by the modified Debye—Hückel equation [6].

RESULTS AND DISCUSSION

Figure 3 shows the advance of the iteration corresponding to the experimental data of Fig. 1 for 10^{-4} M chloride solution before the equivalence point. The straight lines show the successive corrections of the initial data until the desired approximation is obtained.

The correction was used successfully in the following cases: A = standard and B = analyte before the equivalence point, or A = analyte and B = standard after the equivalence point. In the other two cases, the correction does not approach the correct V_e sufficiently when C_A^0 or C_B^0 are about 10^{-4} M or less. Adsorption of ionic species on the silver chloride precipitate was not taken into account but it can introduce some deviations [7].

Some conclusions can be reached from eqns. (14) and (16) about the concentration range where the correction made is significant. As an example, eqn. (14) is used, and the required error is taken as less than 1%. The relation between the correction term and the main term should then be: $(x/y)S\ 10^{16.9n(E'-K_2)/f}/10^{16.9n(E-K_2)/f} < 0.01$. By cancelling out $10^{16.9nK_2}$, introducing eqn. (10) and assuming $f = 1$, we then get $(x/y)S\ 10^{16.9n(E-E')} = (x/y)S/C_A < 0.01$.

Rearrangement gives $100(x/y)\ S < C_A$, which implies that the concentration of the electroactive species should be more than 100 times the solubility of the precipitate formed when $x = y$. A general form of this expression for a required error of less than ϵ% would be

$$(100/\epsilon)\ (x/y)S < C_A \qquad (17)$$

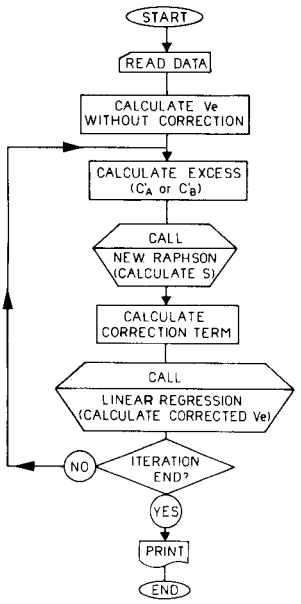

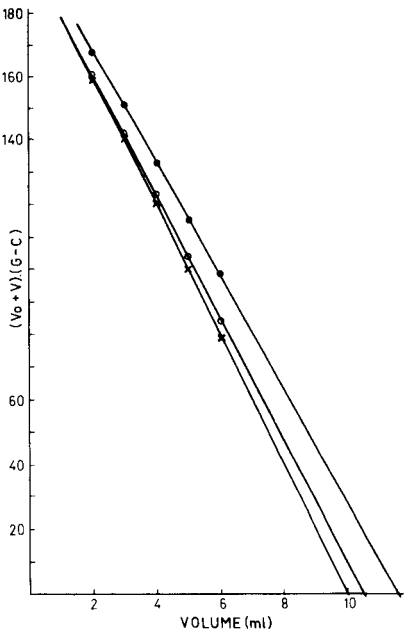

Fig. 2. Flow chart of calculation program.

Fig. 3. Successive approaches in the V_e calculation for the titration of 100 ml of 10^{-4} M chloride with 10^{-3} M silver nitrate in 1 M HNO_3. (•) First iteration (without correction); (○) second iteration; (×) fifth iteration. G is the Gran term ($= 10^{16.9\,n(x/y)(K_2-E)/f}$), and C is the correction term ($= (y/x)(S_A/K_{so}^{1/y})\ 10^{16.9\,n(x/y)(K_2-E')/f}$).

Expression (17) is simpler than others given in the literature [2], and is easily evaluated if the calculations must be done with the correction term. Use of eqn. (16) leads to the same conclusion. In the example given, $K_{so}(AgCl) = S^2 \approx 10^{-10}$, i.e. $S \approx 10^{-5}$, which explains why there are no appreciable errors for titrations of 10^{-3} M chloride but significant errors in titrations of lower concentrations.

The authors thank Dr. Stephen Feldberg for discussions during the preparation of the manuscript.

REFERENCES

1 G. Gran, Analyst, 77 (1952) 661.
2 C. McCallum and D. Midgley, Anal. Chim. Acta, 65 (1973) 155.
3 A. F. Isbell, Jr. and R. L. Pecsok, Anal. Chem., 45 (1973) 2363.
4 E. Still, Anal. Chim. Acta, 107 (1979) 377.
5 G. Horvai, L. Domokos and E. Pungor, Fresenius Z. Anal. Chem., 292 (1978) 132.
6 J. N. Butler, Solubility and pH calculations, Addison-Wesley, 1964, p. 24.
7 R. A. Durst, (Ed.), Ion Selective Electrodes, National Bureau of Standards Special Publication, No. 314, 1969, p. 401.

Analytica Chimica Acta, 133 (1981) 209—213
Computer Techniques and Optimization
Elsevier Scientific Publishing Company, Amsterdam — Printed in The Netherlands

Short Communication

IMPROVED SENSITIVITY USING A MICROCOMPUTER FOR ELECTROTHERMAL ATOMIC ABSORPTION SPECTROMETRY WITH A METAL MICROTUBE

MASAMI SUZUKI*, KIYOHISA OHTA and TATSUYA YAMAKITA

Department of Chemistry, Faculty of Engineering, Mie University, Kamihama-cho, Tsu, Mie-ken 514 (Japan)

(Received 2nd June 1980)

Summary. Data enhancement by signal accumulation, scale expansion after background subtraction, and smoothing with the aid of the microcomputer enables limits of detection to be improved by up to an order of magnitude. Data are reported for 15 elements.

Electrothermal atomization provides increased sensitivity in atomic absorption spectrometry. The commonly used graphite atomizers are difficult to heat uniformly and quickly, and have the disadvantage of carbide formation for some elements. Lining of graphite furnaces with tantalum foil has been used to overcome these difficulties. Compared to graphite furnaces, microtube atomizers [1] have several advantages such as higher possible heating rates, lower input power, less thermal gradient over the atomizer, no problems with carbide formation and lower background emission in the 250—350 nm spectral region. In particular, molybdenum microtubes give more reproducible atomization profiles than other metal atomizers; the formation of intermetallic compounds between the atomizer surface and the analyte has not been observed. The principal drawback with this atomizer is the fluctuation of background at increased heating rate. This drawback can be simply overcome by using a microcomputer. Furthermore, the computer permits the tracing of precise atomization profiles which are necessary to obtain information on atomization. The increased sensitivity obtainable is described in this communication.

Experimental

Instrumentation. A block diagram of the system is shown in Fig. 1. The monochromator, fast-response amplifier and Memoriscope were the same as used previously [2]. The light sources were hollow-cathode and electrodeless discharge lamps (Hamamatsu TV Co.). The atomizer was a molybdenum or a tungsten microtube (20 mm long, 1.5 mm i.d.) which was machined from molybdenum or tungsten sheet (0.05 mm thick). An argon/hydrogen mixture was used as purge gas in the absorption chamber (see Table 1). Atomic absorption signals from the amplifier were fed to a microcomputer through

0378—4304/81/0000—0000/$02.50

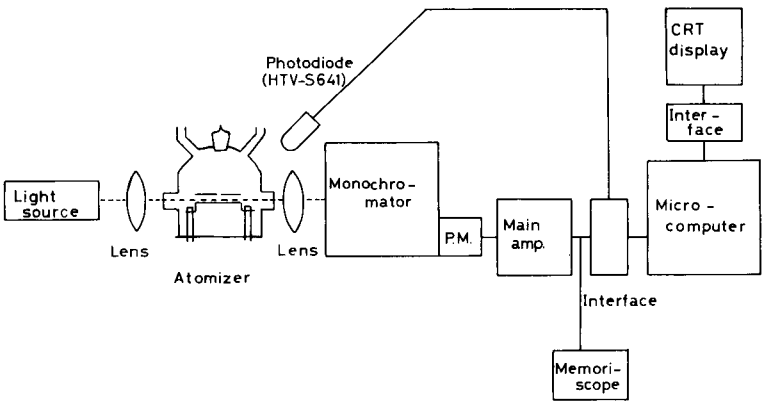

Fig. 1. Block diagram of the instrument.

an A/D converter (DATEL ADC-HX 12BGC) and multiplexer (DATEL MX-808). Signals were also monitored on a Memoriscope. The tube temperature was measured with a photodiode (Hamamatsu TV Co., S641); the signal was calibrated with an optical pyrometer. The signals from the photodiode were fed to the microcomputer and Memoriscope, and recorded simultaneously with the absorption signals.

The microcomputer (SORD M223) used was mounted with an 8-bit microprocessor (Zilog Z-80) as the central processing unit and equipped with 64 kbytes of main memory; the memory capacity was 64000 words, and the basic cycle time was 500 μs. The BASIC program was operated by an interpretative routine. The memory capacity of the floppy disc used as sub-memory was 350 kbytes.

Atomization procedure. An aliquot (1 μl) of sample solution was injected into the microtube atomizer with a glass micropipet and dehydrated at 100°C. Then, the element was atomized by heating to 2100—2200°C under the optimized conditions. Sample solutions were prepared by dissolving the element or its oxide, nitrate or tartrate salt in hydrochloric or nitric acid and evaporating excess of acid.

Stock solutions (1 mg ml^{-1}) were 0.1—6 M in acid. Working solutions were prepared by diluting stock solutions just before use. The concentration of acid was 10^{-5} M for working solutions, which caused no interference on atomization of elements.

Computer program. The programs were written in BASIC. The capacity was 36.5 kbytes. A flow chart is shown in Fig. 2. Data acquisition, calculation and logic operation are done as follows. First, the number of accumulations is input. The computer detects a trigger pulse from the atomizer feeder and data acquisition is started. Typical data acquisition rates are about 125—250 Hz which corresponds to interruptions of 4 ms. Atomic absorption and background profiles are measured alternately and the data are accumulated automatically in the disc memory. This step is repeated a pre-

TABLE 1

Sensitivities and detection limits for various elements

Element	Line (nm)	Sensitivities (pg)			Detection limits (pg)		
		Present work[a]		Graphite atomizer[b]	Present work[a]		Graphite atomizer[b]
		With computer	Without computer		With computer	Without computer	
Ag	328.1	0.14	0.26	5	0.097	0.29	0.1
Al	309.3	0.74[c]	250[c]	50	0.76[c]	5.9[c]	5
As	193.7	2.8	14	25	3.4	12	20
Co	240.7	3.0	29	40	4.8	13	5
Cr	357.9	1.3	3.3	20	1.1	7.4	10
Cu	324.8	0.023	2.6	30	0.0092	0.050	2
Fe	248.6	3.4	6.7	25	1.4	20	5
Ga	294.4	2.8	15	400	1.1	14	200
Ni	232.0	2.5	12	100	1.6	7.6	20
Pd	244.8	9.2	110	20	6.0	53	20
Sb	217.6	0.68	2.2	200	1.5	3.9	5
Se	196.1	2.1	23	200	1.2	6.7	100
Sn	224.6	2.8	8.6	100	2.9	22	100
Sr	460.7	0.15	0.76	20	0.22	0.62	5
Te	214.3	0.5	1.2	100	0.92	3.5	50

[a]Flow rates of purge gas: 495 ml Ar min^{-1} and 5 ml H_2 min^{-1} for As, Cu, Fe, Sb, Se and Te; 490 ml Ar min^{-1} and 10 ml H_2 min^{-1} for Ag; 480 ml Ar min^{-1} and 20 ml H_2 min^{-1} for Al, Co, Cr, Ni, Pd and Sn; 400 ml Ar min^{-1} and 100 ml H_2 min^{-1} for Ga and Sn.
[b]Ref. 3.
[c]Tungsten microtube was used for Al and molybdenum microtube for other elements.

scribed number of times. The background is subtracted from the atomic absorption profile, and the baseline variation with time is compensated to give zero absorption. Then, the position of the peak on each atomic absorption profile is established and the signals at other points away from the peak are accumulated. The resulting atomic absorption profile is displayed on the CRT. If necessary, the smoothing, differentiation and integration of the atomic absorption signal are done by the program.

Results and discussion

The rate of heating of the atomizer affects the atomization profiles. Provided that the rate of response of the amplifier is sufficiently high, increased rates of heating would result in the formation of denser atom clouds and thus higher absorption signals over very short periods of time. Higher rates of heating are achieved by increasing the input power. Unfortunately, very high rates of heating distort the microtube atomizer, and this disturbs the normal passage of the light beam through the atomizer, resulting in fluctuation of the absorption signal. The variation of the source intensity with time also hinders accurate atomic absorption measurement. These drawbacks were overcome by using the system described.

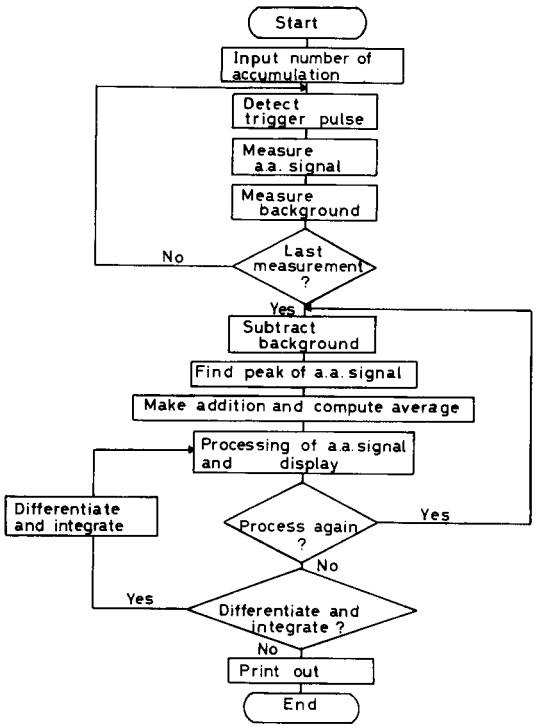

Fig. 2. Flow chart of program.

In the conventional measurement system, there is very little indication of tellurium when the sample atomization profile is compared to the background (Fig. 3A, Te). Instrumental noise may contribute significantly to the final profile even if the computer subtracts the background from the atomization profile. Data enhancement is provided by scale expansion with the aid of the computer. Further smoothing improves the appearance of the data by removal of some noise components such as white noise and noise from electric and magnetic fields. Figure 3 shows typical examples of computer processing compared with Memoriscope traces for tellurium, silver and aluminium. Ten-accumulation processing was applied and smoothing was done by the equation: $(-2x_{n-3} + 3x_{n-2} + 6x_{n-1} + 7x + 6x_{n+1} + 3x_{n+2} - 2x_{n+3})/21$.

The sensitivities and detection limits obtained by the proposed system are presented in Table 1. The sensitivity denotes the amount required to cause 1% absorption and the detection limit is calculated for a S/N ratio of 2. It is evident that the application of the computer to electrothermal atomic absorption spectrometry enhances the S/N ratio considerably.

Differentiation and integration of atomic absorption signals results in a well-defined indication of the appearance and peak temperatures on the atomization profiles. This is available for studies of atomization mechanism. Time for warming-up the light source is unnecessary because of automatic

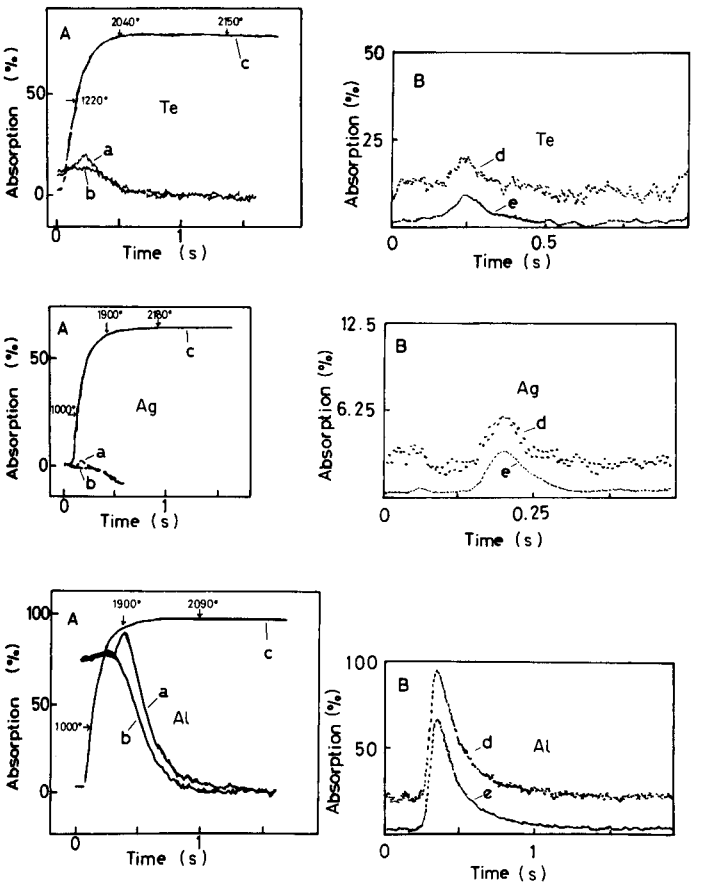

Fig. 3. Memoriscope traces and microcomputer processing of atomization profiles for tellurium (5 pg), silver (0.5 pg) and aluminium (50 pg). (A) Memoriscope traces: (a) atomic absorption signal; (b) background; (c) temperature increase. (B) Atomization profiles by computer processing: (d) no smoothing applied; (e) smoothing applied.

compensation by the computer. The application of the microcomputer facilitates the absorption measurement from the atomization profile, because of the absence of noise. This improves the precision as well as the sensitivity. This method may serve for the determination of elements in biological and some environmental samples when only small samples are available. Practical applications will be reported later.

This work was financially supported by the Ministry of Education, Science and Culture, Japan, under a Grant-in-Aid for Special Project Research.

REFERENCES

1 K. Ohta and M. Suzuki, Talanta, 25 (1978) 160.
2 K. Ohta and M. Suzuki, Anal. Chim. Acta, 110 (1979) 49.
3 C. W. Fuller, Electrothermal Atomization for Atomic Absorption Spectrometry, The Chemical Society, London, 1977.

ACA announcements

ANNOUNCEMENT OF MEETING

6th INTERNATIONAL CONFERENCE ON COMPUTERS IN CHEMICAL RESEARCH AND EDUCATION

The 6th ICCCRE will be held in the Washington, DC area on July 11–16, 1982, and will cover broad areas of computer applications in chemical research and education. There will be lectures in the mornings and evenings, with afternoons open for informal discussions and poster sessions. There will be no parallel sessions. Among the topics to be included are: Chemical Synthesis, Structure Elucidation, Structure/Activity Relationships, Theoretical Chemistry, Chemical Graph Representations, Pattern Recognition, Factor/Cluster Analysis, Computers in the Labs, Computers in the Classroom. Chemical Graph Searching, and U.S. Government Activities in the Field of Computers in Chemistry.

The international organizing committee will consist of S. Heller, Chairman (U.S.A.), V. Koptyug (U.S.S.R.), J. Zupan (Yugoslavia), S. Sakaki (Japan), J.T. Clerc (Switzerland) and P. Lykos (U.S.A.).

Since the conference is expected to have limited facilities, attendence will be held to 150 participants. There will be a spouse program.

For more information contact: Dr. Stephen R. Heller, Chairman, 6th ICCCRE, EPA, MIDSD, PM–218, 401 M Street, S.W., Washington, DC 20460, U.S.A. Tel: (202) 755–4938; Telex: 89–27–58.

CALENDAR OF FORTHCOMING MEETINGS

May 11–15, 1981 Avignon, France	**Vth International Symposium on Column Liquid Chromatography** Contact: Prof. G. Guiochon, Ecole Polytechnique, Laboratoire de Chimie Analytique Physique, Route de Saclay, 91128 Palaiseau Cedex, France. (Further details published in Vol. 118, No. 1)
May 12–15, 1981 Frankfurt am Main, G.F.R.	**5th European Experimental NMR Conference** Contact: 5th EENC, H. Caspari, Iwan Stranski-Institut der Technischen Universität Berlin, Strasse des 17 Juni 112, D-1000 Berlin 12, G.F.R.
May 18–20, 1981 Jekyll Island, Georgia, U.S.A.	**11th Annual Symposium on the Analytical Chemistry of Pollutants** Contact: Prof. Dr. Roland W. Frei, The Free University, De Boelelaan 1083, 1081 HV Amsterdam, The Netherlands.
May 20–22, 1981 Eger, Hungary	**Symposium on the Analysis of Steroids** Contact: Prof. S. Görög, c/o Hungarian Chemical Society, 1061 Budapest VI., Anker köz 1, Hungary.
May 26–28, 1981 Washington, DC, U.S.A.	**3rd International Symposium on Rapid Methods and Automation in Microbiology** Contact: Dr. Richard C. Tilton, Chairman, ISRMA Planning Committee, University of Connecticut Health Center, Department of Laboratory Medicine, 263 Farmington Avenue, Farmington, CT 06032, U.S.A.
June 1–5, 1981 Metz, France	**International Conference on Elemental Analysis** Contact: conference administrators, S. International, 27 Rue du Mans, 92400 Courbevoie, Paris, France. Tel. (01) 333 44 10.
June 1–5, 1981 Stresa, Lago Maggiore, Italy	**2nd European Symposium on Organic Chemistry** Contact: Prof. Giorgio Modena, Istituto di Chimica Organica, Via Marzolo, 1, 35100 Padova, Italy.

June 9–11, 1981 Scarborough, Great Britain	**The 34th Chemists' Conference** Contact: J. Davey, Teesside Laboratories, British Steel Corporation, P.O. Box 11, Grangetown, Middlesbrough, Cleveland TS6 6UB, Great Britain (Further details published in Vol. 124, No. 2)
June 15–29, 1981 Toronto, Canada	**6th International Conference on Modern Trends in Activation Analysis and Exhibition** Contact: Prof. R.E. Jervis, Chairman, Organizing Committee, 6th ICMTAA, Department of Chemical Engineering and Applied Chemistry, University of Toronto, Toronto, Ontario, Canada M5S 1A4.
June 16–17, 1981 Venice, Italy	**1st International Symposium on Chromatography in Biochemistry, Medicine and Environmental Research** Contact: Dr. A. Frigerio, Italian Group for Mass Spectrometry in Biochemistry and Medicine, c/o Istituto di Ricerche Farmacologiche "Mario Negri", Via Eritrea 62, 20157 Milan, Italy. Tel: 35.54.546.
June 18–19, 1981 Venice, Italy	**8th International Symposium on Mass Spectrometry in Biochemistry, Medicine and Environmental Research** Contact: Dr. A. Frigerio, Italian Group for Mass Spectrometry in Biochemistry and Medicine, c/o Istituto di Ricerche Farmacologiche "Mario Negri" Via Eritrea 62 20157 Milan, Italy. Tel: 35.54.546.
June 22–25, 1981 Berkeley, CA, U.S.A.	**2nd International Topical Meeting on Photoacoustic Spectroscopy** Contact: Optical Society of America, Photoacoustic spectroscopy, 1816 Jefferson Place, NW, Washington, DC 20036, U.S.A.
June 22–26, 1981 Veldhoven, The Netherlands	**4th International Symposium on Affinity Chromatography and Related Techniques** Contact: Dr. T.C.J. Gribnau, Organon Scientific Development Group, P.O. Box 20, 5340 BH Oss, The Netherlands. (Further details published in Vol. 118, No. 1)
June 23–27, 1981 Karl–Marx–Stadt, G.D.R.	**Tagung Festkorperanalytik** Contact: Dr. K. Danzer, Technische Hochschule, Karl–Marx–Stadt, Sektion Chemie und Werkstofftechnik, PSF 964, 9010 Karl–Marx–Stadt, G.D.R. (Further details published in Vol. 118, No. 2)
June 30–July 2, 1981 Amsterdam, The Netherlands	**International Conference on Ion and Plasma Assisted Techniques** Contact: CEP Consultants, 26 Albany Street, Edinburgh EH1 3QH, Great Britain.
July 5–10, 1981 Jerusalem, Israel	**Fourth International Conference on Surface and Colloid Science** Contact: The Secretariat, Fourth International Conference on Surface and Colloid Science, c/o Conventions (Kopel Tours) Ltd., P.O. Box 3054, Tel Aviv 61030, Israel.
July 5–10, 1981 Swansea, Wales	**The Third Swansea Summer School of Automatic Chemical Analysis** Contact: Prof. D. Betteridge, Department of Chemistry, University College of Swansea, Singleton Park, Swansea SA2 8PP, Great Britain.
July 6–9, 1981 Strasbourg, France	**27th IUPAC Symposium on Macromolecules** Contact: Secretariat, Macro 1981, Société de Chimie Industrielle, 28, rue Saint-Dominique, 75007 Paris, France.
July 12–17, 1981 Exeter, Great Britain	**5th International Conference on NMR Spectroscopy** Contact: Dr. J.F. Gribnau, Royal Chemical Society, Burlington House, London W1V 0BN, Great Britain.
July 13–17, 1981 Srinagar, India	**International Conference on the Application of the Mössbauer Effect** Contact: Dr. V.G. Bhide, National Physical Laboratory, Hillside Road, New Delhi, 110012, India.
July 13–17, 1981 Durham, Great Britain	**International Symposium on Advances in Polymer Characterization** Contact: Dr. W.J. Feast, Chemistry Department, University of Durham, South Road, Durham DH1 3LE, Great Britain

July 14–16, 1981 Cambridge, Great Britain	**International Conference in Microscopy and X-Ray Diffraction – Inter/Micro '81** Contact: McCrone Research Institute Ltd., 2 McCrone Mews, Belsize Lane, London NW3 5BG, Great Britain.
July 19–24, 1981 Tokyo, Japan	**8th International Congress of Pharmacology** Contact: Int. Union of Pharmacology, IUPHAR, Pharmakologisches Institut im Neuenheimer, Feld 366, D-6900 Heidelberg, G.F.R.
July 20–23, 1981 Prague, Czechoslovakia	**22nd Prague Microsymposium on Characterization of Dynamic and Geometrical Structure of Polymer Systems by NMR Spectra** Contact: B. Sedláček, Institute of Macromolecular Chemistry, Czechoslovak Academy of Sciences, Heyrovského n.2, CS–162 06 Praha, Czechoslovakia.
July 20–23, 1981 Oxford, Great Britain	**7th International Symposium on Synthesis in Organic Chemistry** Contact: Dr. John F. Gibson, Royal Society of Chemistry, Burlington House, London W1V 0BN, Great Britain
July 28–31, 1981 New Hampton, NH, U.S.A.	**30th Anniversary Meeting of the Gordon Research Conference on Statistics in Chemistry and Chemical Engineering** Contact: Dr. Alexander M. Cruickshank, Director, Gordon Research Conferences, Pastore Chemical Laboratory, University of Rhode Island, Kingston. RI 02881, U.S.A. Tel. (401) 783–4011.
Aug. 2–6, 1981 Fort Collins, CO, U.S.A.	**International Symposium on Organometallic Chemistry Directed to Organic Synthesis** Contact: Dr. L.S. Hegedus, Department of Chemistry, Colorado State University, Fort Collins, CO 80523, U.S.A.
Aug. 3–7, 1981 Denver, CO, U.S.A.	**30th Denver Conference on Applications of X-Ray Analysis** Contact: Mrs. Mildred Cain, Denver Research Institute, University of Denver, Denver, CO 80208, U.S.A. Tel: (303) 753–2141.
Aug. 9–14, 1981 Toronto, Canada	**10th International Conference on Organometallic Chemistry** Contact: Dr. H.C. Clark, V-P Academic, University of Guelph, Guelph, Ontario, Canada N1G 2W1.
Aug. 9–14, 1981 Maryland, U.S.A.	**6th International Conference on Chemical Education** Contact: Dr. Marjorie Gardner, Division Director, Division of Science Education Resources Improvement, National Science Foundation, Washington, DC 20550, U.S.A.
Aug. 16–21, 1981 Vancouver, Canada	**28th Congress International Union of Pure and Applied Chemistry** Contact: Congress Secretariat, 28th IUPAC Congress, c/o The Chemical Institute of Canada, 151, Slater Street, Suite 906, Ottawa, Ontario, Canada K1P 5H3.
Aug. 17–21, 1981 Meriden, NH, U.S.A.	**Gordon Research Conference on Ion Exchange** Contact: Dr. A.M. Cruickshank, Director, Gordon Research Conferences, Pastore Chemical Laboratory, University of Rhode Island, Kingston, RI 02881, U.S.A. Tel. (401) 783–4011, or (401) 783–3372.
Aug. 20–21, 1981 Helsinki, Finland	**Symposium on Harmonisation of Collaborative Analytical Studies** Contact: Dr. H. Egan, Laboratory of the Government Chemist, Cornwall House, Stamford Street, London SE1 9NQ, Great Britain.
Aug. 23–28, 1981 Espoo, Finland	**Euroanalysis IV – Triennal Conference of the Federation of European Chemical Societies** Contact: Professor L. Niinistoe, Department of Chemistry, Helsinki University of Technology, SF–02150 Espoo 15, Finland. (Further details published in Vol. 109, No. 1)
Aug. 23–28, 1981 Canberra, Australia	**Sixth Australian Symposium on Analytical Chemistry** Contact: Hon. Secretary, Miss B.J. Stevenson, P.O. Box 1397, Canberra City, A.C.T. 2601, Australia.

Aug. 23–28, 1981 New York, NY, U.S.A.	**National American Chemical Society Meeting** Contact: American Chemical Society, 1155 Sixteenth Street, NW, Washington, DC 20036, U.S.A.
Aug. 30–Sep. 5, 1981 Vienna, Austria	**XI International Congress of Clinical Chemistry – IV European Congress of Clinical Chemistry** Contact: Congress Secretariat, Interconvention, P.O. Box 35, A-1095 Vienna, Austria. Tel. (0222) 42 13 52.
Sep. 1–3, 1981 Houston, TX, U.S.A.	**"EXPOCHEM '81"** Contact: Dr. A. Zlatkis, Chemistry Department, University of Houston, Houston, TX 77004, U.S.A. Tel. (713) 749–2623
Sep. 1–4, 1981 Siofok, Hungary	**3rd Danube Symposium on Chromatography** Contact: Hungarian Chemical Society, H–1368 Budapest, P.O.B. 240, Hungary. Tel: Budapest 427–343. (Further details published in Vol. 115)
Sep. 1–4, 1981 Aberdeen, Scotland	**ESTA 2 – The Second European Symposium on Thermal Analysis** Contact: Dr. F.P. Glasser, Chairman of the Organising Committee, ESTA 2, Department of Chemistry, University of Aberdeen, Meston Walk, Old Aberdeen, AB9 2UE, Scotland.
Sep. 4–8, 1981 Tokyo, Japan	**9th International Conference on Atomic Spectroscopy and XXII Colloquium Spectroscopicum Internationale** Contact: The Japan Society for Analytical Chemistry, 9th ICAS/XXII CSI, Gotanda Sanhaitsu, 26-2 Nishigotanda 1-chome, Shinagawa-ku, Tokyo 141, Japan. (Further details published in Vol. 118, No. 1)
Sept. 9–11, 1981 Chicago, IL, U.S.A.	**2nd International Symposium on Radiopharmacology and Exhibition** Contact: Dr. Lelio G. Colombetti, Pharmacology Department, Loyola University, Stritch School of Medicine, Maywood, IL 60153, U.S.A.
Sept. 9–11, 1981 Coventry, Great Britain	**International Conference on Advances in Flow Measurement Techniques** Contact: Conference Organizer, BHRA Fluid Engineering, Cranfield, Bedford, Great Britain.
Sept. 20–25, 1981 Philadelphia, PA, U.S.A.	**8th Annual Meeting of the Federation of Analytical Chemistry and Spectroscopy Societies (FACSS)** Contact: Richard J. Knauer, Publicity Chairman, ARMCO INC., P.O. Box 1697, Baltimore, MD 21203, U.S.A.
Sep. 21–24, 1981 Loughborough, England	**Particle Size Analysis Conference** Contact: P.J. Lloyd, PSA 81 Conference, Particle Technology Group, Chemical Engineering Department, University of Technology, Loughborough, Leics. LE11 3TU, Great Britain. (Further details published in Vol. 120)
Sep. 22–25, 1981 Leipzig, G.D.R.	**Analytiktreffen 1981 – Strukturanalytische Methoden in der Stereochemie** Contact: Sektion Chemie der KMU Leipzig, Liebigstrasse 18, DDR–7010 Leipzig, G.D.R.
Sep. 28–Oct. 1, 1981 Barcelona, Spain	**16th International Symposium on Advances in Chromatography** Contact: Professor A. Zlatkis, Chemistry Department, University of Houston, Houston, Texas 77004, U.S.A.
Sep. 29–Oct. 2, 1981 Basle, Switzerland	**ILMAC'81 – 8th International Exhibition of Laboratory, Chemical Engineering, Measurement and Automation Techniques in Chemistry** Contact: D. Gammeter, Secretariat, ILMAC '81, Postfach, CH–4021 Basle, Switzerland. Tel: 061–2620 20.
Oct. 27–29, 1981 London, Great Britain	**Petroanalysis 81** Contact: Miss I.A. McCann, Conference Officer, Institute of Petroleum, 61 New Cavendish Street, London W1M 8AR, Great Britain. (Tel: 01–636 1004, Telex: 264380)

Evaluation and Optimization of Laboratory Methods and Analytical Procedures

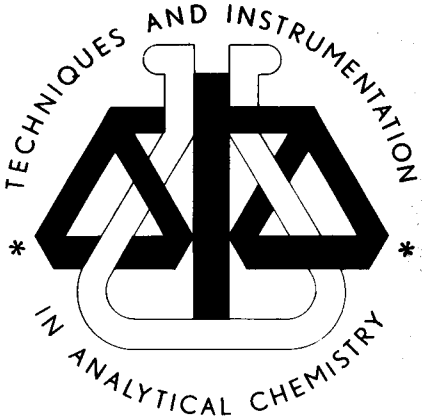

A Survey of Statistical and Mathematical Techniques

D.L. MASSART, A. DIJKSTRA *and* L. KAUFMAN.

with contributions by S. Wold, B. Vandeginste *and* Y. Michotte

Techniques and Instrumentation in Analytical Chemistry - Volume 1

This book provides detailed treatment, in a single volume, of formal methods for optimization in analytical chemistry. It is a comprehensive and practical handbook which no analytical laboratory will want to be without.

All aspects of optimization are discussed, from the simple evaluation of procedures to the organization of laboratories or the selection of optimal complex analytical programmes. Quantitative discrete analysis as well as qualitative and continuous measurement techniques are evaluated.

The book consists of 30 chapters divided into 5 main parts.The main sections are: Evaluation of the Performance of Analytical Procedures, Experimental Optimization, Combinatorial Problems, Requirements for Analytical Procedures, and Systems Approach in Analytical Chemistry.

This work will be of practical value not only to those involved with optimization problems in analytical chemistry, but also to those in related fields such as clinical chemistry or specialized fields such as chromatography. Because it discusses the application of many mathematical techniques in analytical chemistry, this book will also serve as a general introduction to the new field of Chemometrics.

1978 1st Reprint 1979 xvi + 596 pages US $68.25 / Dfl. 140.00
ISBN 0-444-41743-5

ELSEVIER

P.O. Box 211,
1000 AE Amsterdam
The Netherlands

52 Vanderbilt Ave
New York, N.Y. 10017

The Dutch guilder price is definitive. US $ prices are subject to exchange rate fluctuations.

STATISTICAL TREATMENT OF EXPERIMENTAL DATA

By J.R. GREEN, *Lecturer in Computational and Statistical Science, University of Liverpool, U.K. and* D. MARGERISON, *Senior Lecturer in Inorganic, Physical and Industrial Chemistry, University of Liverpool, U.K.*

PHYSICAL SCIENCES DATA 2

This book first appeared in 1977. In 1978 a revised reprint was published and in response to demand, further reprints appeared in 1979 and 1980. Intended for researchers wishing to analyse experimental data, this work will also be useful to students of statistics. Statistical methods and concepts are explained and the ideas and reasoning behind statistical methodology clarified. Noteworthy features of the text are numerical worked examples to illustrate formal results, and the treatment of many practical topics which are often omitted from standard texts, for example testing for outliers, stabilization of variances and polynomial regression.

What the reviewers had to say:

"The index is detailed; the format is good; the presentation is clear; and no mathematics beyond calculus is assumed".
–CHOICE

"A lot of thought has gone into this book and I like it very much. It deserves a place on every laboratory bookshelf".
–CHEMISTRY IN BRITAIN

1977. Reprinted 1978, 1979, 1980.
xiv + 382 pages
US $39.25/Dfl.90.00
ISBN: 0-444-41725-7

ELSEVIER

P.O. Box 211, 1000 AE Amsterdam, The Netherlands.
52 Vanderbilt Ave., New York, NY 10017.

The Dutch guilder price is definitive. US$ prices are subject to exchange rate fluctuations.

VOL. 133, No. 2 ANALYTICA CHIMICA ACTA May 1, 1

(Computer Techniques and Optimization, Vol. 5, No. 2)

CONTENTS